Technische Universität München, Fakultät für Medizin

Somatic multiplexed CRISPR/Cas9-based mutagenesis

Roman Maresch

Vollständiger Abdruck der von der

Fakultät für Medizin

der Technischen Universität München zur Erlangung des akademischen Grades

eines Doktors der Naturwissenschaften

genehmigten Dissertation.

Vorsitzender: Prof. Dr. Carsten Schmidt-Weber

Prüfende/-r der Dissertation:

1. Prof. Dr. Radu Roland Rad

2. Prof. Dr. Bernhard Küster

3. Prof. Dr. Claus Belka

Die Dissertation wurde am 28.05.2020 bei der Technischen Universität München
eingereicht und durch die

Fakultät für Medizin am 29.12.2020 angenommen.

Somatic multiplexed CRISPR/Cas9-based mutagenesis

First advisor: Prof. Roland Rad

Second advisor: Prof. Bernhard Küster

Mentor: Dr.med. Maximilian Reichert

Table of contents

1. List of figures

2. List of tables

3. List of abbreviations

AAV	Adeno-associated virus
aCGH	Array comparative genomic hybridization
ADM	Acinar-to-ductal metaplasia
AFN	MMF antagonizing combination of atipamezole, flumazenil and naloxone
ARID	AT-rich interaction domain
ATF2	Activating transcription factor 2
BSA	Bovine serum albumin
Cas9	CRISPR-associated protein 9
CBh	Chicken ß-actin promoter
CCDS	Consensus coding sequence
CK19	Cytokeratin19
CMV	Cytomegalovirus
CNA	Copy number alteration
CREB	cAMP response element-binding protein
CRISPR	Clustered regularly interspaced short palindromic repeat
CRISPRi	CRISPR interference
CRISPRa	CRISPR activation
crRNA	CRISPR RNA
dCas9	Dead Cas9
DMEM	Dulbecco's Modified Eagle Medium
DMSO	Dimethyl sulfoxide
DSB	Double strand break
EDTA	Ethylenediaminetetraacetic acid
EGFR	Epithelial growth factor receptor
EMT	Epithelial-to-mesenchymal
ERK	Extracellular-signal related kinase
FCS	Fetal calf serum
FFPE	Formalin-fixed paraffin embedded
FLP	Flippase
GAP	GTPase-activating protein
gDNA	genomic DNA
GDP	Guanosine diphosphate
GEF	Guanine exchange factor
GEMM	Genetically engineered mouse model
GFP	Green fluorescent protein
GPCR	G protein-coupled receptor
GTP	Guanosine triphosphate
H&E	Haematoxylin and eosin
HDR	Homology directed repair
HTVI	Hydrodynamic tail vein injection
i.p.	Intraperitoneal
IHC	Immunohistochemistry

Indel	Insertion/deletion
IPMN	Intraductal papillary mucinous neoplasm
LB	Liquid broth
LSL	*loxP*-stop-*loxP*
MAPK	Mitogen-activated protein kinase
MCN	Mucinous cystic neoplasm
MEK	Mitogen-activated protein kinase kinase
M-FISH	Multispectral-fluorescence in situ hybridisation
MMF	Combination anesthetic of medetomidine, midazolam and fentanyl
MRI	Magnetic resonance imaging
MTOR	Mammalian target of rapamycin
MTT	3-(4,5-dimethyl-2-thiazolyl)-2,5-diphenyl-tetrazolium bromide
NF-kB	Nuclear factor-kB
NGS	Next generation sequencing
NHEJ	Non-homologous end joining
P/S	Penicillin/streptomycin
PAM	Protospacer associated motif
PanIN	Pancreatic intraepithelial neoplasm
PBS	Phosphate buffered saline
PCR	Polymerase chain reaction
PDAC	Pancreatic ductal adenocarcinoma
Pdx1	Pancreatic duodenum homeobox 1
PE	Post electroporation
PGK	Phosphoglycerate kinase
PH	Pleckstrin homology
PI3K	Phosphoinositide 3-kinase
PIP2	Phosphatidylinositol 4,5-biphosphate
PIP3	Phosphatidylinositol 3,4,5-triphosphate
PK	*Pdx1-Cre* or *Ptf1a$^{Cre/+}$* intercrossed to *Kras$^{LSL-G12D/+}$* mouse
PP	Poring pulse
PTEN	phosphate and tensin homolog
Ptf1a	Pancreas associated transcription factor 1a
PVDF	Polyvinylidene difluoride
Q61	*Kras* glutamine residue 61
QM	Quasimesenchymal
RALGEF	Ras-like GEF
RNAi	RNA interference
RTK	Receptor tyrosine kinases
S. pyogenes	*Streptococcus pyogenes*
SB	*Sleeping beauty* transposase
SDS-PAGE	Sodium dodecyl sulfate polyacrylamide gel electrophoresis
sgRNA	Single guide RNA
SNV	Somatic nucleotide variant
SWI/SNF	Switch/sucrose non-fermentable

TF	Transcription factor
TP	Transfer pulse
tracrRNA	Trans-activating CRISPR RNA
TSG	Tumour suppressor gene
UMI	Unique molecular identifier
WGS	Whole genome sequencing

4. Summary

Pancreatic cancer patients have a poor prognosis with a 5-year survival rate below 5%. Next generation sequencing of human tumour samples provided scientists with a wealth of novel candidate genes, which still require the validation for their relevance in cancer biology. Genetically engineered mouse models have opened the possibility to study gene function during tumorigenesis at unprecedented depth; however, generation of alleles/models is limited by the long duration and high expenses for the mouse line maintenance.

Here, we have developed a method for transfection-based *in vivo* delivery of multiplexed CRISPR/Cas9 target vectors in mice, which enabled the high-throughput study of candidate genes in pancreatic cancer. We have found that simultaneous CRISPR/Cas9 gene editing of multiple relevant tumour suppressor genes in single cells of the pancreas led to a significantly shortened time to cancer development compared to a control cohort. The possibility to inactivate several genetic target sites in one cell allowed the fast generation of complex cancer genotypes in adult mice, thus recapitulating sporadic somatic mutations seen in cancer patients. We further demonstrated important applications of multiplexed *in vivo* CRISPR/Cas9 gene editing in cancer research, such as combinatorial gene editing, *in vivo* synthetic lethality screening and phylogenetic studies on individual cancer founding clones. CRISPR/Cas9 multiplexing substantiated negative selection of lethal *Brca2*-inactivation in a pure *Kras*^{G12D} background. Furthermore, unique CRISPR-induced mutational signatures were exploited to phylogenetically trace metastatic cancer clones and revealed the evolutionary origin of distinct morphological phenotypes in one cultured cancer sample. Additionally, multiplexed CRISPR/Cas9 delivery induced somatic intra- as well as inter-chromosomal rearrangements, offering for the first time the opportunity to model this frequent phenomenon in the adult mouse pancreas.

In summary, we have established a transfection-based methodology for the mosaic delivery of multiple CRISPR/Cas9 vectors into individual pancreatic cells of adult mice, mimicking the stochastic nature of human tumorigenesis. Our pancreatic cancer model will increase the speed and the scalability for generating complex pancreatic cancer genotypes in mice. Thus, this advancement will open the possibility for basic research to study functional genomics and translational research to gain insights into different critical biological aspects of pancreatic cancer.

5. Zusammenfassung

Das Pankreaskarzinom besitzt eine äußerst schlechte Prognose für Patienten. Next-Generation Sequenziertechnologien haben zu einem starken Anstieg von neuen Kandidatengenen aus Patiententumoren geführt, welche allerdings noch auf ihre biologische Relevanz für den Krebs untersucht werden müssen. Transgene Mausmodelle haben zu einem tieferen Verständnis der Funktion von Genen in der Entstehung von Krebs geführt. Jedoch sind traditionelle Mausmodelle für die große Zahl an Kandidat-Genen sehr teuer und die Erhaltung von komplexen Mausgenotypen aufwendig.

Hier stellen wir ein neues Modell des Pankreaskarzinoms durch parallele Transfektion von multiplen CRISPR/Cas9 Vektoren in adulten Mäusen vor, welches eine beschleunigte Analyse von potenziellen Krebsfaktoren ermöglicht. Die synchrone Editierung von vielen Pankreaskrebs-relevanten Zielgenen in einzelnen Zellen des adulten Pankreas führte zu einer signifikanten Verkürzung der Zeit zur Tumorentstehung im Vergleich zu einer äquivalenten Kontrollgruppe. Die Möglichkeit, viele Tumorsuppressorgene in einer Zelle gleichzeitig zu inaktivieren beschleunigt die Herstellung von komplexen Krebs-Genotypen in Mäusen.

Unser Krebsmodell ist geeignet für die Erforschung von kombinatorischen Gennetzwerken, und ermöglicht die Untersuchung der metastatischen und morphologischen Evolution von Krebseinzelzellklonen, sowie die Durchführung von Screens für die Entdeckung von synthetisch letalen Krebsfaktoren in Mäusen.

Gemultiplexte CRISPR/Cas9 Geneditierung bestätigte die negative *in vivo* Selektion der *Brca2* Inaktivierung im reinen *Kras^{G12D}* Hintergrund. Weiters konnte durch die einzigartigen CRISPR/Cas9-induzierten Mutationssignaturen die phylogenetische Abstammung einzelner metastasierten Krebszellklone, als auch die Evolution eines morphologisch unterschiedlichen Tumors untersucht werden. Die parallele Transfektion von CRISPR/Cas9 konnte intra- als auch inter-chromosomale Strukturveränderungen in den Pankreastumoren induzieren, wobei eine erste Grundlage für die Erforschung dieser Phänomene im adulten Organ geschaffen wurde.

Zusammenfassend haben wir eine Transfektion-basierende Methode zur Einbringung von multiplen CRISPR/Cas9 Vektoren zur simultanen Veränderung von mehreren Kandidatengenen in individuellen Pankreaszellen der adulten Maus entwickelt, um deren Validierung und Durchsatz zu beschleunigen. Unser Krebsmodell erlaubt daher die Charakterisierung von kritischen biologischen und klinischen Eigenschaften des Pankreaskarzinoms, welche für die präklinische Forschung von höchstem Interesse sind.

6. Introduction

6.1. Clinical aspects of pancreatic cancer

The pancreas is a glandular organ that consists of the exocrine compartment, producing digestive enzymes (proteases, lipases, etc) and the endocrine system, secreting important hormones into the circulation for the regulation of carbohydrate, fat and protein levels in the blood (insulin, glucagon, pancreatic polypeptide etc). The exocrine pancreas is separated in the acinar and ductal compartment. In most cases pancreatic malignancies affect the exocrine lineage. Among exocrine cancers, pancreatic ductal adenocarcinoma (PDAC) is the most common type of pancreatic cancer in humans accounting for approximately 90% of exocrine-originating tumours (Ryan *et al.*, 2014). Less common cancers of the exocrine pancreas are acinar cell carcinoma (1-2%), serous or mucinous cystadenocarcinomas (~1%) and rarer ductal adenocarcinomas such as mucinous noncystic carcinomas, adenosquamous carcinomas and undifferentiated carcinomas.

PDAC is today the fourth leading cause of cancer-related deaths worldwide and projected to become second within the next couple of years (Rahib *et al.*, 2014). Globally, the incidence of pancreatic cancer ranges from 1 to 10 cases per 100,000 people with higher rates in Western societies and among men (Siegel *et al.*, 2018). Unlike other tumour entities, the genetic basis for familial aggregation is unclear. However, rare genetic syndromes are associated with an increased risk of developing pancreatic cancer including hereditary pancreatitis (Rebours *et al.*, 2008), Peutz-Jeghers syndrome (Giardiello *et al.*, 2000) and familial atypical multiple mole and melanoma syndrome (Vasen *et al.*, 2000). In addition, biological risk factors are non-hereditary chronic pancreatitis (Duell *et al.*, 2012), smoking (Bosetti *et al.*, 2012), long-lasting diabetes mellitus (Ben *et al.*, 2011) and obesity (Aune *et al.*, 2012). Over the past decades, the curative treatment options in the advanced disease have been extremely limited with 5-year survival rates of around 5% (Rahib *et al.*, 2014). In contrast to other solid cancer entities, targeted therapeutic interventions and pre-tumour screening efforts for risk patients have improved the overall survival. Unfortunately, there are currently no similar clinical approaches available for the care of pancreatic cancer patients (Ryan *et al.*, 2014). Reasons for this clinical situation are the comparatively long-lasting asymptomatic phase in which the cancer already turned invasive, early metastatic dissemination into distant organs, stroma-richness of primaries, aggressive growth into life-sustaining vessels (vena cava), local-neural invasion of nerves facilitating re-colonization after complete surgical removal of the tumour and resistance to chemo- as well as radiotherapy.

For more than a decade, single agent drug gemcitabine has been the standard care for advanced metastatic pancreatic cancer resulting in a median survival of 5.6 month (Burris *et al.*, 1997). In 2011, combinatorial drug FOLFIRINOX consisting of folinic acid, fluorouracil, irinotecan and oxaliplatin comprised a significantly prolonged overall survival in metastatic disease to median 11.1 months, and also improved patient's quality of life (Conroy *et al.*, 2011). A more recent study added nanoparticle albumin-bound paclitaxel (nab-paclitaxel) to gemcitabine and thereby achieved significant elongation of survival to 8.5 month to gemcitabine alone (Von Hoff *et al.*, 2013). Disappointingly, none of these studies are close to complete remission and prolong life of the patients only marginally by a few weeks compared to treatment options already available in the 1990s.

6.2. Exocrine pancreas development in the mouse

At mouse embryonic day 8.5, inhibition of hedgehog signalling in discrete regions of the foregut endoderm initiates the development of the pancreas (Hebrok *et al.*, 1998; Offield *et al.*, 1996). Concomitantly, expression of different transcription factors (TFs) specify the multi-potent pancreatic cell lineage that later form the exocrine and endocrine compartment of the pancreas. Among these TFs, *Pdx1* (pancreatic duodenum homeobox 1) has a critical role for pancreatic development. Mice that carry a deletion of this gene feature pancreatic agenesis (Offield *et al.*, 1996). During the onset of pancreatic bud formation at embryonic day 11.5, *Pdx1*-positive multi-potent pancreatic precursor cells start to express *Ptf1a* (pancreas associated transcription factor 1a), a protein that critically regulates the lineage commitment and maintenance of exocrine pancreatic cells (Krapp *et al.*, 1998; Kawaguchi *et al.*, 2002; Kim *et al.*, 2002). Between embryonic day 11.5-15, pancreatic epithelium in the bud is separated in tip regions containing acinar *Ptf1a*-positive cells and trunk regions containing bi-potent duct- and endocrine cells that are marked by *Pdx1* expression. Activating Notch ligand essentially regulates the trunk/tip patterning of the pancreas as the ablation of the signalling leads to the loss of the bi-potent trunk cell population (Horn *et al.*, 2012). In this phase, expansion of the defined cell lineages occurs. Here, canonical Wnt-signalling regulates the exocrine cell expansion as the conditional knock-out of critical Wnt ligands leads to the attenuation of the development of the exocrine compartment (Wells *et al.*, 2007). Notably in adulthood, committed exocrine cells lose *Pdx1* expression, but especially acinar cells maintain *Ptf1a* expression (Pan *et al.*, 2013). At embryonic day 17.5, the main duct is connected via several interlobular ducts and many intralobular ducts to the acini. In this stage, the endocrine compartment is also completely developed.

6.3. Progression model of exocrine pancreatic cancer (Hruban *et al.*, 2000a)

Mucinous cystic neoplasms (MCNs), intraductal papillary mucinous neoplasms (IPMNs) and pancreatic intraepithelial neoplasms (PanINs) form the three main precursor lesions of pancreatic cancer, with PanINs being the most prevalent. PanINs arise over a sequence of normal duct epithelium to low-grade precursor lesions (PanIN1a, PanIN1b and PanIN2a) with low- to moderate dysplasia peaking to highly dysplastic PanIN3 (carcinoma *in situ*) (Hruban *et al.*, 2000a). Sequencing studies have revealed that over 90% of low- and high-grade PanINs carry an activating mutation in the *KRAS* oncogene (Kanda *et al.*, 2012) and most recently, it was shown that the mutated *KRAS* locus is already amplified in pre-cancerous lesions (Mueller *et al.*, 2018). Oncogenic *KRAS* mutations are in most cases the foundation for de-differentiation processes of exocrine pancreatic cells leading to ductal structures in PanIN1a. These lesions are described by a flat epithelium with nuclei located close to the basal membrane. Already PanIN1b lesions display papillary structures. PanIN2 lesions are characterized by nuclear movement to the lumen and are typically enlarged and/or elongated compared to normal duct epithelium. Architecturally, elevated micro-papillary structures and cytological disorganization, increased nuclear irregularities such as magnified nucleoli or abnormal mitoses and cribriform luminal necrosis and mucinous cytoplasm characterize PanIN3 lesions. In high-grade PanINs as well as in invasive PDAC, genetic mutations in important cancer genes such as *TP53*, *CDKN2A*, *SMAD4* and TGFBR2 pathway genes occur in increasing frequencies setting up the framework for the extensive genomic heterogeneity observed in this entity (Jones *et al.*, 2008; Biankin *et al.*, 2012; Waddell *et al.*, 2015; Bailey *et al.*, 2016a; Witkiewicz *et al.*, 2015). Beyond these recurrent mutations in cancer pathway genes, allelic imbalances of oncogenic *KRAS* itself can influence the biology and clinical outcome of the tumour (Cancer Genome Atlas Research Network, 2017; Mueller *et al.*, 2018). Most recently, our lab could show through microdissection of human PanINs that oncogenic *KRAS* amplification can already occur in these pre-cancerous lesions (Mueller *et al.*, 2018). As this work only aimed to characterize *KRAS* hotspot-mutations in codon 12 and 13, it would be of high interest to analyse other recurrently mutated cancer genes or quantify the structural rearrangements in precursor lesions by whole genome sequencing (WGS). At metastatic stage, PDACs have frequently acquired a high degree of genomic instability compared to other solid cancers. It is currently a matter of debate whether genomic instability itself can be a driver of tumorigenesis (Jones *et al.*, 2008; Griffin *et al.*, 2007; Notta *et al.*, 2016). If PanINs (and likely other pancreatic cancer precursor lesions) already possess an "almost cancer genome", this observation could explain

the rapid metastatic progression seen in pancreatic cancer patients, however it raises a bundle of other unsolved questions.

Today, it is still not unambiguously resolved whether the acinar (larger fraction of exocrine pancreas) or ductal (morphologically more similar to PanINs) compartment gives rise to PDAC or to which subtypes of PDAC (Kong *et al.*, 2011). Historically, ductal-like PDAC histology implicated the ductal compartment as "cell of origin" (Kong *et al.*, 2011; Hruban *et al.*, 2000b). More recent findings show that oncogenic *Kras* is not sufficient to transform mouse duct cells alone and even in combination with mutant *Tp53*, PDAC development from duct cells is less efficient compared to acinar cells (Kopp *et al.*, 2012; Bailey *et al.*, 2016b). Already a couple of years ago, Miyatsuka et al. reported that persistent adult expression of *Pdx1* transcription factor in the mouse pancreas induces a shrinkage of the acinar compartment and a concomitant replacement by duct-like structures in the pancreas, a process called acinar-to-ductal metaplasia (ADM) (Miyatsuka *et al.*, 2006). Analysis of human ADM and PanIN samples without PDAC diagnoses showed that PanIN-independent ADM lesions are wildtype for *KRAS*, whereas ADMs associated with focal PanIN dedifferentiation featured identical oncogenic *KRAS* mutations suggesting retrograde expansion of neoplastic PanIN cells in ADM foci (Shi *et al.*, 2009). Today it is known, that forced expression of oncogenic *Kras* in 4 weeks old mice induces predominantly ADM lesions. However, at later time points, neoplastic PanIN cells can be found in ADM foci, raising the possibility that oncogenic *Kras*-expressing acinar cells can give rise to PanIN lesions and eventually, invasive PDAC (Zhu *et al.*, 2007; Guerra *et al.*, 2007). In general, it is nowadays accepted that acinar plasticity through ADM precedes PanIN formation and thus, represents an early event in pancreatic cancer development in mouse and human (Reichert *et al.*, 2016).

Acinar to ductal trans-differentiation represents a physiological response to acute pancreatic injury. After clearance of the inflammation, certain pro-differentiation factors mediate termination of this metaplastic-feedback loop (e.g. NOTCH1) allowing the recovery of functional acini (Murtaugh *et al.*, 2015). Furthermore, transient signalling pathway activity, such as canonical Wnt/ß-catenin signalling is required for efficient acinar regeneration during inflammatory and regenerative processes (Morris *et al.*, 2010). If the initial stimulus (e.g. chronic pancreatitis) cannot be resolved by the organ, repopulation of the acinar compartment through ductal to acinar trans-differentiation of ADM structures is blocked. In this situation, more pathogenic long-term adaptations such as precancerous PanIN lesions and fibrotic degeneration of destroyed pancreatic parenchyma can occur. Similarly, it was shown that acinar regeneration after ADM induction by acute pancreatitis is abrogated through oncogenic *Kras*

activity (Morris *et al.*, 2010). Guerra *et al.* found that activation of oncogenic *Kras* alone does not lead to neoplastic PanIN lesions and subsequent pancreatic cancer in adult mice unless the mice were challenged with chronic (not acute) pancreatitis (Guerra *et al.*, 2007). This shows that oncogenic *Kras* mutations alone are not sufficient to induce pancreatic tumorigenesis in adult mice, but requires an additional persistent pancreatitis to initiate malignant transformation.

Because none of the studies to date excludes the participation of either ductal or acinar cells in exocrine pancreatic cancer development, it is likely that both compartments can induce tumour formation. Additionally, it is also conceivable that the likelihood of the acinar or ductal population giving rise to an exocrine-originating cancer can be altered through certain intrinsic (e.g. genetic) or extrinsic (e.g. cytokines) factors. Recent work also suggested that PanIN lesions can co-occur with other precursor lesions (Ferreira *et al.*, 2017). This seminal work by Ferreira et al. showed that identical oncogenes trigger PDAC formation from both, the acinar and ductal compartment with similar patho-histology but different marker gene expression (Ferreira *et al.*, 2017). While PDACs of the acinar compartment are preceded by ADM and PanIN precursor stages, duct-derived cancers developed independently of PanIN lesions. Notably, in both acinar and ductal-originating PDACs, "bystander PanIN-like" lesions can be found in surrounding healthy tissues, distinguishing them from true PanIN precursor lesions.

In the near future, the comparison of the normal acinar and ductal exocrine pancreas to pancreatic cancer methylation profiles will shed light on the controversial cell-of-origin debate as distinct epigenetic patterns are conserved over the process of transformation in humans (Jakel *et al.*, 2017). However, a higher number of epigenetic profiles of pancreatic cancer patients is required to allow detailed conclusions. Furthermore, as it was recently demonstrated for central nervous system tumours, methylome data will support histopathological diagnoses with methylation-based classification of the exact cellular origin of individual cancers. In general, the knowledge of the cell of origin will optimize the management of cancer therapy for the patient (Capper *et al.*, 2018).

6.4. Biology of oncogenic *Ras*

The RAS family of proteins build up an essential node within various important signalling pathways. Their main function is to transduce signals from a variety of different membrane receptors to immediate downstream kinases and to the nucleus. In the nucleus, the activation of transcription factors orchestrates distinct cellular responses to each external signal. In general, oncogenic RAS mutations lead to permanent (over-)activation of distinct Ras-related signalling axes. Thereby, these mutations can induce crucial biological processes for cancer development

by promoting proliferation, suppressing cell death, re-wiring metabolism, changing motility and cell adhesion and shaping the tumour microenvironment (Review in Pylayeva-Gupta *et al.*, 2011).

In humans, three *RAS* genes code for three RAS proteins: HRAS, NRAS and KRAS, the latter being spliced in two alternative variants: KRAS4A and KRAS4B. All proteins are ~21kDa small GTPase and share a high degree of amino acid sequence and structural homology. RAS proteins are critical regulators of various signal transduction pathways. For activation, RAS family members are usually tethered to the plasma membrane at micro-domains, where they can form functional multiprotein signalling complexes (Reviewed in (Plowman *et al.*, 2005)). HRAS and NRAS are attached to the cell membrane due to prenylation and palmitoylation. In case of KRAS, the combination of prenylation and a polybasic sequence next to the prenylation modification enables plasma membrane tethering. For protein homeostasis and modulation of the signalling output, RAS proteins can retract from the membrane and compartmentalize to the endoplasmic reticulum or Golgi complex. RAS proteins can allosterically switch between an inactive "OFF" guanosine diphosphate (GDP)- and an active "ON" guanosine triphosphate (GTP)- bound state (Bourne *et al.*, 1990; Field *et al.*, 1987; Wittinghofer *et al.*, 1991). Under normal conditions, RAS proteins remain in their GDP-bound inactive states ($t_{1/2}$=6min, k_{off}= $2x10^{-3}s^{-1}$ at 20°C), unless distinct factors promote GDP-to-GTP exchange (Hunter *et al.*, 2015). Guanine exchange factors (GEFs, e.g. BRAG2) provoke activation of RAS proteins by stimulating GDP to GTP exchange leading to an active conformational state (Wolfman *et al.*, 1990). The hydrolysis of GTP back to GDP is significantly accelerated by GTPase-activating proteins (GAPs, e.g. NF1) leading to inactivation of Ras signalling (Trahey *et al.*, 1987).

Somatic mutations of the proto-oncogene *Kras* occur frequently in leukaemia, pancreatic, colorectal and lung cancer, whereby other Ras family members are involved in tumorigenesis of other entities (Review in (Pylayeva-Gupta *et al.*, 2011)). Oncogenic mutations mostly affect RAS activity by impairing GTP hydrolysis and thus, cause an unphysiological pro-longed GTP-bound state of RAS causing its hyperactivation. In *Kras*, oncogenic point mutation of glutamine residue 61 (Q61) strongly counteracts the nucleophilic attack on the gamma-phosphate and thereby, impairs GTP hydrolysis (Scheidig *et al.*, 1999; Buhrman *et al.*, 2010). However, most common point mutations in *KRAS* occur in codon 12 and 13 of exon 2. Both code for the glycine residues (G12 and G13) that are mostly mutated to an aspartic acid or valine substitution. G12/G13 oncogenic substitutions prohibit the formation of van der Waals bonds between RAS and the associated GAP. G12/G13 residues facilitate the steric re-orientation of catalytic Q61

residue for the initiation of the γ-phosphate nucleophilic attack of the bound GTP leading to the inactivation of active Ras (Scheffzek *et al.*, 1997).

Downstream of active Ras signalling, activation of a variety of important transcription factors such as FOS, JUN, ETS domain-containing transcription factor ELK1, nuclear factor-κB (NF-κB) and activating transcription factor 2 (ATF2) (Stacey *et al.*, 1987; Gutman *et al.*, 1991; Urich *et al.*, 1997; Westwick *et al.*, 1994; Finco *et al.*, 1997) is induced. Eventually, prolonged expression of these TFs culminates in the expression of cell cycle-related G_1 cyclin, cyclin D1, that bundles *Ras*-induced growth signals and introduces a non-dividing G_0 cell to an active cycling G_1 cell (Filmus *et al.*, 1994; Winston *et al.*, 1996). Although oncogenic Ras mutation leads to cyclin D1-mediated mitotic progression, the cell has evolved several scavenging mechanisms counteracting oncogenic insults on different regulatory levels. Roughly, these tumour-suppressing mechanisms (e.g. inducing cell death) are in direct opposition to the "interest" of the developing neoplastic lesion summarized in the hallmarks of cancer (Hanahan *et al.*, 2011).

6.5. *Kras* effector pathways

Ras mutations play causal roles in the development of cancer. This is due to its central upstream position in a plethora of important signalling pathways, that regulate essential functions in development, homeostasis and disease. In mammalian cells, KRAS protein can activate rapidly accelerated fibrosarcoma (RAF)/mitogen-activated protein kinase kinase (MEK)/extracellular-signal related kinase (ERK)-, phosphoinositide 3-kinase (PI3K)/AKT/mTOR-, Ras-like (RalGEF)- and the Rho-family GTPase Rac-signalling. However, Raf/Mek/Erk and PI3K/Akt signalling have the highest relevance for the disease and, thus have been studied most extensively.

As first Ras effector, the RAF/MEK/ERK, or also known as RAF/mitogen-activated protein kinase (MAPK) pathway was described in the early 1990s (Moodie *et al.*, 1993; Warne *et al.*, 1993; Zhang *et al.*, 1993). RAF kinases belong to the serine/threonine-specific protein kinases and can be recruited to the inner layer of the plasma membrane to bind GTP-bound RAS, and thereby initiate the protein kinase cascade for signal transduction (Marais *et al.*, 1995). There exist three mammalian RAF proteins A-, B- and C-RAF that can exert oncogenic functions in several tumour entities themselves, most notably BRAF in melanoma patients (Review in (Maurer *et al.*, 2011)). After binding of RAF to GTP-loaded RAS, the intrinsic inhibition of the cysteine-rich domain on RAF's kinase domain is relieved. Now homo- or hetero-dimerized RAF can phosphorylate and activate MEK which in turn activates ERK by its kinase activity. Sustained phospho-ERK can exert its pro-proliferative function by phosphorylating its

downstream targets, mostly transcription factors that express genes required for the cell's entry into mitosis (e.g. Cyclin D complex) and by suppressing negative regulators of the cell cycle (Chambard *et al.*, 2007). However, phospho-ERK also possesses an immanent negative feedback loop as it has the capacity to phosphorylate RAF residues and thereby terminate its dimerization (Dougherty *et al.*, 2005).

Additionally to the activation of RAF/MEK/ERK signalling through oncogenic *Kras*, development of PanIN lesions and progression to pancreatic cancer requires additional tumorigenic stimulation of phospho-ERK from the epithelial growth factor receptor (EGFR) (Navas *et al.*, 2012; Ardito *et al.*, 2012). Deletion of C-RAF fails to block $Kras^{G12D/+}$-induced tumorigenesis rendering it dispensable for pancreatic cancer, while it is essential for the development of non-small cell lung cancer (Eser *et al.*, 2013; Blasco *et al.*, 2011). These results outline the conceptual framework of tissue- as well as isoform-specificity that characterize oncogenic RAF/MEK/ERK signalling in *Ras*-driven cancers.

The PI3K/AKT/mTOR signalling pathway can control cellular proliferation, quiescence, metabolism and longevity (all being important hallmarks of cancer) and thus, is frequently dysregulated in neoplastic lesions (Janku *et al.*, 2018). Being important in cancer, Class I PI3K signalling complex enzymes consist of heterodimeric lipid kinases that contain a regulatory and one out of three catalytic subunits, namely p110α, p110β and p110γ. Encoding for p110α, *PIK3CA* is commonly mutated in human cancers causing augmented enzyme activity even in the absence of receptor binding (Engelman, 2009). Upstream PI3K signalling complexes can be recruited to the plasma membrane via three different ways: (i) interaction with receptor tyrosine kinases (RTKs), (ii) direct binding with small GTPases such as Ras and Rac1 or (iii) after G protein-coupled receptor (GPCR) activation to dimeric Gßγ (Baer *et al.*, 2014; Guillermet-Guibert *et al.*, 2008). Upon activation, phosphatidylinositol 4,5-biphosphate (PIP_2) is converted to phosphatidylinositol 3,4,5-triphosphate (PIP_3) by PI3K's catalytic subunit leading to the recruitment of several effectors at the inner leaflet of the plasma membrane. Among other factors, PIP_3 recognises pleckstrin homology (PH) domain containing proteins and thereby, recruits 3-phosphoinositide-dependent protein kinase 1 (PDK1) and one out of three isoforms of the serine/threonine kinase AKT (AKT1, AKT2 and AKT3) (Review in (Cantley, 2002)). Being in close vicinity, PDK1 now phosphorylates AKT at threonine residue T308 which activates several downstream (oncogenic) effectors directly (e.g. cAMP response element-binding protein (CREB)) or indirectly (e.g. mammalian target of rapamycin (mTOR)) (Alessi *et al.*, 1997).

As mentioned above, PI3K/AKT signalling is frequently deregulated in neoplastic lesions (Engelman, 2009). In PIK3CA, hotspot mutations cluster around the catalytic domain and are often aetiological to various cancers (Samuels *et al.*, 2004). Notably, the phosphate and tensin homolog (PTEN) serves as a negative feedback mechanism to excessive phospho-AKT by antagonizing PIP$_2$ to PIP$_3$ conversion otherwise leading to uncontrolled PI3K/AKT signalling. PTEN is established as a major tumour suppressor gene in several cancer entities with high incidence rates for example in prostate cancer (Cairns *et al.*, 1997). In pancreatic cancer, PTEN is often found to be target of mutation or reduced protein levels (e.g. due to haploinsufficiency; 4/17 human PDAC samples showed absence of PTEN expression) (Asano *et al.*, 2004; Cancer Genome Atlas Research Network. Electronic address *et al.*, 2017). The importance of PTEN in *Kras*^{G12D}-driven pancreatic cancer is reflected by the demonstration that mice lacking PTEN show reduced time to cancer formation accompanied by pro-tumorigenic infiltration of immune cells, stromal reaction and frequent liver metastasis (Hill *et al.*, 2010; Ying *et al.*, 2011). Further evidence for the essentiality of PI3K/AKT signalling for pancreatic cancer development comes from the finding that oncogenic *Pik3ca*^{H1047R} signalling in mouse pancreas leads to a similar cancer progression as seen in the engineered *Kras*^{G12D} situation (Eser *et al.*, 2013). In contrast in adult animals, inducible endogenous activation of oncogenic *Pik3ca*^{H1047R} failed, while *Kras*^{G12D} *Braf*^{V600E} was able to trigger PanIN lesions. This highlights the necessity of increased RAF/MEK/ERK signalling in adult exocrine cells for precursor lesion initiation (Collisson *et al.*, 2012). Strengthening the co-dependence of both pathways in pancreatic cancer initiation and progression, *Kras*^{G12D} mice featuring concomitant *Pdk1* deletion do not show signs of carcinogenesis nor precursor lesions in adolescence, but instead, comprise fatty degeneration of the pancreas in aged animals (Eser *et al.*, 2013). It is becoming increasingly clear that during tissue homeostasis RAF/MEK/ERK and PI3K/AKT/mTOR signalling intersect and co-regulate each other to fulfil vital downstream functions of the pancreatic cells and the organ itself. In contrast, during the development of malignancies individual signalling pathways can be altered and hyperactivated by mutagenic insults (review in (Mendoza *et al.*, 2011)).

6.6. Molecular subtypes of pancreatic cancer

In humans, pancreatic cancer and its metastases feature a complex genomic heterogeneity beyond a limited number of frequently mutated cancer "drivers" such as *KRAS*, *TP53*, *CDKN2A* and *SMAD4* (Jones *et al.*, 2008; Campbell *et al.*, 2010; Biankin *et al.*, 2012; Waddell *et al.*, 2015; Witkiewicz *et al.*, 2015; Bailey *et al.*, 2016a; Cancer Genome Atlas Research Network. Electronic address *et al.*, 2017). However, in recent years, vast transcriptome analyses of human pancreatic cancers established a platform for the interpretation of genotypes and phenotypes

that allowed a deeper understanding of the underlying tumour biology. In 2011, global gene expression analyses of a large number of human pancreatic cancer patients lead Collisson et al. to the designation of three subtypes, namely classical, quasimesenchymal (QM) and exocrine-like (Collisson *et al.*, 2012). These molecular subtypes could be stratified to different tumour progression rates and treatment responses in patients. Lately, individually aberrantly regulated signalling pathways (as indicated by the differential expression of genes within a gene set describing the pathway) could be associated to molecular subclusters (Bailey *et al.*, 2016a). In example, integrated data analyses revealed the enrichment of squamous/QM type carcinoma for TP53 and KDM6A mutations and hypermethylation of pancreatic endodermal cell-fate determining genes (Bailey *et al.*, 2016a). Likewise, other pancreatic cancer subtypes featured regulatory alterations in other functionally relevant cancer pathway genes impacting the observed phenotype. Larger cohorts and *multi-OMICS* data integration will help researchers to precisely pinpoint cancer subtype-specific oncogenic networks and to novel insights into the pathophysiology of pancreatic cancer. In the future all these findings need to be experimentally validated in adequate model systems to understand the oncogenic mode of action.

Limitations to these transcriptomic studies are the lack of pancreatic cancer samples as patients qualify as non-resectable at the point of diagnosis and in cancer samples, the high and variable stromal content (Witkiewicz *et al.*, 2015). Additionally, in contrast to the mouse, human pancreatic cancers are difficult to grow *in vitro*. Here, the systematic characterisation (genotypes, pathohistology, metastatic status, isolation of primary cultures etc.) of tumours derived from different genetic mouse models of PDAC allowed our group to establish biological characteristics and *in vitro/in vivo* phenotypes. Genomic and transcriptomic analyses of these cancers in a petri dish (no contamination with non-tumour material) in combination with the clinical manifestation, we could generate associations between genetic mutation types and disease phenotypes and furthermore, delineate distinct evolutionary principles for tumorigenesis (Mueller *et al.*, 2018). Notably, using this approach we could uncover the association of the metastatic phenotype to distinct molecular clusters. The cross-validation with human transcriptomic data sets highlighted genomic species differences but also showed conserved oncogenic networks between mouse and human molecular subclusters. Collisson classifier gene sets revealed the presence of "classical-equivalent", "QM-equivalent" and the formerly unknown "mesenchymal-equivalent" subtypes in mouse pancreatic cancer transcriptomes (Collisson *et al.*, 2012; Mueller *et al.*, 2018). The latter subtype is described by the strong upregulation of epithelial-to-mesenchymal (EMT) gene sets and a substantial increase of mutant *Kras* dosage compared to the "QM-equivalent". In accordance, the

pathohistology of these cancers show predominantly undifferentiated characteristics and primary cultures only mesenchymal growth patterns (Mueller *et al.*, 2018).

In summary, the availability of OMIC tools and robust models of pancreatic cancer will facilitate the study of pancreatic cancer, as the reliable molecular classifications of tumours will uncover principal oncogenic networks across different layers of cancer cell gene regulation. In genetically engineered mouse models, one would be able to interrogate conserved subtype-specific oncogenic networks, which could potentially point to specific therapeutic vulnerabilities. Pancreatic cancer patients will profit from the combined molecular and histologic subtype classification as physicians could better predict the clinical manifestation and decide on a molecularly tailored therapy (Collisson *et al.*, 2012; Moffitt *et al.*, 2015; Bailey *et al.*, 2016a).

6.7. Mouse models of pancreatic cancer

Hotspot mutations affecting *KRAS* proto-oncogene are found in over 90% all patients with PanIN lesions and pancreatic cancer (Witkiewicz *et al.*, 2015). In IPMN lesions, mutations in *GNAS* are often found alone or in combination with oncogenic *KRAS* (Wu *et al.*, 2011; Patra *et al.*, 2018). Genetically engineered mouse models (GEMMs) have been used in cancer research to study human tumorigenesis by introducing the same driver mutations into the mouse genome. In the early 2000's, Jackson et al. developed a mouse cancer model through the knock-in of the $Kras^{G12D}$ mutation silenced by a *loxP*-stop-*loxP* (LSL) cassette into the endogenous *Kras* locus (Jackson *et al.*, 2001). The $Kras^{G12D}$-allele can be conditionally activated by Cre-recombinase expression and subsequent *LSL* element excision that enables expression of the downstream oncogene. Here, the pancreatic and duodenal homeobox 1 (*Pdx1*) (Gannon *et al.*, 2000) and the pancreas specific transcription factor 1a (*Ptf1a*) genes (Nakhai *et al.*, 2007) are widely used developmental transcription factors in the mouse pancreas to achieve pancreas-specific conditional expression of the *Cre* recombinase. The *Pdx1* homeobox gene becomes expressed earlier at mouse embryonic day E8.5, while the *Ptf1a* starts at E9.5, both supporting the *LSL* excision in the exocrine pancreatic compartment (Offield *et al.*, 1996; Kawaguchi *et al.*, 2002). A limitation to *Pdx1* as tissue-specific Cre recombinase promoter is the "off-target" expression in the rostral duodenum, bile duct and antral stomach owing to its activity during foregut development. Because *Ptf1a* is only expressed in exocrine pancreatic cells it is more specific than *Pdx1*, however *Ptf1a* gene product can also be detected in the retina and the brain (Nakhai *et al.*, 2007).

The inter-crossing of *Pdx1-Cre* or $Ptf1a^{Cre/+}$ with $Kras^{LSL-G12D/+}$ mice (PK) triggers formation of PanIN lesions which later progress to invasive PDAC that can metastasize to distant organs

(Hingorani *et al.*, 2003). PK mice show progressive PanIN development as reflected by the increase of PanIN cells as well as their grading over the mouse's lifespan. At the age of 9 months, PK mice generally present more neoplastic ductal-like structures than normal ducts together with singularized invasive PanIN-3 (Hingorani *et al.*, 2003). Because important tumour suppressor genes including *TP53*, *CDKN2A*, *SMAD4* are frequently inactivated in humans, these mutations have been engineered in the PK pancreatic mouse cancer models in the past. Not surprisingly, the R172H substitution mutation of *Trp53* (mouse ortholog of human R175H) in PK mice lead to a dramatic acceleration of invasive cancer formation and metastasis (Hingorani *et al.*, 2005). These primary tumours and metastasis exhibited a high degree of genomic instability as seen in human PDAC. However, mutations in other important cancer genes could not be detected highlighting a strong oncogenic cooperation between *Kras* and *Trp53*. The homozygous deletion of the *Cdkn2a* locus in addition to $Kras^{G12D}$ also shows strong convergent effects on neoplastic development and distant dissemination as these mice carried full-blown disease already with 11 weeks of age (Aguirre *et al.*, 2003). A comparative study of $p16^{Ink4a}/p19^{Arf}$ and *Trp53* inactivation alleles in PK mice noted the propensity of heterozygous mice to lose the other copy during tumour progression and indicated histopathological differences between both genotypes (Bardeesy *et al.*, 2006). Most recently, our group found patterns of copy number alterations in relevant cancer genes of primary cultures isolated from PK mice conferring oncogenic gene dosages for the tumour growth (Mueller *et al.*, 2018). Through the systematic genomic characterization of these GEMMs, we could reconcile evolutionary routes as only the complete loss of *Cdkn2a* and *Trp53* is permissive for the amplification of $Kras^{G12D}$ driving more aggressive cancer phenotypes. In contrast, heterozygous or wild-type copy number states of *Cdkn2a* and *Trp53* cooperate with heterozygous $Kras^{G12D}$ and tolerate genetic gains of alternative drivers of pancreatic cancer such as *Myc*, *Yap1* or *Nfkb2*. Transcriptional profiles of PK cancers also largely overlap with classifier genes proposed for human pancreatic cancer subtypes (Mueller *et al.*, 2018). Overall, these data pinpoint to conserved evolutionary contingencies of *Kras*-driven oncogenesis.

Recently, advanced recombination-based systems have been engineered in mice for the study of pancreatic cancer (Schonhuber *et al.*, 2014). The combination of the Cre/Flippase (Flp) technology allows for the inducible dual-recombination to target cancer-associated genes in subpopulations of the tumour or the study of effects arising from simultaneously targeted genes in specific cell types of the microenvironment that modulate the crosstalk between the tumour and its originating organ. As carcinogenesis is a genetic multistep process, this mouse model can reconcile evolutionary routes over time or point towards genetic vulnerabilities of

molecular cancer subtypes. As a proof of concept, by targeting different immune cell populations, the selective depletion of mast cells from the pancreatic cancer's microenvironment showed the dispensability of this cell type for tumour formation process (Schonhuber *et al.*, 2014). Hence, pancreas-specific modelling of tumorigenic events in the mouse recapitulates molecular and histologic phenotypes as found in humans and allows the in-depth and unbiased study of cancer development (pre-malignant PanIN lesions) and progression (invasive, metastatic pancreatic cancer).

6.8. CRISPR/Cas9-based gene editing

Bacteria and archaea have evolved adaptive immune strategies to defend their organismal homeostasis against contagious DNA pathogens (e.g. bacteriophages) by destroying the genomic cargo of the invading virus. Within the bacterial genome, the type II clustered regularly interspaced short palindromic repeats (CRISPR) system consists of *foreign* DNA sequences arranged in a repetitive order that is interspersed with palindromic CRISPR DNA stretches (Wiedenheft *et al.*, 2012; Fineran *et al.*, 2012; Horvath *et al.*, 2010; Barrangou *et al.*, 2007). These genetic clusters are transcribed as single CRISPR RNAs (crRNAs) containing the "protospacer" cassette complementary for the DNA sequences of the exogenous DNA pathogen. The crRNA can hybridize with another trans-activating CRISPR RNA (tracrRNA) which is processed from the palindromic stretches of the CRISPR locus (Deltcheva *et al.*, 2011). Both RNA transcripts form a base-paired crRNA:tracrRNA structure that initiates the coupling of the RNA structure to the CRISPR-associated protein 9 (Cas9) protein (Jinek *et al.*, 2012). Now, the functional endonuclease complex can introduce a double strand break, if the protospacer portion of the crRNA recognizes complementary DNA and if an adjacent protospacer associated motif (PAM) resides in the bound DNA. Moreover, fragmented exogenous DNA can also be incorporated into the bacterial CRISPR locus serving as an acquired immunity in case of renewed infection with the same DNA pathogen.

In the simplest variant, the *Streptococcus pyogenes* (*S. pyogenes*) programmable crRNA (recognizing DNA) and fixed tracrRNA (guiding Cas9) were fused to function in mammalian cells as single RNA chimera (known as sgRNA or gRNA) to direct the Cas9 nuclease for the introduction of double strand breaks (DSBs) in the genome (Jinek *et al.*, 2012; Cong *et al.*, 2013). The 5' crRNA portion of the sgRNA consists of 20 nucleotides that can hybridize with target sequences by RNA-DNA base pairing rules. The 3' sgRNA portion of the tracrRNA attracts the Cas9 to the site of binding. For its endonuclease function, the *S. pyogenes* Cas9 requires a PAM consisting of the NGG trinucleotide 3' of the crRNA. Summarizing,

CRISPR/Cas9-mediated genome editing can be achieved at every position in the locus of interest that harbours a N_{20}-NGG motif.

Before the CRISPR/Cas9 era, zinc finger nucleases (ZNFs), transcricption activator-like effector nucleases (TALENs) and meganucleases were used as genome editing tool in different organisms. However, these methods suffer from individual disadvantages. Meganucleases are difficult to engineer since target-specific because DNA binding and nuclease function occur in the same domain (Wolfe *et al.*, 2000). ZNF construction is hampered by context-dependent interactions of individual finger domains recognizing the target region (Urnov *et al.*, 2010). TALENs are more robust in terms of sequence-specific genome editing, however assembling large repetitive TALEN repeats in a vector can be laborious and difficult in viral vectors (Joung *et al.*, 2013). CRISPR/Cas9 outperforms previous methods in terms of simplicity for target vector construction, robustness of the delivery and genome editing efficiency. After the proof of concept in 2012 in bacteria (Jinek *et al.*, 2012), a series of studies could show genome editing in human cell lines, stem cells (Mali *et al.*, 2013; Cong *et al.*, 2013; Jinek *et al.*, 2013) and in zebra fish (Hwang *et al.*, 2013). Following to this initial series of studies, other higher-level organisms were genetically engineered by CRISPR/Cas9-based mutagenesis such as mice (Wang *et al.*, 2013; Shen *et al.*, 2013), rats (Li *et al.*, 2013) and drosophila (Yu *et al.*, 2013; Bassett *et al.*, 2013). The simplicity and efficiency of the CRISPR/Cas9 tool enabled researchers to perform genome-wide positive and negative forward genetic screening approaches to identify critical genes that are responsible for a particular phenotype (Wang *et al.*, 2014).

CRISPR/Cas9 introduces a cut between the third and fourth nucleotide 5' of the NGG motif. The re-ligation of the Cas9-induced DSB involves one of at least two possible cell-autonomous repair mechanisms. The more frequent pathway functions via non-homologous end joining (NHEJ) and promotes error-prone DNA repair by introducing insertion/deletion (Indel) mutations of variable lengths leading to the disruption of the translational reading frames of targeted genes. On the other hand, homology directed repair (HDR) causes the precise reconstruction of the DNA sequence, whereby the donor template can be the sister chromatid or exogenous DNA (e.g. generation of point mutations). Furthermore, mutations within Cas9 can modify the nuclease function. For example, D10A or H840A substitutions in the nuclease domain generate nickase variants of the original Cas9 enzyme that only cut a single DNA strand, respectively (Jinek *et al.*, 2012; Gasiunas *et al.*, 2012). Recently, sgRNA-Cas9 interaction was used as a platform for different approaches to repress or activate transcription of genes known as CRISPR interference (CRISPRi) or CRISPR activation (CRISPRa),

respectively. Already the sgRNA-directed interference of an inactivated "dead Cas9" (dCas9) variant in the intragenic region caused the disruption of the transcriptional elongation of the gene message (Qi *et al.*, 2013). More advanced fusions of dCas9 to transcriptional enhancers or to silencer elements lead to an activation or repression of gene expression, respectively (Gilbert *et al.*, 2013). The development of dCas9 fusions to enzymes controlling the epigenome of a cell also made the targeted study of epigenetic regulation of specific genes feasible (Kearns *et al.*, 2015; Hilton *et al.*, 2015; Kennedy *et al.*, 1995). Hence, CRISPR/Cas9-based mutagenesis as well as CRISPR-based modification of epigenetic as well as transcriptional regulation have already and will further deepen our understanding of the cell's signalling machinery.

6.9. *In vivo* CRISPR/Cas9 gene editing in mice

For *in vivo* delivery of sgRNA/Cas9 functional units into adult mice, two general methodologies can be deployed. Firstly, using the ability of viruses to infect cells and release their DNA/RNA message, CRISPR/Cas9 can be cloned into viral vectors to edit any locus of interest and study the effects of targeted gene(s) in the organism. Already in 2014, *Rivera* et al. designed a lentiviral construct comprising the programmable sgRNA cassette and *Cre* recombinase tethered to the Cas9 enzyme by a P2A element. CRISPR-containing lentivirus was delivered intratracheally to the lungs of $Kras^{LSL-G12D}$ mice to induce oncogenic *Kras* and concomitantly inactivate putative tumour suppressor genes (TSGs) (Sanchez-Rivera *et al.*, 2014). Similar lentiviral CRISPR/Cas9 constructs were also used to infect mouse pancreatic cells with functional CRISPR/Cas9 units. To increase the tissue specificity of lentiviral infection and thus, genome editing of ductal cells (otherwise also infecting the stromal compartment) in $H11^{LSL-Cas9}$ mice, *Chiou* et al. performed retrograde pancreatic ductal injection (Chiou *et al.*, 2015). Here, a sgRNA targeting the *Lkb1* locus and phosphoglycerate kinase (PGK) promoter-driven *Cre* recombinase were packed in a lentiviral backbone. This lentivirus was next delivered into $H11^{LSL-Cas9/+}$; $Kras^{LSL-G12D/+}$; $Trp53^{flox/flox}$ mice to induce somatic gene editing and ultimately pancreatic tumourigenesis in all mice (3/3). Similarly, direct injection of lentiviral particles into the pancreatic parenchyma of adult $Kras^{LSL-G12D/+}$; $Trp53^{flox/flox}$ mice induced Cas9-mediated target gene editing and tumour onset in the pancreas (Sanchez-Rivera *et al.*, 2014). Other viral delivery systems include retrovirus, adenovirus, baculovirus and most notable, adeno-associated virus (AAV) (Senis *et al.*, 2014). AAVs for CRISPR/Cas9 genome editing feature several advantages over other viral delivery strategies, for example: (i) different AAV capsids have distinct tissue/cell specificities, (ii) AAVs comprise a high targeting efficiency and (iii) they tend to rarely integrate into the host genome and thus, reducing the probability of off-target

cutting. A disadvantage of AAV-based approaches would be the comparatively low cargo size of the viral genome, that can partially be circumvented by using Cas9 knock-in mice. Because of these advantages, the delivery of CRISPR/Cas9 by AAV enabled for direct *in vivo* screening for functional tumour suppressors (Chow *et al.*, 2017) but also allows for novel and efficient gene therapeutic approaches (Yang *et al.*, 2016; Chew *et al.*, 2016; Kotterman *et al.*, 2014).

Secondly, CRISPR/Cas9 tool kit can also be directly delivered into specific tissues. In general, one can transfect the nucleic acids coding for CRISPR/Cas9 or introduce functional mRNA/protein complexes into the cell. In the latter case, CRISPR/Cas9 is thereby coupled to liposomes or nanoparticles allowing the uptake of the cell by endocytosis (Glass *et al.*, 2018).

In the following paragraph, I will focus on available strategies involving *in vivo* delivery of plasmid DNA. The tissue of interest critically defines which methodology for the CRISPR/Cas9 delivery should be chosen for optimal gene editing of the target site. For example, as blood vessels converge from the mouse tail to the liver, hydrodynamic tail vein injection (HTVI) is a comparatively easy, fast and non-invasive method to transfect liver cells with CRISPR/Cas9 plasmid DNA for somatic gene editing (Xue *et al.*, 2014). Our group performed pioneering work as we used the advantages of HTVI for *in vivo* CRISPR/Cas9 genome editing. These include the high range of targeted cells and the potential to deliver multiple vectors to individual cells to allow for simultaneous (multiplexed) mutagenesis of large gene sets. This work facilitated functional genomic analyses of hepatobiliary cancers in mice (Weber *et al.*, 2015).

Electroporation can be used to target different organs of mice for pDNA delivery with variable delivery efficiencies (Kobayashi *et al.*, 2017; Renaud *et al.*, 2008; Barnabe-Heider *et al.*, 2008; Seehawer *et al.*, 2018; Aihara *et al.*, 1998; Michaelis *et al.*, 2014). Using *in utero* electroporation of mouse cerebella in combination with CRISPR/Cas9, Zuckermann et al. could generate medulloblastomas by targeting the *Ptch1* locus in *Trp53*^{-/-} or *Trp53*^{+/-} mice. Furthermore, the disruption of the combined gene functions of *Trp53*, *Nf1* and *Pten* lead to the onset of glioblastomas in adult wild-type mice (Zuckermann *et al.*, 2015).

6.10. Aim of the study

Traditional genetically engineered mouse models suffer from certain limitations, such as the long time frames required for the generation of complex genotypes or expensive mouse line maintenance. Furthermore, lineage tracing of individual cancer clones or *in vivo* mutagenesis screening are difficult to achieve by directly manipulating the genome of mice.

In this study, I aimed for the adaptation of the CRISPR/Cas9-based gene editing tool to mutate multiple relevant cancer genes directly in the adult mouse pancreas to induce cancer development. We hypothesised that this cancer model would enable for the fast *in vivo*

combinatorial gene editing, evolutionary study of edited cancer clones, synthetic lethality screenings and chromosome engineering. This approach can build the framework for the study of gene functions, gene interaction networks and chromosomal rearrangements in pancreatic cancer. We also aimed to address limitations of high-level sgRNAs multiplexing, that will provide a guidance for appropriate use of the method.

7. Materials

7.1. Technical equipment

Table 1. Technical equipment.

Equipment	Source
Agilent Bioanalyzer 2100	Agilent Technologies
Analytical balance A 120 S	Sartorius AG
Autoclave 2540 EL	Tuttnauer Europe B.V.
AxioCam HRc	Carl Zeiss AG
AxioCam MRc	Carl Zeiss AG
Class II Biological Safety Cabinet	Thermo Fisher Scientific
Centrifuge 5424	Eppendorf
Centrifuge 5810 R	Eppendorf
CUY650P3	Nepa Gene Co., Ltd.
DynaMag™-96 Side Skirted Magnet	Thermo Fisher Scientific
Electrophoresis power supply Power Pac 200	Bio-Rad Laboratories GmbH
Gel Doc™ XR+ system	Bio-Rad Laboratories GmbH
Glass ware, Schott Duran®	Schott AG
Heated paraffin embedding module EG1150 H	Leica Microsystems GmbH
Homogenisator Precellys® 24	Bertin Instruments
Horizontal gel electrophoresis system	Biozym Scientific GmbH
Incubator NCU-Line® IL 23	VWR International
Magnetic stirrer D-6010	neoLab
MiSeq System	Illumina
Microscope Axio Imager.A1	Carl Zeiss AG
Microtome Microm HM355S	Siemens AG
Microwave	Thermo Fisher Scientific Inc.
Mini-PROTEAN® Tetra Cell	Bio-Rad Laboratories GmbH
NEPA21 Super Electroporator	Nepa Gene Co., Ltd.
Neubauer hemocytometer, improved	LO-Laboroptik GmbH
NextSeq 550 System	Illumina
Odyssey® infrared imaging system	Li-Cor Biosciences
Paraffin tissue floating bath Microm SB80	Thermo Fisher Scientific Inc.
pH meter 521	WTW GmbH
Pipettes Reference®, Research®	Eppendorf AG
Primovert Microscope	Carl Zeiss
Qubit® 2.0 Fluorometer	Thermo Fisher Scientific
ROCKER 2D digital	IKA-Werke
StepOne Plus Real-Time PCR System	Applied Biosystems
Surgical instruments	Thermo Fisher Scientific Inc.
Thermocycler Tpersonal 48	Biometra
Thermocycler TProfessional Basic 96	Biometra
Thermocycler TProfessional Basic Gradient 96	Biometra
ThermoMixer® comfort 5355	Eppendorf
Tissue processor ASP300	Leica Microsystems GmbH
Ultra Low-Temperature Freezer Innova® U725	Eppendorf
UVsolo 2 Gel Documentation System	Analytik Jena
Vortex-Genie 2	Scientific Industries
Weighing Scale A120S	Sartorius
Western blot system SE 260 Mighty Small II	Hoefer Inc.

7.2. Reagents and enzymes

Table 2. Reagents and enzymes.

Reagent/Enzyme	Source
1kb DNA Ladder	New England Biolabs
1,4-Dithiothreitol (DTT)	Carl Roth GmbH
2-Mercaptoethanol, 98%	Sigma-Aldrich Chemie GmbH
2-Propanol (isopropanol)	Carl Roth GmbH
100bp DNA Ladder	New England Biolabs
Acetic acid	Sigma-Aldrich
Agarose	Sigma-Aldrich
Ampicillin	Sigma-Aldrich
Ammonium persulfate	Sigma-Aldrich
BbsI (10,000 units/mL)	New England Biolabs
Bovine serum albumin, fraction V	Sigma-Aldrich
Bromphenol blue	Sigma-Aldrich
Calcium chloride	Carl Roth
EDTA-free, protease inhibitor cocktail tablets	Roche Deutschland Holding GmbH
ExonucleaseI	New England Biolabs
Deoxynucleotide Mix, 10 mM each	Sigma-Aldrich
Dimethyl sulfoxide (DMSO)	Carl Roth
DirectPCR Lysis Reagent (Cell)	Viagen Biotech
dNTP mix, 10mM each	Fermentas GmbH
Dodecylsulfate Na-salt in pellets (SDS)	Serva Electrophoresis GmbH
Eosine	Waldeck
Ethanol absolute	Carl Roth
Ethidium bromide	Sigma-Aldrich
Ethylenediaminetetraacetic acid *(EDTA)*	Sigma-Aldrich
Forene® isoflurane	Abbott
Formalin	Carl Roth
Gel Loading Dye, Purple (6x)	New England Biolabs
Glycerol	Sigma-Aldrich
Glycin Pufferan®	Carl Roth
Hematoxylin	Merck
HotStarTaq DNA polymerase	Qiagen GmbH
Hydrochloric acid (HCl)	Merck
Isopropanol absolute	Carl Roth
Isotonic sodium chloride solution	Braun Melsungen AG
LB-Agar (Luria/Miller)	Carl Roth
LB-Medium (Luria/Miller)	Carl Roth
Lipofectamine® 2000	Thermo Fisher Scientific
Magnesium chloride (MgCl$_2$)	Carl Roth
Magnesium sulfate (MgSO$_4$)	Carl Roth
Nonidet P40	Roche Deutschland Holding GmbH
NEBuffer 2	New England Biolabs
Pertex mounting medium	Medite
Phosphate buffered saline	Sigma-Aldrich
Polyethylene glycol 4000	Sigma-Aldrich
Potassium chloride (KCl)	Carl Roth
Precision Plus Protein™ all blue standard	Bio-Rad Laboratories GmbH
Proteinase K	Sigma-Aldrich
Q5® High-Fidelity DNA Polymerase	New England Biolabs
REDTaq® ReadyMix™ PCR reaction mix	Sigma-Aldrich
RNAlater	Sigma-Aldrich
RNase-free DNase set	Qiagen GmbH
RNaseA	Fermentas GmbH
Roti®-Histofix 4 %	Carl Roth
Rotiphorese® gel 30	Carl Roth

Reagent/Enzyme	Source
Shrimp Alkaline Phosphatase *(rSAP)* (1,000 units/mL)	New England Biolabs
Sodium chloride (NaCl)	Carl Roth
Sodium hydroxide solution (NaOH)	Merck KGaA
Surveyor® Mutation Detection Kit	Integrated DNA Technologies
SuperScript II	Thermo Fisher Scientific
SYBR® Select Master Mix	Thermo Fisher Scientific
T4 DNA Ligase	New England Biolabs
T4 Polynucleotide Kinase	New England Biolabs
TaKaRa Ex Taq DNA Polymerase	Takara Bio
Taq DNA Polymerase	New England Biolabs
TEMED	Carl Roth
Tris(hydroxymethyl)aminomethane	Sigma-Aldrich
Tris(hydroxymethyl)aminomethane hydrochloride	Sigma-Aldrich
Tween® 20	Carl Roth
Xylene	Carl Roth

7.3. Reagents for cell culture

Table 3. Reagents for cell culture.

Reagent	Source
Collagenase Type II	Worthington Biochemical
DMEM, high-glucose	Sigma-Aldrich
Dimethylsulfoxide (DMSO)	Carl Roth GmbH
DPBS, no calcium, no magnesium	Thermo Fisher Scientific
FCS Superior	Biochrom
L-Glutamine (200 mM)	Thermo Fisher Scientific
MEM Non-Essential Amino Acids Solution (100X)	Thermo Fisher Scientific
MTT reagent	Sigma-Aldrich
Penicillin-Streptomycin (5,000 U/ml)	Thermo Fisher Scientific
RPMI 1640 Medium	Thermo Fisher Scientific
Trypsin-EDTA (0.5%)	Thermo Fisher Scientific

7.4. Kits used in this study

Table 4. Kits used in this study.

Kit	Source
DNeasy Blood & Tissue Kit	Qiagen
MinElute Reaction Cleanup Kit	Qiagen
NucleoBond® Xtra Midi EF	Macherey-Nagel
QIAprep Spin Miniprep Kit	Qiagen
QIAquick Gel Extraction Kit	Qiagen
QIAquick PCR Purification	Qiagen
QIAshredder	Qiagen
Qubit® dsDNA BR Assay Kit	Thermo Fisher Scientific
RNeasy Mini Kit	Qiagen

7.5. Reagents for library preparation and sequencing

Table 5. Reagents for library preparation and sequencing.

Reagent	Source
Agencourt AMPure XP magnetic beads	Genewiz
Agilent High Sensitivity DNA Kit	Agilent Technologies
EB buffer	Qiagen GmbH, Hilden

KAPA DNA Standards and Primers for Illumina	Kapa Biosystems
KAPA HiFi HotStart ReadyMix (2x)	Kapa Biosystems
KAPA SYBR Fast qPCR ABI Mix (2x)	Kapa Biosystems
MiSeq Reagent Kit v2 (300 cycle)	Illumina
MiSeq Reagent Kit v3 (600 cycle)	Illumina
NEBNext DNA Sample Prep Reagent Set 1	New England Biolabs
NEBNext® Ultra DNA Library Prep Kit for Illumina®	New England Biolabs
Nextera XT Kit	Illumina
Sodium hydroxide (NaOH)	Carl Roth

7.6. Disposables

Table 6. Disposables.

Consumable	Source
ABgene Storage Plate, 96-well, 2.2 mL, square well, conical	Thermo Fisher Scientific
Adhesive PCR Plate Foils	Thermo Fisher Scientific
Biopsy/tissue embedding cassettes	Simport
Cell culture dishes (100 mm)	Greiner Bio-One
Cell culture flasks (50 mL, 250 mL, 550 mL)	Greiner Bio-One
Cell culture plates (6-well, 12-well, 24-well, 96-well)	Corning
Cell scrapers	Sarstedt
Cell strainers (70 µm, 100 µm)	Corning
Combitips advanced® (0.2 mL, 0.5 mL, 1 mL, 5 mL, 10 ml)	Eppendorf
Conical tubes (15 mL, 50 mL)	Greiner Bio-One
Cover slips	Gerhard Menzel B.V.
Cryotubes (1.6 mL)	Sarstedt
Disposable blades	Swann-Morton
Disposable reservoirs	Integra Biosciences
Disposable scalpels	B. Braun Melsungen
Disposable spatulas	Carl Roth
DNA LoBind Tubes (1.5 mL)	Eppendorf
Glass slides SuperFrost™ Plus	Thermo Fisher Scientific
Hard-Shell® 96-Well PCR Plates, high profile, semi skirted	Bio-Rad Laboratories
Hard-Shell® Low-Profile Thin-Wall 96-Well Skirted PCR Plate	Bio-Rad Laboratories
MicroAmp® optical 96-well reaction plate	Thermo Fisher Scientific
MicroAmp® Optical Adhesive Film	Thermo Fisher Scientific
Microtome blades S35	Feather Safety Razor
microTUBE AFA Fiber Snap-Cap 6x16mm Case	Covaris
Needles 27 gauge	Seidel medipool
Pasteur pipettes	Brand
PCR stripes (8 tubes)	Sarstedt
Petri dishes (100 mm)	Greiner Bio-One
Pipette tips (10 µL, 200 µL)	Biozym
Pipette tips with filter (10 µL, 100 µL, 200 µL, 300 µL, 1250 µL)	Biozym
Reaction tubes safe-seal (0.5 mL, 1.5 mL, 2 mL)	Sarstedt
Reaction tubes safe-seal (5 mL)	Eppendorf
Serological pipettes (5 mL, 10 mL, 25 mL, 50 mL)	Greiner Bio-One
Syringes (1 mL, 30 mL)	B. Braun Melsungen

7.7. Buffers and solutions for molecular biology

Table 7. Buffers and solutions for molecular biology.

Buffer	Ingredients
5x Protein loading buffer (Laemmli), pH 6.8	10% SDS 50% Glycerol

	228 mM Tris hydrochloride
	0.75 mM Bromphenol blue
	5% 2-Mercaptoethanol

50x Tris acetate EDTA (TAE) buffer, pH 8.5	2 M Tris
50x Tris acetate EDTA (TAE) buffer, pH 8.5	50 mM EDTA
	5.71% Acetic acid

IP buffer, pH 7.9	50 mM HEPES
	150 mM NaCl
	1 mM EDTA
	0.5% Nonidet P40
	10% Glycerol
	Phosphatase inhibitor (add prior to use)
	Protease inhibitor (add prior to use)

| Stacking gel buffer | 0.5 M Tris, adjusted to pH 6.8 with HCl |
| Resolving gel buffer | 1.5 M Tris, adjusted to pH 8.8 with HCl |

Running buffer	25 mM Tris
	192 mM Glycine
	0.1% SDS

Transfer buffer, pH 8.3	25 mM Tris
	192 mM Glycine
	20% Methanol

7.8. Bacterial strains

Table 8. Bacterial strains.

Bacterial strain	Source
One Shot® Stbl3™ chemically competent E. coli	Thermo Fisher Scientific
One Shot™ TOP10 Chemically Competent E. coli	Thermo Fisher Scientific

7.9. Plasmids

Table 9. Plasmids.

Plasmid	Source
CRISPR-SB	(Weber *et al.*, 2015)
pcDNA6.2	LifeTech
PGK-Cre	Addgene #11543
pLentiX1-PURO	Addgene #17297
pX330	Addgene #42230

7.10. On-Target sgRNA sequences

Table 10. sgRNA sequences for target genes. Ensembl ID, consensus coding sequence (CCDS) and targeted exon are given for each target gene. sgRNA were chosen

Gene	Ensembl ID	CCDS	sgRNA sequence (genomic PAM)	Exon
Apc	Apc-001 (ENSMUST00000079362)	CCDS29125	TCAGTTGTTAAAGCAAGTTG (AGG)	2
Arid1a	Arid1a-201 (ENSMUST00000105897)	CCDS38908	TTAGTCCCACCATACGGCTG (AGG)	2
Arid1b	Arid1b-201 (ENSMUST00000115797)	CCDS49929	CTGTGCACCTGGGGGACCGT (AGG)	2
Arid5b	Arid5b-201 (ENSMUST00000020106)	CCDS35929	GCTATGCAAATCGGATCCTT (TGG)	2
Atm	Atm-001 (ENSMUST00000118282)	CCDS40636	GGCTGTCAACTTCCGAAAAC (GGG)	7

Brca1	Brca1-001 (ENSMUST00000017290)	CCDS25474	AAATCTTAGAGTGTCCGATC (TGG)	2
Brca2	Brca2-201 (ENSMUST00000044620)	CCDS39411	TAGGACCGATAAGCCTCAAT (TGG)	3
Cdkn2a-ex1β	Cdkn2a-201 (ENSMUST00000107131)	CCDS18350	TGGTGAAGTTCGTGCGATCC (CGG)	1
Cdkn2a-ex2	Cdkn2a-001 (ENSMUST00000060501)	CCDS38812	GTGCGATATTTGCGTTCCGC (TGG)	2
	Cdkn2a-201 (ENSMUST00000107131)	CCDS18350		
Cdkn2b	Cdkn2b-201 (ENSMUST00000097981)	CCDS18351	GGCGCCTCCCGAAGCGGTTC (AGG)	1
Pten	Pten-001 (ENSMUST00000013807)	CCDS29753	GCTAACGATCTCTTTGATGA (TGG)	1
Rosa26.1	Gt(ROSA)26Sor	OTTMUSG00000034748	ATATGGTAGCCAATAATCAA (TGG)	intergenic
Rosa26.2	Gt(ROSA)26Sor	OTTMUSG00000034748	TAGTCCCACAAGACTATCTG (AGG)	intergenic
Smad4	Smad4-001 (ENSMUST00000025393)	CCDS29337	GACAACCCGCTCATAGTGATA (TGG)	2
Trp53	Trp53-202 (ENSMUST00000171247)	CCDS48826	GACACTCGGAGGGCTTCACT (TGG)	3

7.11. On-Target Primer

Table 11. Sequence of primer pairs used for amplification of sgRNA target sites.

Gene	Forward Primer	Reverse Primer
Apc	GCGAATAAGCACCACTCCTC	AAGAATGAACCAACACCAAGG
Arid1a	GTTCTGATTCCTGTGCTCGC	TCCATCACCTACCTGCTGTG
Arid1b	AGTTCTGGGGTACTTGGAATCA	GGTACTGCAAGCCTCCCA
Arid5b	TGGCTTGCACGGACCTTATA	ATCAGCAGTTGGACGGTCTT
Atm	TCCTTTTCAACTGTTCCTGTTACA	GACAATGGAAAGGCGAGTCA
Brca1	AGCGTGAGAACTCCTCCAAA	CTGCCATGAGGAAGAACACA
Brca2	TCACGAGTTTCTCCGTGTCA	GCTCTGGCTGTCTCGAACTT
Cdkn2a-ex1β	TCTCACCTCGCTTGTCACAG	AAGTACTCCATCTCCCGGGA
Cdkn2a-ex2	TCAACTACGGTGCAGATTCG	CGGGTGGGTAAAATGGGAAC
Cdkn2b	CCGAAGCTACTGGGTCTCC	CACTTGCCCAGCTTGTACG
Pten	TGCGAGGATTATCCGTCTTC	CATCCGTCTACTCCCACGTT
Rosa26.1	TCTGATGCCCTCTTCTGGTG	GGCTAAACTCTGGCCCTACA
Rosa26.2	GGAAGGATTGTCTGTGCCCT	ATTTTCCAAAGCCCTCCCCA
Smad4	TGCAGTGTCACAGATGCTCA	CTCAGGAACTGGAGGAAGCA
Trp53	ACATAGCAAGTTGGAGGCCA	CCACTCACCGTGCACATAAC

7.12. Off-Target sgRNA sequences

Table 12. sgRNA sequences for off-target genetic sites. Off-target IDs for each delivered sgRNA, targeted chromosome and DNA strand, position in mm10 genome, genomic off-target sequence, number of mismatches to each sgRNA and genetic location of the off-target binding are given. The top 5 intergenic off-target binding regions and at least the top 3 intragenic binding sites were submitted to amplicon-based deep sequencing for off-target CRISPR/Cas9 mutagenesis. The probability of off-target binding was computed using the total number, the pair-wise distribution of aligned nucleotides and the proximity of mismatches to the respective PAM site (Wiedenheft *et al.*, 2012).

Guide ID	chr	Str	Position (mm10)	Sequence	# mis-mat-ches	Gene
Apc_1	9	-1	26933897	TCAGTTATTAAAGCAAATTGGGG	2	None
Apc_2	14	1	77604446	GCAGTTGAGAAAGCAAGTTGGAG	3	None
Apc_3	3	-1	114376816	TCAGATTATAAAGCAAGTTGTGG	3	None
Apc_4	5	1	75817666	TTAGCTGTTAAAGCAAGTTACAG	3	None
Apc_5	10	1	94379839	TCAGATGGGAAAGCAAGTTGCAG	3	None
Apc_6	13	1	106857412	TAAGTTGCTATAGCAACTTGAAG	4	NM_029665
Apc_7	7	1	12984855	TCAGTTCCTACAGCAAGTTCCAG	4	NM_001168561
Apc_8	10	-1	52195004	AGAGTTCTTAAAGCAAGGTGGAG	4	NM_011282
Arid1a_1	17	1	27452698	CCAGGCCCACCATATGGCTGAGG	4	None
Arid1a_2	5	-1	122707741	TGAGCCCCACTTTACGGCTGCGG	4	NM_011026
Arid1a_3	8	1	89565625	TGGGACCCACCATACCGCTGTGG	4	None
Arid1a_4	16	-1	13032943	TTAAACCCACCATACGCCTAAAG	4	None
Arid1a_5	8	-1	126296723	ATAGTCCATCCATAGGGCTGAAG	4	None
Arid1a_6	15	1	79917925	TGTGTCCCACCACAAGGCTGGAG	4	NM_144811
Arid1a_7	1	1	164211867	ATAGACCCACCCTTCGGCTGGAG	4	NM_007976
Arid1b_1	18	-1	34860543	CCGCCCACCTCGGGGACCGTGGG	4	None
Arid1b_2	1	1	166651815	CTAGGCAACTGGGGGACCCTGAG	4	None
Arid1b_3	12	-1	21167366	CTGAGCACACTGGGGACCGTGAG	4	None
Arid1b_4	16	-1	85798156	CTGGGGACCATGGGGACCGTGGG	4	NM_009621
Arid1b_5	9	-1	45838687	CTTTGCAGCTTGGGGACCGACAG	4	NM_011792
Arid1b_6	9	1	49250583	CTCAGCTCCTGGGGGACCCTGGG	4	NM_177701
Arid5b_1	16	-1	64165874	TCTATGCAAGTCAGATCCTTTAG	3	None
Arid5b_2	13	-1	8753315	GCTATGCCACTCTGATCCTTCAG	3	None
Arid5b_3	10	-1	87808962	GCTGTTCAAATCGGATCCTGTAG	3	None
Arid5b_4	3	1	20285892	AGTTTGCAAATGGGATCCTTGGG	4	None
Arid5b_5	1	1	107504467	CCTATGCAAATCTGATCCTAAAG	3	None
Arid5b_6	7	1	123235828	CCTGTGCAAATCCTATCCTTTGG	4	NM_146198
Arid5b_7	6	1	125679494	CCTATGCAAATTGTATCCCTCAG	4	NM_011708
Atm_1	13	-1	46896751	TGTTATCAACTACCGAAAACTAG	4	None
Atm_2	10	-1	80700847	ACCTGAGAACTTCCGAAAACCAG	4	None
Atm_3	13	-1	37858202	CTCTGAAAACTTCCGAAAACTGG	4	None
Atm_4	3	1	120488144	GATTGTCTACTTCCCAAAACTGG	4	None
Atm_5	7	-1	49024377	GACTGTCAACTTCCTAAAAACAG	3	None
Atm_6	9	-1	116131633	GACTGTCCACTTGCGACAACCAG	4	NM_029575
Atm_7	18	-1	67878014	GGCACTCAACATCCCAAAACTGG	4	NM_027556
Atm_8	9	-1	59327354	GGCTATCAGCTGCCTAAAACGAG	4	NM_175325
Brca1_1	18	1	24000244	AAATCTTGGAGTGTCCGGTCAAG	2	None
Brca1_2	10	-1	125354400	AAATTTTAGTGTGTCCCATCAAG	3	None
Brca1_3	11	1	111491635	AATTCTTAGAATGTCCCATCCAG	3	None
Brca1_4	5	-1	34202516	ACATCTGTGAGTGTCCCATCCAG	4	None
Brca1_5	3	-1	7612625	AAGTCTGGGAGTTTCCGATCCAG	4	None
Brca1_6	17	1	35127508	GAACCTTGGAGTGTCCGCTCAAG	4	NM_033477
Brca1_7	12	1	110855953	ACATCTTACAGTGTCAGATGGGG	4	NM_001199785
Brca1_8	1	1	60486355	AAATCTTAAATTGTCTTATCTGG	4	NM_001045513

31

Brca2_1	16	1	7627804	TATGACCAATGAGCCTCAATAAG	3	None
Brca2_2	5	-1	37348530	GATGACCCATAAGCCTCAAAGAG	4	NM_145920
Brca2_3	7	-1	83675639	TGGAACAGCTAAGCCTCAATCAG	4	None
Brca2_4	6	1	101239153	TTAGACCTATAAACCTCAATGAG	4	None
Brca2_5	X	-1	10836554	GAGAACTGATTAGCCTCAATAGG	4	None
Brca2_6	12	-1	36476693	AAGGACAGATAAACCTCATTAGG	4	NM_178629
Brca2_7	5	-1	123819253	TAGGAACGCTACGGCTCAATAGG	4	NM_001042421
Cdkn2a ex1ß_1	8	1	44728100	TGATTAAGTTCGTGAGATCCTGG	3	None
Cdkn2a-ex1ß_2	2	-1	30208726	CAGTGAAGTGCCTGCGATCCCAG	4	None
Cdkn2a-ex1ß_4	6	-1	87833508	AGGTGTGGTGCGTGCGATCCCAG	4	None
Cdkn2a-ex1ß_5	16	1	39487042	AAGTGAAGTTTGTGCGTTCCCAG	4	None
Cdkn2a-ex1ß_6	13	-1	50417915	TGCTGCAGTTCGTGCGGGCCAAG	4	NM_175401
Cdkn2a-ex1ß_7	11	-1	120809527	TGTGGAAGTTCGTCAGATCCTGG	4	NM_007988
Cdkn2a-ex1ß_8	X	1	58919170	TGGTGAAGTTTCTGAGCTCCAAG	4	NM_023774
Cdkn2a-ex2_1	4	1	148874074	GTGGGAGATCTGCGTTCCGTAAG	4	None
Cdkn2a-ex2_2	7	1	126924957	GTGCGTTCTTTGCGTTGCGTGGG	4	None
Cdkn2a-ex2_3	4	1	45255256	GTGCCATATTCCAGTTCCGCAAG	4	None
Cdkn2a-ex2_4	2	1	180925924	GTGGGACATTTGGGTTCCTCTGG	4	None
Cdkn2a-ex2_5	8	-1	72157092	GTTCAATATTTGTGTTCTGCCAG	4	None
Cdkn2a-ex2_6	11	-1	95675148	GTGTGATATTGACGTTCTGCAAG	4	NM_008831
Cdkn2a-ex2_7	3	-1	53474746	GTGCGATAGTTGCATGCGGCCGG	4	NM_173382
Cdkn2b_1	11	1	116110179	ACCGGCTCCCGGAGCGGTTCCAG	4	NM_172570
Cdkn2b_2	17	-1	25067936	GGGGCCTCCTGAAGGGGTTCTGG	3	None
Cdkn2b_3	5	-1	112046540	GGCGGCTGCAGAAGCGGTTGAGG	4	None
Cdkn2b_4	14	1	21750555	CCCGCCTCCCGAAGCAGTTCCGG	3	NM_026283
Cdkn2b_5	14	1	25710848	GGATGCTCCCGAAGCGGTGCTGG	4	None
Cdkn2b_6	2	-1	148044131	TGCGCCGCCAGAAGCGCTTCAAG	4	NM_010446
Pten_1	1	-1	96400219	CCTATCGATTTCTTTGATGATGG	3	None
Pten_2	10	1	11786839	AATACCGGTCTCTTTGATGATGG	4	None
Pten_3	6	1	110140664	TGTCACGATGTCTTTGATGAAGG	4	None
Pten_4	1	-1	146699106	GCTTACGATGTATTTGATGATGG	3	None
Pten_5	12	-1	8410402	AGTAGCTATCTCTTTGATGAGAG	4	None
Pten_6	2	1	37427652	TGTAACAATGTCTTTGATGAAAG	4	NM_146253
Pten_7	3	1	138451237	GCTGACACTGTCTTTGATGATAG	4	NM_007410
Pten_8	10	-1	63017546	GGAAACGATGGCTTTGATGACAG	4	NM_001079824
Rosa26.1_1	16	1	19408733	TTGATTATTTGATACCATATAAG	2	None
Rosa26.1_2	8	-1	55887271	TTGTTTAATGTCTACCATATGGG	3	None
Rosa26.1_3	4	-1	93809596	TTGATTAATTTCTACCATATTGG	3	None
Rosa26.1_4	10	1	37034194	ATGTTTCTTTGCTACCATATTAG	4	None
Rosa26.1_5	6	-1	38705196	CTTCTTATTGACTACCATATCAG	4	None
Rosa26.1_6	X	1	155324145	TTGATTGTTGTATACCATATCAG	3	NM_016764
Rosa26.1_8	17	-1	85607421	CTGATTATTACCTGCCATATCGG	4	NR_015387

Rosa26.2_1	13	-1	54604762	TGGACCCAGAAGACTATCTGTAG	3	None	
Rosa26.2_2	2	-1	42198522	TAGGACCAAAAGACTATCTGTAG	3	None	
Rosa26.2_3	3	-1	95594328	TAATTCCACAAGACTATCTCAAG	3	None	
Rosa26.2_4	10	-1	70183548	TTGTCCCTCAAGTCTATCTGCAG	3	None	
Rosa26.2_5	X	-1	51672728	TGCTCCCTGAAGACTATCTGTGG	4	None	
Rosa26.2_6	3	1	96637363	TTATCCTACAAGACTATGTGTAG	4	NM_011069	
Rosa26.2_7	11	-1	96447670	AAGTCCCCCATGACTTTCTGCAG	4	NR_033524	
Rosa26.2_8	4	-1	117897880	CAGTCCCACATAACTATATGAGG	4	NM_146152	
Smad4_1	18	1	39700412	AATAGCAGCTCATAGTGATAGAG	4	None	
Smad4_2	6	-1	127223185	ATAACCCGCTTATAGTGATGTGG	3	None	
Smad4_3	8	-1	85849958	ACAGCCCTTACATAGTGATAGGG	4	None	
Smad4_4	13	1	31135739	ACAAACATCTCCTAGTGATATGG	4	None	
Smad4_5	1	1	168232264	GAAACCAGCTCAAAGTGATAGAG	4	None	
Smad4_6	10	1	21148552	ACTATCTGCTCAAAGTGATACGG	4	NM_001198914	
Trp53_2	5	-1	106714108	ATCACTTGGAGGGCTTCACTCAG	3	None	
Trp53_3	10	-1	109647934	GGCTGTCAGAGGGCTTCACTCAG	4	None	
Trp53_4	9	-1	49800050	GTCTGTCAGAGGGCTTCACTGAG	4	None	
Trp53_5	5	-1	117024931	CACACTGGGAAGGCTTCACTTAG	3	None	
Trp53_6	2	-1	35730631	GGCAGTCAGAGGTCTTCACTCAG	4	NM_001114125	
Trp53_7	2	-1	62501156	GACAGTCTGAAGGCTTCACATGG	4	NM_007986	
Trp53_8	2	-1	158261400	AACACTCGGAGGCCATCACTGGG	3	NM_177850	

7.13. Off-Target Primer

Table 13. Sequence and annealing temperature for each primer pair used to recognize indicated sgRNA off-target site.

Off-target	Forward primer	Reverse primer	T_a [°C]
Apc_1	CTGAGTGTGGTGCTATACTCAAG	ACTAGGATTAGGACCTAGGAAACA	60
Apc_2	AGATCTGCAGTTCACCCCAA	GGGAGTCCAGGAAGCAGAAT	60
Apc_3	AGTTACTGGTGGCTGTAAGACA	AGAGTGGCAGTTCAAGGTAGT	60
Apc_4	ATCCAACGCTGATTCCTTGC	GGGAGGTGATTGAGAGGGAC	60
Apc_5	CCTGGTTTTACGTTGCTGCT	CTATTTGCCTGCACCTCCAG	60
Apc_6	CAATGCAAAAGGTGTTCTGACA	TCACCACCCTTGCTGTAACT	60
Apc_7	CACTTGCTTCAGTCTGAGCC	CCTGCAGTCAACCTTGGTTC	60
Apc_8	CGAACCTGTCAGTTGCAAGT	TGCGATGTTCTGGGCTATCT	60
Arid1a_1	TCCAGATGCCAACCCCTATC	GCCACAGACCCTATTCCTCA	60
Arid1a_2	TGAGAGGGTCACGAGTTGG	CTATTGCCCCAGACCCAGAG	60
Arid1a_3	TGTCTACGATCACAGTGCAGT	ACACAGGCTGTAACTCTGAAGA	60
Arid1a_4	CAGAGGAAGTTGGGTGAGGA	TCATGCTCATCAGGGCTTCT	60
Arid1a_5	GCCAACAGGTGAGTCTTCTAAC	CAGGCCCATGTTGTCTGAAG	60
Arid1a_6	CGGCAAGTTCTGTTTGTGCT	GTCTGGGTCTCATCTCCTGG	60
Arid1a_7	TCCTCGAAGTAGACATATCCACA	TGCAAAGGTTCTTCTGGAGC	60
Arid1b_1	GGCTCTAAAACCCCCAACCT	GTTCCCAACTGGGAGCCTGA	60
Arid1b_2	GTGGTAGGAGCTTGGAGTCG	AACCAGGGGATCAAGGACTG	60
Arid1b_3	TGCTACATCTGGAGCCTCTTG	CACCTTCAGAGAGCAGCAGTA	60
Arid1b_4	TGAAAAGAGAACGACGGCGA	ACTCCTCTACCTGTGTCCCG	60
Arid1b_5	CATCCCAGACCCCTTTCAGC	GAGTGGGCAGGAGAAATCCG	60
Arid1b_6	GTGGTGTGTCTGATTGCCTT	GCGCAGCACTCCTGTAAGA	60
Arid5b_1	CACAACCAAAGGTCTGACGC	AAGCTGAAAGTCCCAGTTGGAT	60
Arid5b_2	ACCAGTTGGTTTGTGCAGGG	TGGTAGCTGGAACCTTTCCC	60
Arid5b_3	GAAAAGCCCAAACAAGCTGGA	TGTGCCATTTGCCCAGGTTT	60
Arid5b_4	GCCAGCTAAACTTATACTCTGGTTG	CTGCACCATGCCTGCCTAT	63
Arid5b_5	GATTTCTGTGGACCAGCACC	TCTGTGCACTTTGGCGCTTA	63

Arid5b_6	ATTGCTTTGCTCTCCCCAGG	GTACCTCAGGCATCCCACAT	60
Arid5b_7	TGGTTGACCTATGCACGACC	GCACATTGCAAAGGGTCTCA	60
Atm_1	TGAGGGTTCAAACCCACCCC	AGAAGATCAGTGGTCAGCCC	63
Atm_2	ACTAGCCCCCTTTTGCTCTT	GGAGCTCAGGAACTAGGGGT	60
Atm_3	CTGGAGCAGCGGCTTTAAGT	CTGCTGTCCCCACATGGAAG	60
Atm_4	ACCTCGAGAATTGCAGGTCC	GGGAATTGAGAAAGTGTTGGAGT	60
Atm_5	GGCCAGTCATCTATGCAGTCA	TCTTTATTCCAGCCGACGCT	60
Atm_6	TGTGATACACGGGACTGTGAG	CATGCCATGCCATTTGTGC	60
Atm_7	CCTGTGAGTGCTGAGGTTCA	CAGCGAAAGCTGAAACCGTA	60
Atm_8	TCGGGTGCTCTTAATCTGCTG	TGTTCCTTGGAGTCCTTGTTGA	63
Brca1_1	GACTTCGTGGACAGAATGGC	TCCAGCCCTGTTTGATTCCT	60
Brca1_2	GAGAACTGCAGAGCCCATTG	ACCGACATTTTCCCCTCCTT	60
Brca1_3	TCCAAAGGCTGCTAGTGGAA	CCTCGACCCCTCCCAATTTT	60
Brca1_4	CCCAACACAGCCCACTACA	ACCTGCAGAGTAAAGGGCTC	60
Brca1_5	TGGATTCCAGCCTCTGTCAA	TGTCCCTAGCCAGTACCTCT	60
Brca1_6	TAGCAGGGACCTCAAAGTGG	ATAGCAGCCCATGAAGCCAG	63
Brca1_7	GCACTGTAAGCTCAACCCAG	CCTCTGCCACATGAGTACCA	60
Brca1_8	ACATGACTGGAGTTAGAAAAGGA	TGTGCTTGCTATTCCTATGATGA	60
Brca2_1	CACAGTAGGTTGGGTCTTCC	GACAGGGTTGGAGAGTGCC	60
Brca2_2	GCGCTGTTATTTCCTCCGTT	AGCAAGGCCAGTGATCTCAT	60
Brca2_3	TGAGCAAGTCACTTTGGAAAACA	AAGTGGGAACTTCAGGAGGG	60
Brca2_4	CACTGAGTGTCATGCTTGGC	ACTAGTGAGCCCTGCCTTTC	60
Brca2_5	GACACAGGAAGAGGGAGACA	ATCAAGCCACCAGAATCCCT	60
Brca2_6	TGCATTTCCTTTGACACCAGT	ATCAGAGATCTCCGTGGCTG	60
Brca2_7	AGAAGGAATTTGGGATTTTGGCA	TGGAGAGTGAGCTAGCCAAG	60
Cdkn2a ex1ß_1	GCTTCCCTGAAACCTGCATC	CATCAAGGACTAGGAGCAATGA	60
Cdkn2a ex1ß_2	GTTGCCCTCATCTCAGACCT	TTCCAAGTGCAGCAAAGGTC	63
Cdkn2a ex1ß_4	GGGGAGAGGGTCTAGAAGGA	TCCACAGATCATTGGCGAGA	60
Cdkn2a ex1ß_5	GGCATCTTTTCATTTGTCAGCC	ACACAGACACACAGATCCAAT	60
Cdkn2a ex1ß_6	ACTTCAGTGATCGCTAGGCC	CACACAGTGGGGCATAGAGA	60
Cdkn2a ex1ß_7	TGAGGACATGCACACAGACT	AATGCTTGGCTGGGTGATTG	60
Cdkn2a ex1ß_8	CTGCAGAGAGTTCCCAGGAA	CTCTTCATTGCTGATCCGCC	60
Cdkn2a-ex2_1	TGGGCTTGTTTTAAAGGGGC	CAATGTCTGCTGCTCACCTG	63
Cdkn2a-ex2_2	GTCTGTTTGGATGCCCTTGG	AGGCTACTCTTGCTGTCTCC	63
Cdkn2a-ex2_3	AAACTGAACTTGCTCGGCTC	TTGAGCATGAGAGGGAAGCA	60
Cdkn2a-ex2_4	TACCACTTCCTTCCCTGCAG	ATTGACTGTCCTACCCTGGG	60
Cdkn2a-ex2_5	TTACCTAACTCCTGGGGCAG	CAGGAAGCTAGACTGTGCCT	60
Cdkn2a-ex2_6	CCATCCTGTCAGTGGTTCCT	GCTACCTACCCACCACTACTC	60
Cdkn2a-ex2_7	ACTGGGGCATCTTCAGTCTC	AGTGAAAAGCCCCAATGATAAGT	60
Cdkn2b_1	GACAGCGTGTGGTTCTTGC	GAAGTCTCAAGAGGGTCGTGC	63
Cdkn2b_2	TTTTGGGCAAAACAGACCCG	TCAACCTGATTGCTGCCTTTC	60
Cdkn2b_3	TCATCCACCTCTCCCTTCTCT	TGTGTAGATGCTCTGGGGAC	63
Cdkn2b_4	AGGACTGACTGAGAAGGGGTT	CTAAGTCGCCGTTGGAGTCG	60
Cdkn2b_5	GATACGGGTCTTGCTTCTGGA	GCCCCTTGAGCATCACTTGG	60
Cdkn2b_6	GAGGCAGGTGCTCCCTTTAG	CCTCTTCCCTTTCTACCGGC	60
Pten_1	CAAGAGAAAGACAAGGCATGGT	AGAAGGGAGGAGGGAAGGAA	60
Pten_2	GGAGCAGCTTGGAGTCTGAT	CATTGCCAGCACAGTTCTCA	63
Pten_3	GGAACATTAAGAGTGAAACAGCT	AAATAGGTGGCAGAACGGGT	63

Pten_4	CATGCAACAACAGAGGACACA	TCCTTCTTCTGACCAAATGTGA	63
Pten_5	AACAATGCTCAGAGGGTCCC	GATGGAATGTTGGGCCTCAA	60
Pten_6	AAGGGTGGACTACAAAAGAGC	ACAGAAAGGTTTGTCTTGGCC	60
Pten_7	GCTGTGGTATTTCAACTGGCT	TGACCTTCACGTTGCCAATG	63
Pten_8	CCATAGCCATGTCCTCCCAT	GCTGCAAACATTAATGAAGAAGC	60
Rosa26.1_1	CCCATGTGTAGTGTCAATCATCC	TCACACAGGTAAAGTAATGTGTTGT	60
Rosa26.1_2	CTGGGGCATCACCAAATTGT	CGGCTGAACTTAATTGCTCCTTT	60
Rosa26.1_3	AAAGCCTGGAGTTTCTGTTGCT	TTTACTAGCTCAGAGATTGGGACT	60
Rosa26.1_4	AACCCAGGGACTGAAAAGCA	AGGGCTTTTGTGCATGCTAAG	60
Rosa26.1_5	CATTCCTGAGGTGGCCAGG	AAAGGCTTCGAACCAAAAATGT	60
Rosa26.1_6	TTACAATGGCAAACGAATATGGT	AGCAGACTCGGTGCTCTTAAC	60
Rosa26.1_8	CCTCAATCCCACTCTACGTTT	AGGGGTGTATTTGCAACTCGT	60
Rosa26.2_1	CTGTCCCCCAGTAGCCAAAG	CTCTGCTATCACAGTGCCCC	60
Rosa26.2_2	TCATAACTGAGATTGTTAAAGACCA	CAGGGTTGGGACACTAGTTGA	60
Rosa26.2_3	GAAATGACATTCCCCAGCCC	TTGGTCCTCAGAACCCTCAG	60
Rosa26.2_4	TGCTTGCCTTCATCTGACCC	TCACGGTAGTGCTGGCTAGA	60
Rosa26.2_5	AGACTTCCATGGGATGTGAGAAAT	AATTTCATTCGAAGGGTGTATCTC	60
Rosa26.2_6	CTGGGGAACTCAACAGATGC	TTGATTCCCAGAGCCCACAT	60
Rosa26.2_7	TATTCTGGGGTGCGTTCAGC	CATGCCAGGCGTTTGTTAGC	60
Rosa26.2_8	AGGCAAAGGGGCACTAAAGG	GTCCTTCACTCTGCCGTCTC	63
Smad4_1	CATCATCTCCAAGGCCCTCA	GCCATTCCAGGGATCAAACC	60
Smad4_2	CAGATATGGTGGTGCATGCC	TTGGAAAGCAGAGCAACAGG	60
Smad4_3	GGGGTTCCTGGGAGTCTTTT	TACTGTGGCCTTGAGAAGCA	60
Smad4_4	TAAGCAGCACTCACCACCAA	GCTCAGTCACCTAAGCTTGT	60
Smad4_5	AAAGTGGGACTCATAGGGCC	TCCCGTCTCAGGTCACAAAA	60
Smad4_6	TAATGCCTGCTGTCCCTTCA	TGAGATCATCTGACGGGCAA	60
Trp53_1	CCTAGCATTCAGGCCCTCAT	TGAGGGGAGGAGAGTACAGT	60
Trp53_2	GGATTGTCCCTTGTACCACTTC	AACAAATGTGCGGGCAACTT	60
Trp53_3	GCATGCACTGAACAGAAATTGG	TCAGAGGAGATTTGCTTGGGA	60
Trp53_4	CCCTGGCTCTTCTGTGTGTA	GAACCCGCAGCATGTGATAG	60
Trp53_5	CATGATGCCTGTTCACGAGG	CTGGTAAAAGGTGCTGGCTT	60
Trp53_6	CATGCTGTTTGGGTGGAAGG	AGAAAAGAGGGGCTGGTTCC	60
Trp53_7	CTACCCGGCAATGAACAGGT	CCAAGTGGCCAAGAAGCAAA	60
Trp53_8	GGCTTGCCGTCTTTGTTGAT	AAGTGGACAGTTCTCCCAGC	60

7.14. Software

Table 14. Software and programs used in this study.

Software	Source
AxioVision 4.8	Carl Zeiss AG
Genomic Workbench 7	Agilent Technologies
GraphPad Prism5	GraphPad Software
Illumina Sequence Analysis Viewer 2.4.5	Illumina
Office 2016	Microsoft Corporation
Odyssey® v1.2	Li-Cor Biosciences
R Software Environment	The R Project, The R Foundation
Snapgene 3.1	GSL Biotech
StepOne™ v2.3	Applied Biosystems, Inc.

7.15. Manufacturer

Manufacturer	(Headquarter) Location

Manufacturer	(Headquarter) Location
Abbott GmbH	Ludwigshafen, Germany
Addgene	Cambridge, Massachusetts, USA
Agilent Technologies, Inc.	Santa Clara, CA, USA
Analytik Jena AG	Jena, Germany
Applied Biosystems, Inc.	Carlsbad, CA, USA
B. Braun Melsungen AG	Melsungen, Germany
BD Biosciences, BD, Inc.	Franklin Lakes, NJ, USA
Bertin Instruments	Montigny-le-Bretonneux, France
Biochrom GmbH	Berlin, Germany
Biometra GmbH	Göttingen, Germany
Bio-Rad Laboratories, Inc.	Hercules, CA, USA
Biozym Scientific GmbH	Hessisch Oldendorf, Germany
Brand GmbH	Wertheim, Germany
Carl Roth	Karlsruhe, Germany
Carl Zeiss AG	Oberkochen, Germany
Cedarlane, Inc.	Burlington, ON, Canada
Corning, Inc.	Corning, NY, USA
Covaris, Inc.	Woburn, MA, USA
DAKO, Agilent Technologies, Inc.	Santa Clara, CA, USA
Developmental Studies Hybridoma Bank	Iowa City, IA, USA
Ditabis AG	Pforzheim, Germany
Eppendorf AG	Hamburg, Germany
Eurofins Genomics GmbH	Ebersberg, Germany
Feather Safety Razor Co., Ltd.	Osaka, Japan
Genewiz, Inc.	South Plainfield, NJ, USA
GraphPad Software, Inc.	San Diego, CA, USA
Greiner Bio-One GmbH	Kremsmünster, Austria
GSL Biotech LLC	Chicago, IL, USA
IKA-Werke GmbH	Staufen, Germany
Manufacturer	**(Headquarter) Location**
Illumina, Inc.	San Diego, CA, USA
Integra Biosciences AG	Biebertal, Germany
Integrated DNA Technologies, Inc.	Coralville, IA, USA
Jackson ImmunoResearch, Inc.	West Grove, PA, USA
Kapa Biosystems, Inc.	Wilmington, MA, USA
Macherey-Nagel GmbH	Düren, Germany
Medite GmbH	Burgdorf, Germany
Merck KGaA	Darmstadt, Germany
Microsoft Cooperation	Redmond, Washington, USA
neoLab Migge GmbH	Heidelberg, Germany
New England Biolabs, Inc.	Ipswich, MA, USA
Qiagen GmbH	Hilden, Germany
R&D Systems, Inc.	Minneapolis, MN, USA
Santa Cruz Biotechnology, Inc.	Dallas, TX, USA
Sarstedt AG	Nümbrecht, Germany
Sartorius AG	Göttingen, Germany
Scientific Industries, Inc.	Bohemia, NY, USA

36

Seidel medipool GmbH	Gauting-Buchendor, Germany
Sigma-Aldrich Corporation	St. Louis, MO, USA
Simport Scientific, Inc.	Beloeil, QC, Canada
Swann-Morton, Ltd.	Sheffield, United Kingdom
Takara Bio, Inc.	Kyoto, Japan
The R Project, The R Foundation	Vienna, Austria
Thermo Fisher Scientific Gerhard Menzel B.V.	Braunschweig, Germany
Thermo Fisher Scientific, Inc.	Waltham, MA, USA
Viagen Biotech, Inc.	Los Angeles, CA, USA
VWR International GmbH	Darmstadt, Germany
Waldeck GmbH	Münster, Germany
Worthington Biochemical Corporation	Lakewood, NJ, USA

8. Methods

8.1. Design of single guide RNA (sgRNA) sequences

Sequence information of all genomic target genes were obtained by downloading consensus coding sequences (CCDS) from ensemble.org (GRCm38.p2). sgRNA sequence cassettes were generated by using the online-based CRISPR design tool (http://crispr.mit.edu). The CRISPR design tool allows the detection of sgRNAs that comprise a high target specificity next to the PAM and flags sgRNAs with a high degree of unspecific genome-wide off-target regions. For each target gene, two sgRNA sequences were chosen based on the position (N-terminal of targeted gene) and their specificity for its target. sgRNA on- and off-target primer sequences and corresponding target regions are shown in Tables 10-13.

8.2. Cloning of sgRNA sequences in CRISPR-SB

For cloning sgRNA target sequences into CRISPR-SB vector, 100µM of each forward and reverse oligo were 5'-phosphorylated by using T4 polynucleotide kinase and annealed in 1x T4 Ligation Buffer by incubating for 30min at 37°C and subsequently ramping down from 95°C to 25°C at 5°C/min. The CRISPR-SB vector contains *Sleeping Beauty* inverted terminal repeats flanking the functional CRISPR/Cas9 units (U6 RNA promoter, sgRNA cassette, hybrid form of the chicken ß-actin (CBh) mRNA promoter and *hSpCas9*) (Weber *et al.*, 2015). The co-activity of *Sleeping Beauty* transposase (SB) could in theory allow the stable mobilization into the host genome, however due to the high efficiency of CRISPR/Cas9 genome editing this feature was not used in the study. One µg of CRISPR-SB vector was *BbsI*-digested for at least 1h at 37°C creating overhangs for the annealed oligo and opened plasmid DNA (pDNA) was PCR purified and eluted in EB buffer following manufacturer's instruction. For each ligation, 50ng of *BbsI*-opened CRISPR-SB, 1:200 diluted oligo duplexes, 1x Quickligation buffer and Quickligase were incubated for 10min at room temperature. For plasmid amplification, *Stbl3*^{TM} chemically competent cells were transformed by incubating for 20min on ice and 10min at room temperature in 1x KCM chemical transformation buffer. After pre-incubation at 37°C on a horizontal shaker, transformed *Stbl3*^{TM} were plated on a liquid broth (LB)-agar plate with 100mg/mL ampicillin as selection marker. After overnight growth, 5mL liquid LB cultures were inoculated with single colonies picked from the agar plate and transformed *Stbl3*^{TM} again grown for over 12h in liquid culture. For long-term storage, 250µl of bacterial suspension was mixed 1:1 in 50% glycerol and frozen at -80°C. For bacteria suspension either the QIAprep Spin Miniprep Kit (in case of 5mL) or the endotoxin-free Plasmid Midi Kit (in case of 150mL) was used for pDNA purification according to manufacturer's instruction. The correct

integration of the sgRNA targeting sequences was verified by Sanger sequencing using a primer binding to the upstream U6 promoter.

8.3. sgRNA cleavage efficiency testing using SURVEYOR™ assay

For the determination of individual sgRNA cleavage efficiencies, we used the mouse primary pancreatic cancer cell line PPT 4072 that comprises wild-type status in all target regions. The cell line was grown under standard culturing conditions (see below). A day before transfection, $5x10^4$ cells were seeded in a 12-well plate and standard medium was changed to Opti-MEM™ (Thermo Fisher Scientific Inc.) one hour before transfection. 500ng of respective cloned CRISPR-SB constructs and 250ng of pLentiX1-Puro (Addgene #17297) vector were co-transfected overnight using the lipofection reagent Lipofectamine 2000™ (Thermo Fisher Scientific Inc.) according to manufacturer's instruction. Following day, transfection reagent was removed, and cells recovered in culturing medium without penicillin/streptomycin (P/S) for approximately 8h. Selection for transfected cells was conducted by the addition of 4µg/mL puromycin to culturing medium without P/S for 72h. When edited PPT 4072 cells reached confluency, gDNA was harvested by using the Direct PCR lysis kit and equivalent volumes of respective gDNA samples submitted to TaKaRa *Ex Taq* proof reading polymerase reactions by following manufacturer's instructions and employing primers listed in Table 11. The yield of the PCR reaction was quantified by Qubit fluorometric measurement and 250ng of each product adjusted in 12µL 1x TaKaRa reaction buffer. Heteroduplex formation of wild-type and edited DNA strands was achieved after multiple melting and annealing cycles of amplicons. SURVEYOR® nuclease assay was performed according to manufacturer's instructions. Processed amplicons of respective samples were diluted 1:6 in DNA loading buffer and agarose gel electrophoresis performed to separate wild-type (un-nicked full-length DNA) and edited (nicked enzymatically cleaved DNA) DNA strands. By calculating integrated intensity of gel bands using ImageJ software, Cas9-mediated indel frequency was calculated on the basis of the fraction of mutated enzymatically cut to full-length wild-type DNA strands (Guschin *et al.*, 2010).

8.4. Animal experiments

All mice were maintained on *C57Bl/6;129S6/SvEv* mixed background and housed under specific pathogen-free conditions according to the institutional guidelines. Female and male mice were randomly subjected to somatic electroporation-based CRISPR/Cas9 vector delivery cohorts. Mouse lines used in this study include *Rosa26^{mT/mG}* (Muzumdar *et al.*, 2007) mice for *in vivo* delivery efficiency testing and double-mutant *Ptf1a^{Cre/+}* (Nakhai *et al.*, 2007);*Kras^{LSL-*

$^{G12D/+}$ mice (Jackson *et al.*, 2001) for the establishment of tumour cohorts. All animal studies were conducted in compliance with European guidelines for the care and use of laboratory animals and were approved by the Institutional Animal Care and Use Committees (IACUC) of Technische Universität München, Regierung von Oberbayern and the UK Home Office.

8.5. Genotyping

Approximately 2-3 weeks after birth, newborn mice were ear punched to label mice in a numeric code and obtain biopsies for genotyping. Briefly, gDNA from ear biopsies was extracted by overnight incubation in 50μL Soriano lysis buffer (20μg/mL Proteinase K) at 55°C and subsequently, Proteinase K heat inactivated at 95°C for 15min. Eventually, the samples were vortexed thoroughly, centrifuged for 10min at >4000g and diluted 1:10 in water in a fresh tube. gDNA samples can be stored for short term at 4°C, and for long term at -20°C. For standard genotyping, 6.25μL of a 2x PCR pre-mix (peqGOLD Taq-DNA-Polymerase kit, VWR) was used containing distilled water, 10x buffer S, 30% sucrose, SucRot, PeqTaq and dNTPs. PCR reaction was filled up to 12.5μL with 1μL gDNA, distilled water and 0.05-1μM forward and reverse primer depending on the locus. Primer sequences for genotyping and PCR product size are given (Ptf1a-generic, CCTCGAAGGCGTCGTTGATGGACTGCA; Ptf1a-mut, GCCACCAGCCAGCTATCAA; Ptf1a-wt, CCACGGATCACTCACAAAGCGT; Kras$^{LSL-G12D}$-generic, CACCAGCTTCGGCTTCCTATT, CCATGGCTTGAG-TAAGTCTGC; Kras$^{LSL-G12D}$-wt, AGCTAATGGCTCTCAAAGGAATGTA; Rosa26-for, CCATGTGATCGCGCTTCTCGT and Rosa26-rev, GTTCGGCTTCTGGCGTGT). PCR conditions were used according to manufacturer's instructions (T_a=60°C for *Ptf1a$^{Cre/+}$*, T_a=55°C for *Kras$^{LSL-G12D/+}$* and T_a=62°C for *Rosa26$^{mT/mG}$*). For *Ptf1a$^{Cre/+}$* genotyping PCR, 5% DMSO was supplemented. PCR products were size-separated by agarose gel electrophoresis. Briefly, 1.5% agarose was dissolved in 1x TAE buffer and microwaved until agarose was completely dissolved. After cooling down, agarose solution was supplemented 1:20'000 with ethidium bromide, casted into the gel chamber and eventually, left for polymerization. Ready-to-use PCR products were loaded onto the gel, separated in the electric field (120V) and DNA bands were visualized by excitation with UV.

8.6. Electroporation-based *in vivo* transfection of pancreatic cells in the mouse

In vivo electroporation-based transfection for gene delivery has been shown in a variety of organs in mice including muscle (Aihara *et al.*, 1998), liver (Liu *et al.*, 2002), lung (Dean *et al.*, 2003) and brain (Zuckermann *et al.*, 2015). Eight-to-15 week old mice were treated orally hours

before surgery with 0.5mg/mL Metacam solution. For surgery, mice were anaesthetised with an intraperitoneal (i.p.) injection of a combination of medetomidine (0.5mg/kg), midazolam (5mg/kg) and fentanyl (0.5mg/kg, MMF) and after assessment of complete anaesthesia, eyes covered in eye ointment for protection. The left flank of the mice is carefully shaved, and the abdomen disinfected locally at the site of the procedure. Now, the spleen can be located through the skin. A one cm left-to-lateral incision of the skin caudal to the spleen is made and the connective tissue carefully detached from the peritoneum. A 0.5cm left-to-lateral incision through the peritoneum allows the location of the pancreas, which is now carefully pulled out from the abdominal cavity with anatomical forceps avoiding the irritation of the organ. The tail of the pancreas is placed on a phosphate buffered saline (PBS)-soaked piece of surgical paper to prevent retraction and dehydration of the organ. For intra-parenchymatic injection, 50µL plasmid mixture were administered slowly into the pancreatic tail at a depth of 2-4mm using a 100µl Hamilton® syringe attached to a 27G cannula. In total, 60µg of the 15 sgRNA mix (=4µg/sgRNA endotoxin-free pDNA) or 8µg control mix targeting the *Rosa26* locus were delivered. After complete injection, the cannula remained for half minute at the position to prevent the leakage of the newly formed bleb. For *in vivo* electroporation of pancreatic cells, the Nepa21 square-pulse generator (Nepa Gene Co., Ltd., Ichikawa, Chiba Japan) is supplied with forceps-type electrodes that are equipped to 3mm^2 platinum disks (CUY650P3) and together, enable the careful "sandwiching" at the area of injection in the organ and allow the electric current flow. Electroporation was performed at indicated settings, using 50V or 70V for the Poring pulse (Pp) and 30V or 40V during the Transfer pulse (Tp), respectively. In case, the Joule heat measurement during Pp remained beneath 0.15Joule indicative of inefficient electric flow, a second series of pulses was applied to increase transfection performance. After electroporation, the pancreas was carefully replaced in the anatomical position in the abdominal cavity. Eventually, the peritoneal wall was closed with interrupted sutures (5-0 Ethilon) and the skin with wound clips. After the procedure, the MMF anaesthesia was antagonized by the subcutaneous injection of 750µg/kg atipamezole, 500µg/kg flumazenil, 1.2mg/kg naloxone (AFN). Until waking up, mice were kept in a 37°C warming chamber and two weeks after surgery, wound clips are carefully removed with forceps.

8.7. Monitoring scheme and scoring of *in vivo* electroporated PK mice

After electroporation procedure, mice were monitored for 5 consecutive days to score signs of acute sickness (e.g. open wound clips, condition of the fur, activity etc.). In case mice featured signs of acute pain due to the surgery (e.g. overreaction to palpation of the abdomen, flight behaviour, hunched posture etc.) mice were treated orally by application of a few drops of

0.5mg/mL Metacam solution for a maximum of 48h. In case, symptoms do not vanish after 48h, mice were euthanized by isoflurane anaesthesia and subsequent cervical dislocation. Following to the acute phase, mice were monitored on a weekly basis for general signs of illness (e.g. activity, condition of the fur, weight, abdominal mass etc.) and starting from 8 weeks post electroporation, abdomen were scanned regularly by magnetic resonance imaging (see below, MRI) for pancreatic tumours. In case mice exhibited prolonged moderate, short-term additive severe signs of sickness, MRI pancreatic cancer diagnosis or single criteria (e.g. palpable abdominal mass above 1.5cm, ascites, weight loss of more than 15% initial body mass) then mice were euthanized and submitted to sample preparation. Kaplan-Meier survival curves were calculated using Prism (GraphPad software version 5.01).

8.8. Efficiency analyses for electroporation-based *in vivo* transfection

For the establishment of targeted cells after *in vivo* electroporation of pancreatic cells, 60μg of pcDNA6.2 (GFP expression plasmid) were mixed with endoscopic marker containing non-pyrogenic carbon particles and injected into pancreata of 8-15week old wild-type mice. *In vivo* electroporation was performed as described above with conditions given in respective Figures. Two days post electroporation, mice were euthanized, ink-labelled pancreatic region located, fixed in HistoFix solution overnight at 4°C and eventually, paraffin embedded. For quantification of pcDNA6.2-targeted GFP-expressing cells, twelve step-wise 2μm thick sections were sampled and immunohistochemistry (IHC) against GFP performed. Stage cutting resulted in the analysis of a total of 1mm cross section of electroporated tissue. As the other half of ink-labelled electroporated tissue was used for direct DNA isolation, resulting values were multiplied by two to calculate the total number of targeted cells per electroporated pancreas. Background positivity (as pancreas has a high intrinsic background) was subtracted by counting identical amount of mock-electroporated anti-GFP stained sections.

For determination of long-term targeted survivor pancreatic cells, we electroporated 30μg of a PGK-*Cre* expression (Addgene #11543) or mock vector controls in 8-15week old *Rosa26^{mT/mG}* mice and harvested pancreata 7 days post procedure. After re-localization of ink-labelled pancreatic tissue, specimens were short-term fixed in 4% paraformaldehyde without methanol for 1h and subsequently, dehydrated by incubation in 15% and 30% sucrose solution in PBS, respectively. Next, specimens were embedded in Tissue-Tek, carefully frozen in isopropanol chilled at -80°C to avoid cracks inside the block and submitted to cryosectioning. For the Cre-mediated deletion of the loxed GFP-stop cassette and concomitant tdTomato expression, one section every other 100μm (in total 10 sections) of an one millimetre thick electroporated tissue region were sampled and counterstained with DAPI (Thermo Scientific Inc.).

8.9. Recombination PCR for detection of Cre-mediated $Rosa26^{mT/mG}$ conversion

For the verification of the excised stop cassette in the $Rosa26^{mT/mG}$ reporter allele after the electroporation of *Cre* recombinase vector, a nested PCR approach was performed. Thus, high-quality double stranded gDNA was extracted seven days post electroporation from ink-labelled site of vector delivery and >100ng submitted to the first PCR run using Taq polymerase (VWR international; 40 cycles; T_a=62°C) and Rosa26 primers. To eliminate primer from the first amplification step, a PCR clean-up was performed according to manufacturer's instructions. For the nested amplification step, 1µl of the sample or 1µl of a 1:10^5 dilution of the positive control (genomic DNA (gDNA) originating from a primary culture isolated from $Ptf1a^{Cre;}Kras^{LSL-G12D/+};Rosa26^{mT/mG}$ mouse) were submitted to a PCR (30 cycles; $_{Ta}$=62°C) using nested primer tdEG-nest-Inf (GCAACGTGCTGGTTATTGTG) and tdEG-nest-INr (CTCGATGTTGTGGCGGATCT) . Nested PCR products were either size separated on a 1.5% agarose gel or PCR purified for Sanger capillary sequencing to verify *Cre*-mediated recombination of the *mT/mG* reporter allele.

8.10. Magnetic resonance imaging (MRI)

For the monitoring of the *in vivo* tumour growth, we performed MRI imaging on a clinical 3-Tesla MRI Philips Healthcare system (Ingenia 3 T) in combination with a human eight-channel wrist coil (SENSE Wrist coil 8 elements). MRI imaging was optimized on 3 T instruments for mouse and rat imaging as described in a previous protocol (Braren *et al.*, 2011). Five to 10 weeks after electroporation procedure, mice were regularly imaged in a one-month interval to screen for solid abdominal masses located in the pancreatic tail. For tumour detection, longitudinal T2-weighted (T2w) turbo spin-echo imaging was performed with following parameter settings: Slice thickness=0.7mm, in-plane resolution=0.3x0.38mm^2, TR/TE=4352ms/101ms, TF=21, NSA=9. In case pancreatic tumour masses reached >2mm diameter, mice were euthanized and submitted to sample preparation.

8.11. Mouse dissection

Before necropsy, mice were anesthetized with isoflurane and subsequently, killed by cervical dislocation. Mice were fixed with needles for necropsy procedure, abdomen disinfected with 80% ethanol and cut open to access peritoneal cavity. Pancreatic tumour mass was extracted and washed in 1x PBS. Regional sampling was performed on primary tumour mass. Briefly, a cross section was cut from the global tumour mass and sampled for histology, representing a complete profile of the tumour. The poles of the primary tumour mass were cut into smaller pieces and submitted to primary culture establishment and stored in RNAlater at -20°C for long

term storage. Routinely, main pancreatic metastatic routes such as liver, lung and lymph nodes were inspected for macroscopic nodules. In case the mouse presented metastasis, nodules were sampled individually for primary culture, gDNA/RNA extraction and histology. Other organs including small and large intestine, spleen and stomach were also taken for histology and gDNA/RNA isolation and tail and ear as "normal gDNA control".

8.12. Histology, hematoxylin and eosin (H&E) staining and IHC

For histology, normal tissue and tumour samples were processed as described above. Paraffin-embedded specimens were cut on a Microm HM355S microtome (Thermo Fisher Scientific) in 2µm thick sections. For H&E staining, sections were dewaxed by incubation in Roti® Histol (2x 5min), rehydrated in decreasing ethanol series (2x 99%, 2x 96% and 2x 70%, 1min each) and incubated in distilled water. Next, sections were placed for 10s in hematoxylin and blued for 5min in running tap water. For acidophilic counter staining, sections were incubated for 30s in eosin solution, washed in distilled water and submitted to an increasing ethanol series (2x 70%, 2x 96%, 2x 99%, 1min each). Eventually, slides were incubated in Roti® Histol (2x 5min) and cover-slipped with mounting medium for long-term storage.

For standard IHC, pre-treatment procedures for the antigen retrieval were adapted to each antibody used. To this end, sections were de-paraffinized as stated above. For primary antibodies Cytokeratin 19 (Hybridoma bank TROMAIIIc, host: rat, 1:500) and GFP (Fitzgerald, host: rabbit, 1:200), samples were boiled in ethylenediaminetetraacetic acid at 100°C solution for 20min and for E-cadherin (Cell signalling, host: rabbit, 1:400) and cleaved caspase 3 (Cell signalling, host: rabbit, 1:200), samples were boiled in 10mM sodium citrate buffer, pH 6.0 at 95°C for 10min. After chilling to room temperature, sections were rinsed with distilled water and pre-incubated in 3% H_2O_2 solution in the dark for 15min to remove endogenous peroxidase activity. Briefly, specimens were washed three times in PBS and blocked for 1h in blocking solution (5% bovine serum albumin (BSA in PBS). After one washing step in PBS, sections were incubated overnight at 4°C in blocking solution supplemented with primary antibodies in stated dilutions. Specimens were washed three times in PBS to remove excess primary antibodies. For visualization, either horseradish mouse anti-rabbit (Dako, 1:300) or secondary rabbit anti-rat antibody (Jackson Immuno Research, 1:1000) were used. Slides were washed carefully with PBS. Detection of peroxidase-labelled secondary-primary antibody complexes was performed by following the manufacturer's instructions of the Bond Polymer Refine Detection Kit on a Bond Max staining instrument. Eventually, slides were counter-stained with hematoxylin and mounted as described above.

8.13. Analysis of stained specimens

For histologic examination, H&E and IHC stainings were recorded on an Axio Imager.A1 microscope attached to an AxioCam HRc and AxioVision 4.8 software package. Scale bars are stated individually in each figure legend and representative pictures are shown. Quantification of cleaved caspase 3 cells was performed by a blinded pathologist. Grading of mouse pancreatic cancers was performed by trained veterinary pathologist Dr. Katja Steiger according to the consensus report of genetically engineered mouse models published in (Hruban *et al.*, 2006).

8.14. Establishment of primary cultures of pancreatic tumours

Primary mouse pancreatic cancer cultures were maintained in standard culturing medium (Dulbecco's Modified Eagle Medium (DMEM) supplemented with 10% fetal calf serum (FCS) and 1x P/S). For isolation of primary mouse cancer cultures, regionally sampled tumour tissues and individual metastasis were washed in PBS and cut into small pieces using a scalpel under sterile biological safety cabinet. Next, cancer samples were transferred in culturing medium without FCS containing collagenase digestion media (200units/mL collagenase type 2 and incubated at 37°C at 750rpm on an orbital shaker for 1-12h depending on the size of the tissue pieces. Cell suspension was centrifuged for 5min at 350g and pelleted cells seeded in a six-well plate. In case primary cultures attached and grew confluent, cells were passaged approximately 1:3 until T175cm^{2-}sized flask was reached. Briefly, culturing medium was removed, cells washed in PBS without Ca$_2$Cl$_2$ and incubated in trypsin/ ethylenediaminetetraacetic acid (EDTA) at 37°C until cells detached. After stopping trypsinization process by adding culturing medium, supernatant was removed by pelleting cells for 5min at 350g and cells seeded in the required dilution in a new vessel containing normal culturing medium. If a precise cell number was needed, a Neubauer counting chamber was used. For cryopreservation, trypsinized cells were re-suspended in ice-cold freezing medium (50% FCS, 40% DMEM, 10% dimethyl sulfoxide (DMSO)), transferred to CryoPure tubes and gradually frozen to -80°C (1-3°C per minute) in an isopropanol-filled freezing container. Primary cultures were kept in liquid nitrogen for long-term storage.

8.15. gDNA isolation and Sanger sequencing

gDNA from mouse tissue (Stored in RNAlater®) was extracted by cutting tissue pieces using a clean scalpel and overnight incubation at 55°C and orbital shaking in proteinase K solution included in the DNeasy blood and tissue Kit. Pelleted primary cultures were lysed for 10min at 55°C in the same proteinase K solution and gDNA extracted by following the manufacturer's instructions (Qiagen). The gDNA concentration of each sample was measured using the Qubit

fluorometer detecting specifically dsDNA. For amplification of targeted loci, proof-reading Q5® High-Fidelity DNA Polymerase was used according to the instruction manual. Primer pairs spanning the genomic region of Cas9 double strand breakage were designed using the latest Primer-BLAST tool (https://www.ncbi.nlm.nih.gov/tools/primer-blast/). All pairs meet the condition of generating a product between 400-500bp, whereby the PAM is located decentralized on the amplicon (SURVEYOR™ assay).

For Sanger capillary sequencing, 25ng of respective gDNA sample were submitted toQ5® PCR for 35 cycles and products inspected on a 1.5% agarose gel in 1x TAE buffer. If successful, amplicons were purified using the QIAquick PCR Purification Kit (Qiagen) according manufacturer's instructions and PCR reactions were sequenced individually using the corresponding primer at an external provider (https://www.eurofinsgenomics.eu/). Sequence traces were aligned to the annotated locus using SnapGene® (3.1.4 software version) and analysed for indel events using the TIDE deconvoluting tool (Brinkman *et al.*, 2014).

8.16. Amplicon-based deep sequencing of CRISPR/Cas9 targets

gDNA extraction of cancer samples and proof-reading PCR of sgRNA on- and off-target sites (Table 11 and 13) were performed as described above. Twenty µL of each PCR reaction covering the CRISPR/Cas9 genomic target region derived from an individual sample were pooled and PCR purified (Qiagen). DNA concentration of pooled samples was measured using the Qubit instrument. Briefly, 1µg of pooled PCR product were end-repaired, A-tailed and adapter ligated following the manual of the NEBNext Ultra DNA Library Prep Kit and adapter sequence published elsewhere (Bronner *et al.*, 2014). For individual sample barcoding and amplification, a 50µL Q5® PCR reaction (12 cycles, T_a=62°C) with overhanging primers including P5 and P7 adapters for binding on the Illumina sequencing flow cell (Bronner *et al.*, 2014). Eventually, magnetic bead-based PCR purification (Agencourt AMPure XP Beads) was performed according to manufacturer's instructions and barcoded amplicons eluted in 45µL (0.9x) EB buffer. Identical volumes of barcoded samples were pooled and the final library quantified using a 2x SYBR Green qPCR mix and primer pairs published in (Bronner *et al.*, 2014) against standardized amount of DNA fragments included in the Kapa Biosystems library quantification kit. Briefly, for loading of the sequencing flow cell, library is denatured after 5min incubation in 0.2N sodium hydroxide and single stranded library fragments buffered in HT1 provided from Illumina. For de-multiplexing sample barcodes, 0.83µM of iPCRtagseq sequencing primer was spiked into the index read slot of the Illumina cartridge (Bronner *et al.*, 2014). In total, 8pM of denatured library including 20% PhiX reference DNA guaranteeing enough complexity to distinguish individual bases at the same position of the read were

sequenced on a MiSeq instrument in combination with the MiSeq Reagent Kit v2 for 600bp in paired-end mode.

8.17. Bioinformatical analyses

Bioinformatic analyses including mapping, filtering and pile-ups of sequenced reads were conducted by the bioinformaticians Maxim Barenboim and Thomas Engleitner in our group. Briefly, paired end reads (300bp from each side) generated on the Illumina MiSeq instrument were mapped using the BBMAP short read aligner (http://bbmap.sourceforge.net) with default setting onto the mouse reference genome (Ensembl release GRCm38p4, Genome reference consortium). Further analyses were performed on R version 3.2.2. Among several tested aligners, this package performed particularly well in annotating large deletions larger than 100bp (Weber *et al.*, 2015). After mapping, generated BAM files were sorted and indexed with samtools (v0.1.19 (Li *et al.*, 2009). BAM files were only extracted from properly paired reads, which were defined by the bitwise flag0x2 integrated in samtools. For display lines containing indel information in a pileup data format of the number of reads covering specific CRISPR/Cas9 target sites, samtools (v0.1.6) command with option (-i) was used. Pileup files were generated using VarScan (v2.3.6) pileup2indel command (Koboldt *et al.*, 2009). Detected indels were only considered true in case the mutation is supported by more than 100 variant reads. Variant allele frequencies were calculated at each CRISPR/Cas9 target sites.

8.18. PCR for detection of CRISPR/Cas9-mediated inter- and intrachomosomal deletions

For every possible intra-chromosomal fusion between sgRNA target sites on a single chromosome and for every multispectral-fluorescence in situ hybridisation (M-FISH)-indicated inter-chromosomal fusion, we performed TaKaRa *Ex Taq* PCR. In brief, 50ng of gDNA of each primary culture were submitted to TaKaRa *Ex Taq* PCR with respective primer pairs used to amplify sgRNA genomic targets (listed in Table 11) according to manufacturer's recommendations (35cycles, T_a=60°C). Five µL of each resulting PCR product were size-separated on a 1.5% agarose gel, and in case of a band present, remaining 25µL of the reaction mix was submitted to PCR purification as described above. Eventually, inter- as well as intra-chromosomal fusion PCR products were verified by Sanger capillary sequencing using appropriate forward primers.

8.19. Multispectral-fluorescence *in situ* hybridisation (M-FISH)

To analyse primary pancreatic tumour cultures for ploidy and inter-chromosomal translocations, M-FISH of chromosomes was performed according to published protocols (Jentsch *et al.*, 2001). Briefly, cells were grown to 50-70% confluency in a T75 flask using

standard culturing medium and treated for approximately 50min with 100µg/mL KaryoMAX™ Colcemid™ solution. Metaphase-arrested cells were washed in 1x PBS, swollen for 12min in pre-warmed hypotonic 0.56% potassium chloride buffer and subsequently fixated by drop-wise addition of Carnoy's solution (ice cold 3:1 methanol and acetic acid) without causing any physical shock to the tube. After spinning down, supernatant was removed; cell pellet re-suspended in 100% Carnoy's solution and flicked to singularize cells. The last step was repeated, and successful metaphase spread verified by dropping fixated instable cells onto a slide and checked under the microscope. Cell suspension was stored at -20°C and M-FISH performed by Dr. Fengtang Yang's lab at the Wellcome Trust Sanger Institute as described elsewhere (Jentsch *et al.*, 2001).

8.20. RNA isolation from cells, cDNA synthesis and qRT-PCR

Total RNA was isolated from cells grown to 60-80% confluency in a 10cm dish cultured in standard medium without P/S. Cells were washed in cold PBS, transferred to 400µL RLT buffer containing 1:100 ß-mercaptoethanol by scraping and homogenized using the QIAshredder micro-centrifugation tubes according to manufacturer's instructions. Homogenate was snap frozen on dry ice and stored at -80°C until further processing. RNA isolation was carried out using the RNeasy mini kit according to its protocols and gDNA was on-column digested following the instructions of the RNase-Free DNase set. Eluted total RNA concentration was determined with the Qubit RNA BR Assay kit. For reverse transcription, the SuperScript II protocol (Thermo Fisher) was performed using 1µg total RNA and random hexamers and oligo-dT primers. Suited mouse *Kras* target and *Gapdh* housekeeping primer pairs and probes were obtained using NCBI's primer-BLAST tool (https://www.ncbi.nlm.nih.gov/tools/primer-blast/) with a pre-defined 50-150bp amplicon size and separation of binding sites by an intron. Real-time qPCR was carried out with the TaqMan qPCR chemistry and on the StepOnePlus system. To check for primer specificity, a melting curve was included within each run. Data were analysed using the StepOne™ software and expression analysed against a standard curve.

8.21. RNA-seq analyses

Bulk 3'transcript end RNA-seq (SCRB-seq) libraries were generated on isolated RNA from primary cultures with the assistance of Rupert Öllinger and as described previously (Parekh *et al.*, 2016). Briefly, RNA was reverse transcribed using oligo-dT primer including sample barcodes, unique molecular identifiers (UMI) and adapter. Sample cDNA was pooled, residual primers digested using ExonucleaseI and amplified with KAPA HiFi ReadyMix. For library generation, 0.8ng of cDNA was tagmented and 3'ends amplified by following instructions of

the Nextera XT Kit (Illumina) combined with specific primers binding the 3'adapter. Eventually, the library was paired-end sequenced on a NextSeq 550 system with inverted P5 and P7 adapters allowing the sequencing of 51 cycles of transcript cDNA in read1 and 16 cycles of UMI and sample barcodes in read2. Sequencing data were processed by our bioinformaticians using the published Dropseq pipeline (version 1.0) (Macosko *et al.*, 2015) to generate gene-wise and UMI-wise transcript count matrices (Mueller *et al.*, 2018). For differential expression analyses, DEseq2 (Love *et al.*, 2014) was used. Genes were considered differentially regulated if the absolute $\log_2$(fold change) was above 0.8 and the adjusted *P* value was smaller than 0.05. Gene set enrichment analyses was conducted with the hypergeometric test implemented in the "Molecular Signature Database" (MSigDB) version 6.0 online tool (http://software.broadinstitute.org/gsea/msigdb/). Only enriched terms with a false discovery rate of $P \leq 10^{-4}$ were considered.

8.22. 3-(4,5-dimethyl-2-thiazolyl)-2,5-diphenyl-tetrazolium bromide (MTT) assay

For the measurement of cellular viability, MTT assay was performed which measures the activity of cytosolic and mitochondrial dehydrogenases. In principal, the MTT reagent is incorporated by living cells and is converted by NADH-dependent reductases into insoluble formazan. Five thousand cells were seeded per well in a 96-well plate in sextuplicates in standard culturing medium. After 24h (= time point 0), cells were changed to serum-depleted or standard culturing medium depending on the condition. Every other day, cells received fresh medium and were measured at indicated time points. For the measurement, cells were changed to DMEM medium containing 0.5mg/mL MTT and incubated for 4h at 37°C. Subsequently, MTT medium was carefully removed and formazan precipitate was re-solubilized by the addition of 100μL 1:1 DMSO/ethanol mixture per well and shaking for 10min protected from light. Eventually, optical density of the formazan was measured at 595nm using an Anthos 2001 spectrophotometer.

8.23. DNA damage response analyses by Western blotting

Doxorubicin treatment was performed in collaboration with Dr. Matthias Wirth. Briefly. mesenchymal and epithelial Panc021 cells were grown to 50% confluency in standard culturing medium without P/S in 10cm dishes. Doxorubicin was purchased from Sigma-Aldrich and cells treated for 24h with 1μM Doxorubicin in standard culturing medium. Briefly, 24h after treatment, bulk protein was harvested by washing twice in ice-cold PBS, scraping down of cells in RIPA buffer supplemented with protease and phosphatase inhibitors and incubation for 30min on ice. Subsequently, cell lysate was centrifuged for 20min at 4°C and >20'000g and

supernatant transferred to a fresh tube. Equal volumes of protein lysate were incubated in 5x Laemmli buffer for 5min at 95°C and submitted to sodium dodecyl sulfate polyacrylamide gel electrophoresis (SDS-PAGE) using 10% separation gel overlaid by a 4% stacking gel (Laemmli, 1970). Eighty µg of protein samples per condition were loaded, electrophoresis conducted initially at low voltage for immigrating of charged linearized protein species into the gel and for size-separation at 100V for approximately one hour. Subsequently, gel was released and blotted onto a polyvinylidene difluoride (PVDF) membrane in a tank blot system at 4°C and 100V for 2h (Towbin *et al.*, 1979). Membranes were blocked with 5% BSA and 0.01% Tween20 in PBS for 1h and gentle rocking. Primary antibodies (ß-actin (A5316, Sigma-Aldrich); p53 (CM5, Leica Biosystems); p21 (sc-397, Santa Cruz Biotechnology); pH2AX (Ser139, Clone JBW301, 05-636, Millipore) and p-Chk1 (S317/A300-163A, Bethyl Laboratories) were diluted according to vendor's recommendation for Western blotting in 5% BSA and 0.1% Tween20 in PBS. After overnight incubation at 4°C, primary antibody solution was washed away three times and membrane incubated with corresponding secondary antibody diluted in 5% BSA in PBS at room temperature for 1h. After three consecutive washing steps in 0.1% Tween20 in PBS, antibody conjugates were visualized using the Odyssey Infrared Imaging System (Licor, Bad Homburg, Germany).

9. Results

Parts of individual figures and respective written contents have been previously published in the scientific paper "Multiplexed pancreatic genome engineering and cancer induction by transfection-based CRISPR/Cas9 delivery in mice", Maresch, Mueller et al. (Nature Communications volume 7, Article number: 10770 (2016)). The establishment of electroporation-based transfection procedure, primary culturing of cancers, sample generation and library preparation for NGS was performed by myself with essential help of Sebastian Müller. The wet-lab contributions and bioinformatic analysis of NGS raw data of co-authors and colleagues are stated in the methods section. All data interpretations and resulting conclusions were conducted by myself. All adapted figures from the previous publication are denoted in respective figure legends.

9.1. Electroporation-based transfection for delivery of pDNA into somatic cells

In this study, I explored the possibility to establish a protocol for the direct transfection of pancreatic cells in adult mice with exogenous DNA particles based on electroporation. In short, electroporation allowed the transfer of large and charged molecules like pDNA through the membranous lipid bilayer of living cells. The application of a certain voltage to amphipathic membranous systems induced a dynamic condition of electrostatic attraction and repulsion in the cellular membrane (Somiari *et al.*, 2000; Neumann *et al.*, 1982). The applied electric voltages generated transient water-filled pores in the lipid bilayer of cells, allowing the electrophoretic passage of charged molecules (e.g. pDNA, molecular probes or drugs) into the cytoplasm. The amplitudes and the duration of applied electric voltages determined the extent of the loss of semipermeability. Mild electric pulses (e.g. 50V per 7mm^2 of tissue lasting for maximally 50ms for the pancreas) caused only a short influx of extracellular components, which facilitated complete recovery of targeted pancreatic cells. Without electrostatic formation of pores, charged molecules would otherwise never passively diffuse through the bilayer membrane of the cell. For direct *in vivo* electroporation of parenchyma cells, forceps-type electrodes were used to apply electric pulses onto the pancreatic tissue and to permeabilize the lipid bilayer for the uptake of pDNA particles into resident cells.

To this end, laparotomy on anaesthetised mice was performed to mobilize the pancreas for the intra-parenchymal injection of pDNA (Figure 1a). After injection of 50µl vector mix, the cannula was carefully retracted to avoid leakage of the bleb. The Nepa21 square-pulse generator was combined with forceps-like electrodes suitable for pDNA transfer to the pancreas. Electrodes were applied to "sandwich" the bleb containing pDNA particles and the

parenchyma. Two sets of electric pulses were generated to enable optimized *in vivo* transfection of local pancreatic cells (Figure 1b,c). After delivery, the pancreas was placed back into the abdominal cavity, the incision sutured, and the mice scored for clinical symptoms on a regular basis (Detailed description is provided in Materials and Methods section).
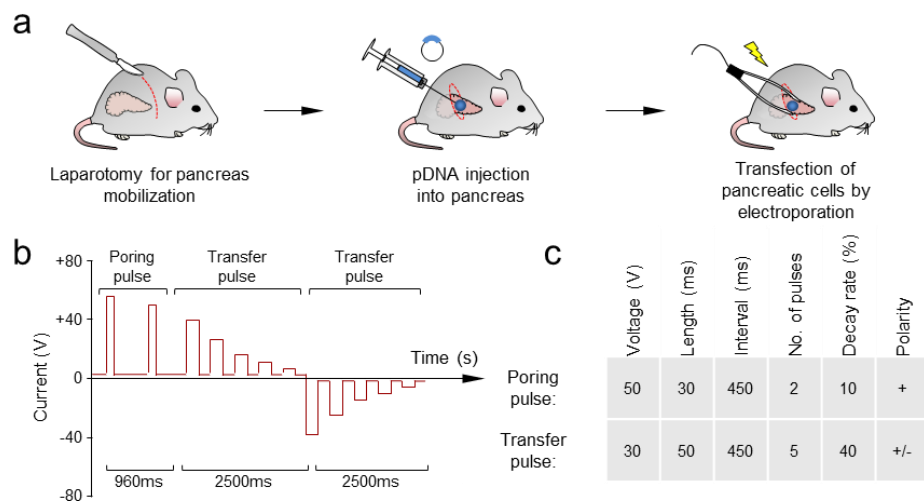
Figure 1 | *In vivo* electroporation for direct transfection of pancreatic cells in mice. a, Illustration of the *in vivo* electroporation procedure. **b**, The square-pulse electroporater was capable to generate four different sets of electric pulses. First, two uniphase peaks of poring pulses induced pore formation in cellular membranes by applying short but high-amplitude electric currents. Second, reversed-phase sets of five long-duration pulses allowed for the electro-kinetic transfer of pDNA into the cells. **c**, Table containing relevant physical properties of the optimized electric pulse sets enabling efficient *in vivo* gene transfer to pancreatic cells. **a-c**, adapted from (Maresch *et al.*, 2016).

9.2. Efficiency of electroporation-based transfection in mouse pancreatic cells

To determine the number of targeted pancreatic cells, electroporation of a green fluorescent protein (GFP) reporter construct was performed. The GFP reporter expression was supported from the cytomegalovirus (CMV) promoter. GFP-positive cells two days post electroporation (PE) were counted (Figure 2a). For the relocation of the electroporated pancreatic tissue area during necropsy, permanent endoscopic marker (1:10) was supplemented to the injection mix (Figure 2b). IHC against GFP was performed on formalin-fixed paraffin embedded (FFPE) specimens. Analysis of endogenous GFP fluorescence by fluorescence microscopy was hampered by the high degree of autofluorescence in the pancreas limiting the identification of low-level GFP-expressing cells (Data not shown). To correct for the number of false positive cells, mock-electroporated mice were included into the analysis. For each electroporated pancreas, twelve cuts over a range of 1mm pancreatic tissue were counted for GFP-positive cells as determined by IHC and projected over the area of electroporation (Methods). On average, 749 transfected cells, which resided exclusively in the ink-labelled region of the pancreas, were detected (Figure 2c,d).
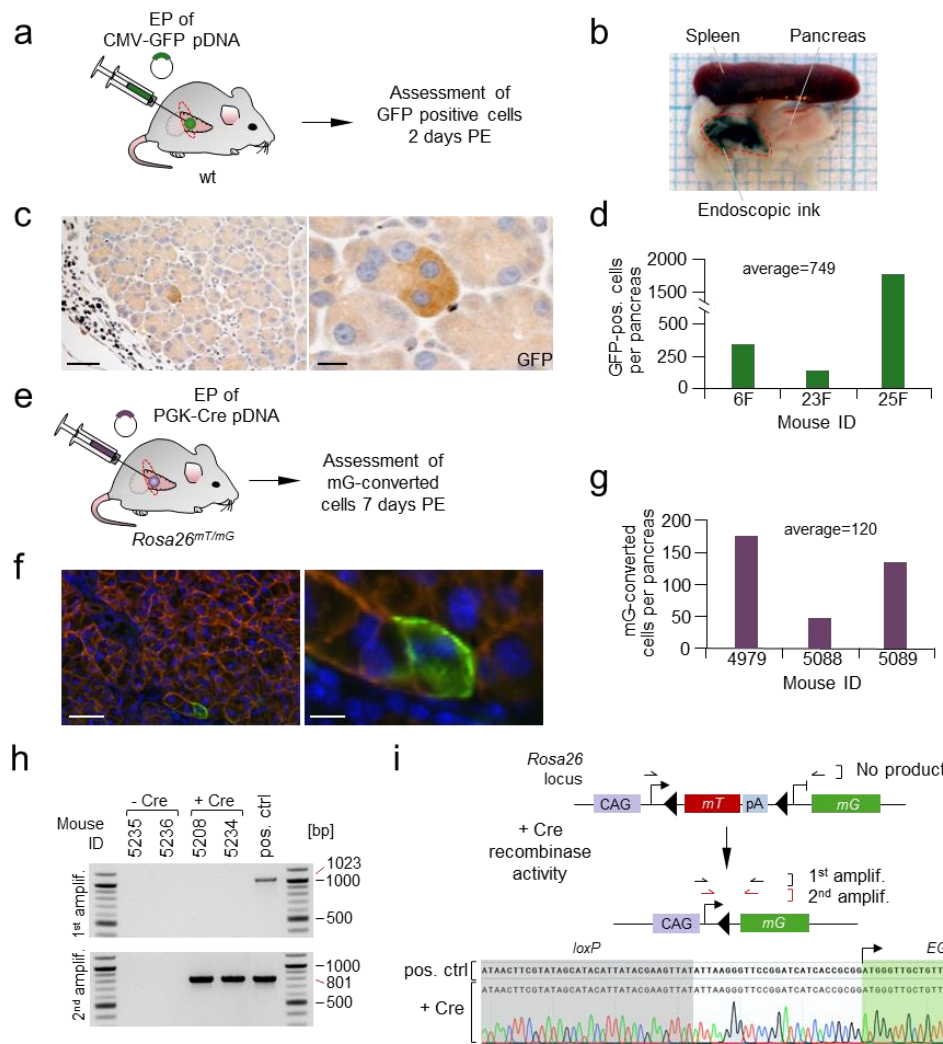
Figure 2 | Determination of the number of pancreatic cells transfected by electroporation in mice. **a**, Illustration of the workflow for the delivery of a GFP-expressing vector into mouse pancreatic cells. **b**, Permanent endoscopic marker was used to relocate area of transfected cells. Note that the range of targeted cells is restricted to the local area of electroporation/ink. **c**, IHC against GFP was performed 2 days PE to analyse the efficiency of transfected cells per mouse. Left image features immune cells clearing endoscopic ink that marks region of interest. Scale bars, 50μm left and 10μm right. **d**, Three GFP-electroporated mice were systemically analysed in the area of electroporation by counting stage cuts to estimate the total number of positive cells per targeted pancreas. **e**, Illustration shows experimental procedure to account for the number of long-term surviving pancreatic cells. **f**, PGK-driven Cre recombinase mediates the excision of the red mT cassette and allowed permanent expression of membranous GFP fluorescent protein in pancreatic cells 7 days PE. Scale bars, 50μm left and 10μm right. **g**, Enumeration of GFP-positive cells in the area of electroporation in three mice after 7 days. **h**, Two *Rosa26^{mT/mG}* reporter mice were electroporated with or without PGK-Cre, gDNA isolated and submitted to nested PCR amplifying only recombined mT/mG reporter allele. gDNA of a *Ptf1a^{Cre/+};Rosa26^{mT/mG}* mouse was used as a positive control (See Methods). Red lines indicate prospected size of amplicons. **i**, Nested PCR products of all samples were Sanger sequenced and confirmed the excision of the mT-Stop cassette in pancreata electroporated with PGK-Cre. **a-i**, adapted from (Maresch *et al.*, 2016).

Because localized acute tissue damage caused by the dissipation of electric energy was observed, we speculated whether the electroporation procedure had detrimental consequences on the number of targeted cells. To elaborate on the number of cells that had survived acute inflammation, electroporation of a PGK promoter-driven *Cre* recombinase into *Rosa26^{mT/mG}* reporter mice was performed (Figure 2e). The knock-in *Rosa26^{mT/mG}* mouse consisted of a loxP-flanked tdTomato cassette and a downstream GFP, that can be localized to the membrane. In presence of *Cre* activity, otherwise red tdTomato-positive cells would convert to green GFP-positive cells. This approach allowed for the permanent labelling of electroporated cells. After seven days, three *Cre* recombinase and mock electroporated *Rosa26^{mT/mG}* pancreata were collected and fluorescence-based quantification of endogenously marked cells was performed (Figure 2f). While mock electroporated mice never showed GFP-converted cells, a mean of 120 long-term surviving cells (n=3 mice) in *Cre*-transfected *Rosa26^{mT/mG}* pancreata was found (Figure 2g). To verify *Cre*-mediated recombination at the genetic level, to exclude the possibility of mutations affecting the GFP expression (a scenario that was conceivable considering the low number of targeted cells) and because of autofluorescence, a nested PCR approach of control and *Cre* recombinase electroporated mice was conducted (n=2 mice per group). While mock electroporated *Rosa26^{mT/mG}* pancreata showed no sign of spontaneous recombination/mutation at the reporter locus, mice that had received the *Cre* expressing plasmid showed a PCR product after second chain reaction at the expected size. The emergence of an amplicon only after a nested PCR approach reflected the low frequency of successfully targeted cells (Figure 2h). For further proof of this finding, the *Cre*-targeted amplicons were submitted to Sanger sequencing. Both nested PCR products shared complete sequence identity compared to the positive control confirming GFP recombination due to *Cre* activity in the mouse pancreatic cells (Figure 2i). As it is known, that excessive loads of *Cre* protein could exert toxic functions to the cell (Schmidt-Supprian *et al.*, 2007) and many individual vector particles could enter single cells by electroporation-based transfection, the actual number of successfully targeted cells might be underrepresented in this experiment. By combining results of both experiments, the short-term GFP expression from the vector and the long-term endogenous reporter allele recombination, we projected that several hundred pancreatic cells could be targeted during the electroporation procedure.

9.3. Effects of electroporation on pancreatic tissue

We further investigated the side effects of the electroporation on the pancreatic tissue. To this end, three mock electroporated wildtype mice at 2-, 7- and 21-days PE were histologically analysed. At the area of electroporation, mild to moderate inter- as well as intralobular

infiltration of macrophages and neutrophils and occasionally, also acinar cell vacuolization was found two days PE (Figure 3a). Seven days PE, the inter- and intralobular immune cell infiltrate contained lymphocytes as well as macrophages that carried phagocytosed dark-brownish pigment (likely residuals of endoscopic ink and cell debris). Moreover, one of three mice comprised focal ADM (Figure 3a). In all wildtype mice, complete tissue regeneration and ablation of inflammatory response was observed 21 days PE, apart from focal accumulations of macrophages removing permanent endoscopic ink (Figure 3a). Likewise, active caspase-3 staining of electroporated pancreata showed increased rates of apoptosis two days PE, which returned back to non-electroporated levels seven days PE (Figure 3b,c). Restricted necrosis of single pancreatic cells, observed two days PE, was abrogated and cleared by the immune system seven days after the procedure.
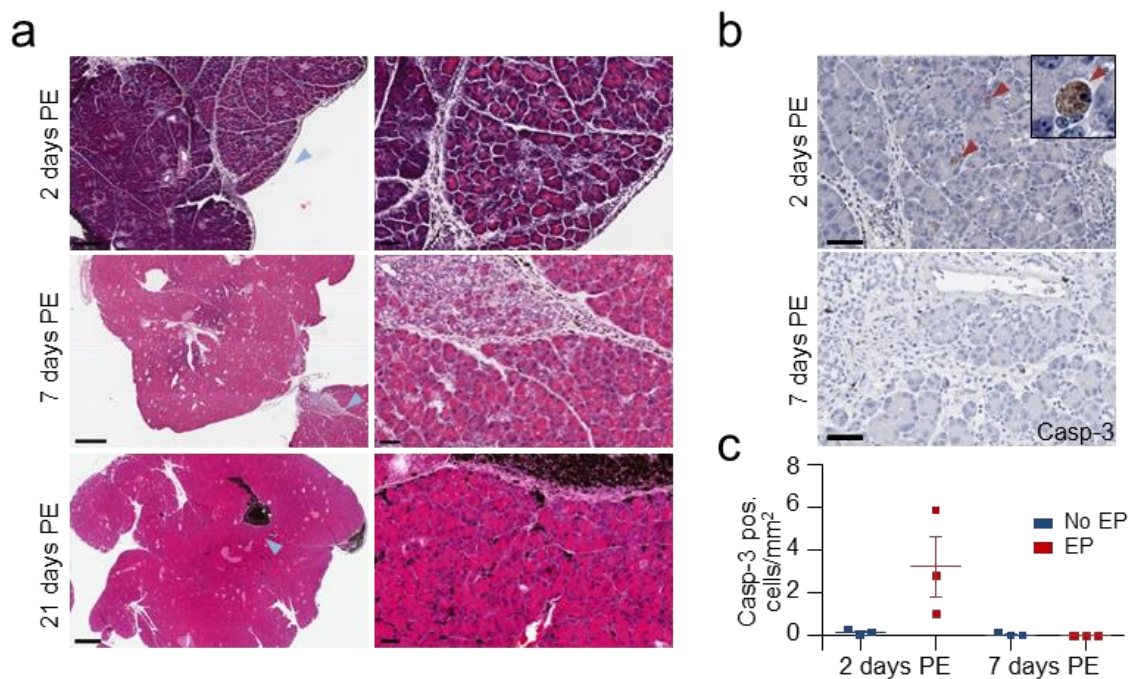
Figure 3 | Pancreatic tissue damage after electroporation. a, Pathohistology of the pancreas in electroporated wild-type mice was analysed 2, 7 and 21 days after procedure (n=3 mice per time point). Representative images are shown. Two days PE (Top panel), H&E staining revealed cytoplasmic vacuolization of few acinar cells and low-grade to moderate inter- as well as intralobular infiltration of neutrophils and macrophages to the site of electroporation. Seven days PE (Middle panel), moderate invasion of lymphocytes was detected together with macrophages and neutrophils. After 21 days, all mice have undergone a full regeneration of the acinar cell compartment of the pancreas and localized inflammation was cleared. Permanent endoscopic ink was present in all time points. Light-blue arrow heads indicate area of magnification. Scale bars, top left 200μm, mid/bottom left 500μm and right 50μm. **b,** Cleaved caspase-3 IHC in wild-type pancreata of mice 2 days PE (top) and 7 days (bottom) after the procedure. Red arrow heads indicate apoptosis in pancreatic cells. Scale bars, 50μm. **c,** Quantification of apoptotic cells per mm^2 in wild-type pancreata of electroporated and mock operated mice at indicated time points. Data is shown as mean ± s.e.m. of three independent replicates. **a-c,** adapted from (Maresch *et al.*, 2016).

In summary, the results of the pathohistological examination revealed that *in vivo* electroporation caused a tolerable completely reversible acute inflammation of wild-type pancreata, which showed no signs of progression to a chronic self-sustaining inflammatory response.

9.4. CRISPR/Cas9 gene editing in transfected pancreata

A major motivation of this study was to use the advantage of the transfection-based electroporation to deliver simultaneously multiple CRISPR/Cas9 constructs to individual cells of the mouse pancreas. This feature of electroporation cannot be achieved to a similar extent using viral somatic gene targeting strategies such as AAV. The multiplexing of sgRNA vectors in combination with the expression of Cas9 nuclease enzyme would allow the editing of several genetic targets in individual cells simultaneously. Most frequently mutated genes in pancreatic cancer were selected for gene editing in the adult mouse pancreas (Table 15). In total, 15 sgRNAs, including two *Rosa26* targeting sgRNAs, were used.

Two additional neutral sgRNAs against the *Rosa26* locus that had no effect on pancreatic tumorigenesis, were also included. All 15 sgRNA sequences were cloned in a modified version of the pX330 vector (CRISPR-SB) supporting the transcription of the sgRNA and the Cas9 nuclease from the U6 and the Cbh promoter, respectively (Figure 4a, (Weber *et al.*, 2015). The CRISPR-SB vector flanked essential CRISPR/Cas9 components with *Sleeping Beauty* inverted terminal repeats. In combination with *Sleeping Beauty* transposase activity, the complete CRISPR/Cas9 cassette could stably integrate into the genome. This would lead to a permanent expression of the CRISPR components; however, this feature was not used in this study. For identification of uniform sgRNA cleavage performance across all genetic targets, 2-3 sgRNAs per locus were tested *in vitro* and the one with the highest cleavage efficiency was used for *in vivo* electroporation (Data not shown). PPT 4072 pancreatic primary culture featured intact alleles for all sgRNA target sites and was therefore transfected with selected sgRNAs. Figure 4b depicts the SURVEYOR™ assay of PPT 4072. The analysis of cleavage bands showed a uniform distribution of insertion/deletion (indel) frequencies across all edited loci (Figure 4c).

Table 15. TSGs reported to be involved in human pancreatic tumorigenesis. Tumour suppressor genes targeted by CRISPR/Cas9 as well as their mutation type and reported frequency of inactivation in human pancreatic cancer are given. Numbers in brackets correspond to mutated cases per total cases included within each individual study. #, acinar cell carcinoma; *, germ line mutation; LOSS, loss of gene expression; DEL, large genetic deletion; MUT, mutation of respective gene; PM, promoter methylation and METH, gene methylation.

Genes	Type	Range	References
APC	MUT	9%	(2/23)# (Jiao *et al.*, 2014)
	DEL, METH, LOSS	48%, 56%, 58%	(12/25, 24/43, 14/24) (Furlan *et al.*, 2014)
ARID1A	MUT	9%	(2/23)#(Jiao *et al.*, 2014)
	MUT	4%	(4/99)(Biankin *et al.*, 2012)
	MUT	8%	(2/24)(Jones *et al.*, 2008)
ARID1B	DEL	4%	(3/77)(Shain *et al.*, 2012)
ARID5B	---	---	---
ATM	MUT	4%	(1/23)#(Jiao *et al.*, 2014)
	MUT	5%	(5/99)(Biankin *et al.*, 2012)
BRCA1	MUT	13%	(15/112)*(Lynch *et al.*, 2004)
BRCA2	MUT	10%	(4/41)*(Goggins *et al.*, 1996)
	MUT	10%	(4/39)*(Ozcelik *et al.*, 1997)
	MUT	4%	(1/23)# (Jiao *et al.*, 2014)
CDKN2A	DEL, MUT	41%, 38%	(15/37, 14/37)(Caldas *et al.*, 1994)
	DEL, MUT, PM	48%, 34%, 14%	(24/50, 17/50,7/50)(Schutte *et al.*, 1997)
CDKN2B	---	---	---
TP53	MUT	70%	(19/27)(Redston *et al.*, 1994)
	MUT	33%	(33/99)(Biankin *et al.*, 2012)
	MUT	75%	(18/24)(Jones *et al.*, 2008)
	MUT	13%	(3/23)#(Jiao *et al.*, 2014)
PTEN	LOSS	63%	(5/8)(Asano *et al.*, 2004)
SMAD4	LOSS, MUT, DEL	37%	(31/84)(Hahn *et al.*, 1996)
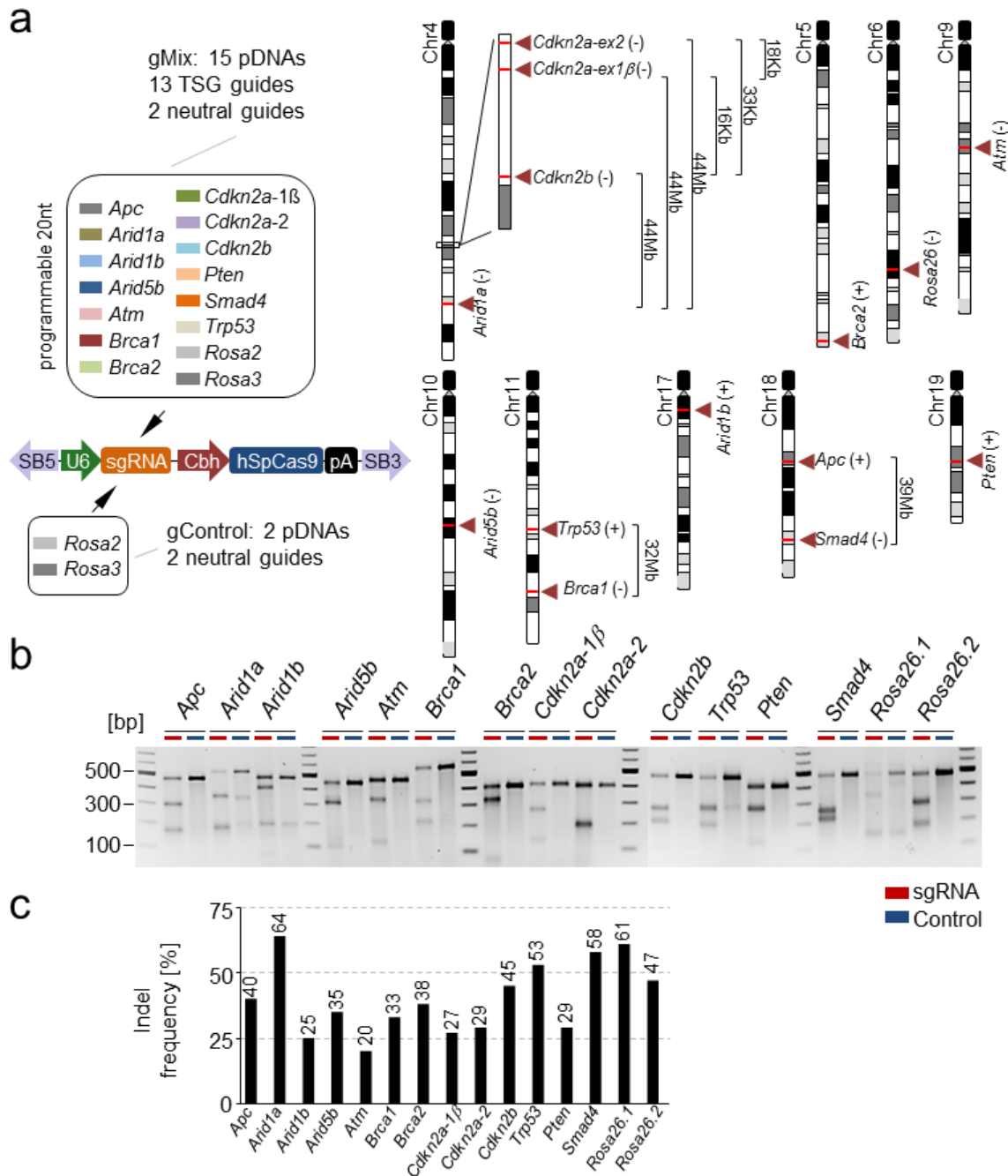
Figure 4 | CRISPR/Cas9 vector generation and validation of sgRNA cleavage efficiency. a, A modified version of the pX330 CRISPR/Cas9 vector was used to clone individual sgRNAs. gMix vector combination includes 13 sgRNAs targeting known pancreatic TSGs and two neutral sgRNAs. As control, the gControl vector mix was used to inactivate only non-oncogenic *Rosa26* gene. In our setting, the SB-CRISPR vector enableed transient codon-optimized *S. pyrogenes* Cas9 (hSpCas9) enzyme expression under the control of a Cbh promoter. sgRNA expression was driven by the human U6 promoter. pA, polyadenylation signal; SB, sleeping beauty inverted terminal repeat. Right panel shows targeted chromosomes and highlights distance between possible intra-chromosomal breakpoints. Chr, chromosome. **b**, SURVEYOR™ endonuclease assay was performed to determine equal sgRNA cleavage potential between individual sgRNAs in a murine primary cancer cell line with intact loci at all binding sites. Control was a sgRNA targeting the *Rosa26* locus. **c**, Graph shows optical density analysis of cut PCR products (harbouring indel mutations) in percentage of the total intensity. On average, sgRNAs cutting efficiency averaged at ~40%. **A-b**, adapted from (Maresch *et al.*, 2016).

9.5. *In vivo* electroporation for CRISPR/Cas9-mediated pancreatic cancer induction

To explore the possibility of multiplexed *in vivo* genome editing in mice, equimolar amounts of different sgRNA vectors targeting relevant TSGs in pancreatic cancer were mixed (Figure 5a). As control cohort to the gMix receiving mice, sgRNAs only targeting the neutral *Rosa26* locus were included into the study (Figure 5a). Around 95% of human pancreatic cancer patients present an activating *KRAS* mutation (Ryan *et al.*, 2014). To model the human situation, *Ptf1a*$^{Cre/+}$ and *Kras*$^{LSL-G12D/+}$ mice (PK) were inter-crossed. As previously published, PK mice showed a median survival of 472 days (Range of 263 to 844 days; n=55) (Eser *et al.*, 2013). Importantly, PK mice only present low-grade PanIN lesions at 3 months of age (~100 days), but no progression to invasive pancreatic cancer (Eser *et al.*, 2013). PK mice were distributed randomly to either the gMix or gControl cohort and *in vivo* electroporated. Subsequently, mice were regularly scored for clinical symptoms and monitored for tumour induction by MRI or palpating over a time course of 6 months (Figure 5a,b). We observed a tremendous acceleration of pancreatic cancer formation in PK mice electroporated with gMix compared to the gControl cohort (Figure 5c). Electroporation of the gMix resulted in a median time to tumour formation of 10.7 weeks after TSG inactivation. Within the observation time, 7 out of 13 gMix-receiving mice (54%) featured pancreatic tumorigenesis compared to none in the "neutral" gControl cohort (n=8; *P*=0.016; log-rank test; Figure 5c).
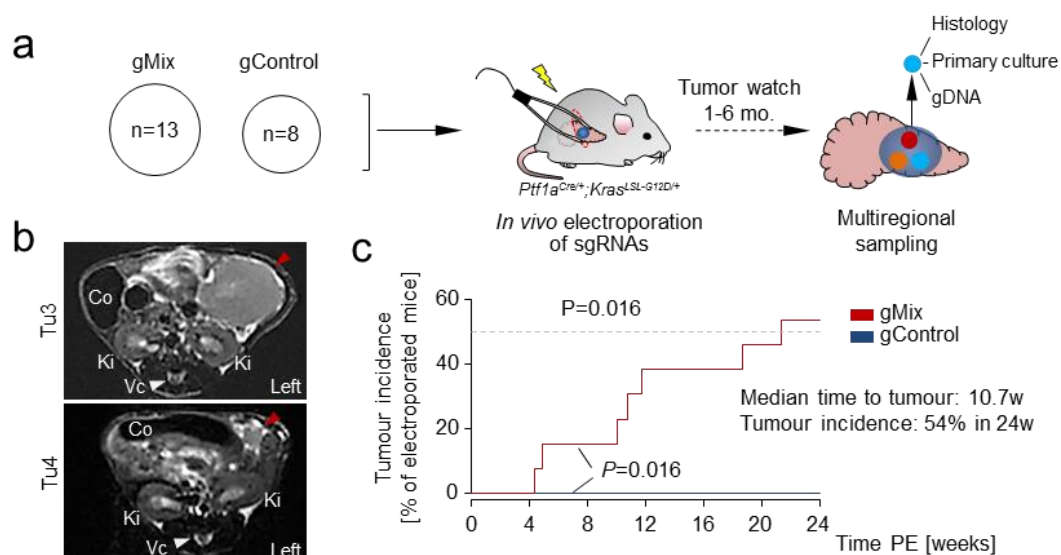

Figure 5 | *In vivo* electroporation with multiple CRISPR/Cas9 vectors targeting PDAC-relevant TSGs lead to an acceleration of pancreatic cancer formation in *Ptf1a*$^{Cre/+}$;*Kras*$^{LSL-G12D/+}$ mice. a, In total, 13 mice were electroporated with the gMix and eight with the gControl equimolar mixture. Cartoon depicts the workflow. Over a time of 6 months, mice were regularly monitored by MRI imaging and palpating of the abdominal cavity for pancreatic cancer growth. In case a tumour was detected, regional sampling was performed. **b**, Representative T2-weigthed MRI sections of a pancreatic tumour mass (top) and a small lesion (bottom) in indicated mice. Red arrow head points at the pancreatic lesion. Co, colon; Ki, kidney and Vc, vertebral column. **c**, Graph shows the time to tumour formation in gMix (n=13) and gControl cohort (n=8). *P*=0.016; log-rank test. **b-c**, adapted from (Maresch *et al.*, 2016).

9.6. Histopathology of CRISPR/Cas9-edited pancreatic cancers

Examination of the histopathology of pancreatic tumours and metastases revealed a broad spectrum of pancreatic cancer histology, from well-differentiated to completely undifferentiated or sarcomatoid/anaplastic tumours (Figure 6a-f). To exclude the possibility, IHC for epithelial markers in all undifferentiated cancer cases was performed. In theory, a sarcoma could also develop through accidental electroporation of sgRNAs targeting resident stromal cells in the pancreas. Cytokeratin19 (CK19) and E-Cadherin staining confirmed pancreatic parenchyma origin because all undifferentiated cancers contained epithelial marker-positive, ductal-like structures (Figure 6g). Primary cancer cultures were isolated from all mice succumbing to pancreatic cancer. In all electroporated cancers, PCR indicated *Cre*-mediated recombination of the engineered *Kras*$^{LSL-G12D}$ allele in PK mice, thus evidencing for the cancer origin from the exocrine *Ptf1a*-expressing cell lineage (Data not shown). Roughly, the morphology of primary 2D cultures resembled histology of respective tumours. Well-differentiated cancers were more of epithelial appearance and undifferentiated displayed a more mesenchymal phenotype (Figure 6h-m).

In summary, electroporation of CRISPR/Cas9 vectors targeting relevant pancreatic TSGs led to a significant reduction of the time to tumour formation compared to the gControl cohort. CRISPR/Cas9-edited cancers represented similar histopathologic phenotypes as observed in other common mouse pancreatic cancer models.
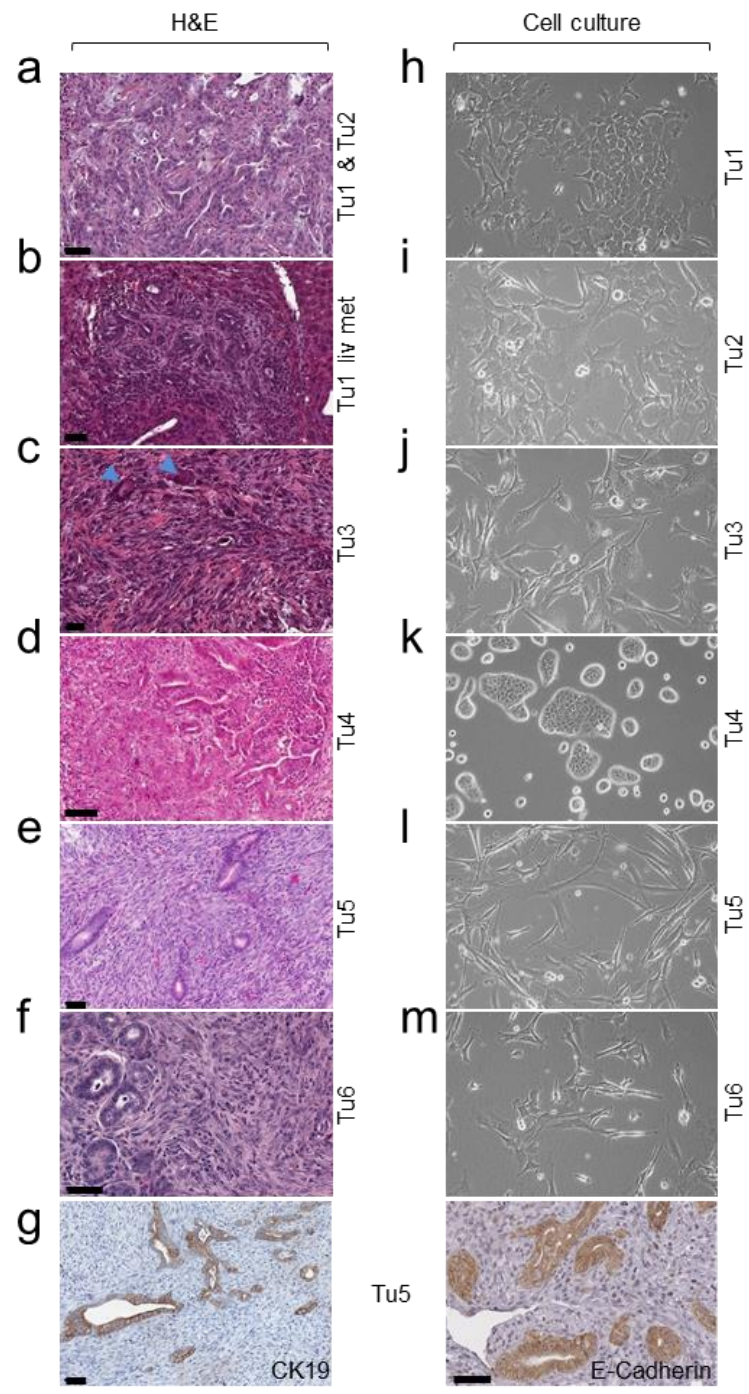
Figure 6 | Histopathology of pancreatic cancers and morphology of isolated 2D primary cultures.
a-f, *In vivo* CRISPR/Cas9-based mutagenesis targeting key pancreatic TSGs in *Ptf1a*$^{Cre/+}$;*Kras*$^{LSL-G12D/+}$ mice lead to PDAC development. Differentiation stage was revealed by H&E staining. **a,d**, H&E stainings show representative areas of moderately (G2-3) differentiated PDACs and associated liver metastasis of Tu1 matching with the primary G2-G3 differentiation. **c,e,f**, Poorly-differentiated sarcomatoid G4 PDAC with typical anaplastic giant cells in Tu3 (**c**, blue arrow heads). **g**, CK19 (ductal marker) and E-cadherin (epithelial marker) IHCs of all sarcomatoid G4 tumours were performed to verify exocrine origin of the pancreas. Representative pictures of Tu5 are shown. Scale bars, 50μm. **h-m**, Brightfield microscopic pictures revealed morphologic heterogeneity in primary cultures. 10x magnification. **a-e** and **g**, adapted from (Maresch *et al.*, 2016).

9.7. CRISPR/Cas9-based genome editing for somatic pancreatic cancer modelling

For the analysis of CRISPR/Cas9-based mutagenesis at individually targeted tumour suppressor loci, amplicon-based next generation sequencing (NGS) was conducted. All cancer tissues as well as the isolated primary cultures originating from different regions of the cancer (regional sampling) and, if available, amplicons of healthy pancreatic tissues from electroporated mice were submitted to NGS analysis (Figure 5a). Therefore, a protocol for the combination of single PCRs from all edited loci in a sample was set up to reduce the workload for the library preparation. A critical problem was the mapping strategy for the analysis of CRISPR/Cas9 gene editing frequencies. Because sequenced reads also contained Cas9-induced large indel mutations, they were often mistakenly filtered out and lost to the analysis. Therefore, standard bioinformatic tools to process and correctly map edited reads sequenced from targeted loci were optimized by bioinformaticians in our group (See in Methods section).

Variant allele frequencies (VAFs) at all CRISPR/Cas9 target sites were determined by amplicon-based deep sequencing. In Figure 7a, multiple mutations at the individual targeted loci were combined as cumulative variant reads in each tumour. Adjacent normal tissues to pancreatic cancers never showed evidence for indels at sgRNA target sites (Figure 7a). The pancreatic tissues of gControl samples also indicated no detectable variant allele reads at *Rosa26* target site or random mutations in 13 other TSGs after 6 months (Data not shown). This result suggested that ultra-deep sequencing (>10,000 reads/amplicon) could not detect variant reads in targeted *Rosa26* locus above sequencing error rates. In contrast, pancreatic cancers of electroporated gMix mice presented high indel frequencies in targeted genes (Figure 7a). The efficiency of CRISPR/Cas9 editing per cancer ranged from 47% (7/15 targets) to 93% (14/15 targets) of potentially targetable loci (Figure 7a, lower bars). This result pointed towards a high level of multiplexing (number of vectors entering and modifying a single cell) during the electroporation procedure. Overall, 72% (69/96, counted without *Brca2* targets) of all possible genetic targets were edited after delivery of CRISPR/Cas9 by electroporation into pancreata of adult mice.
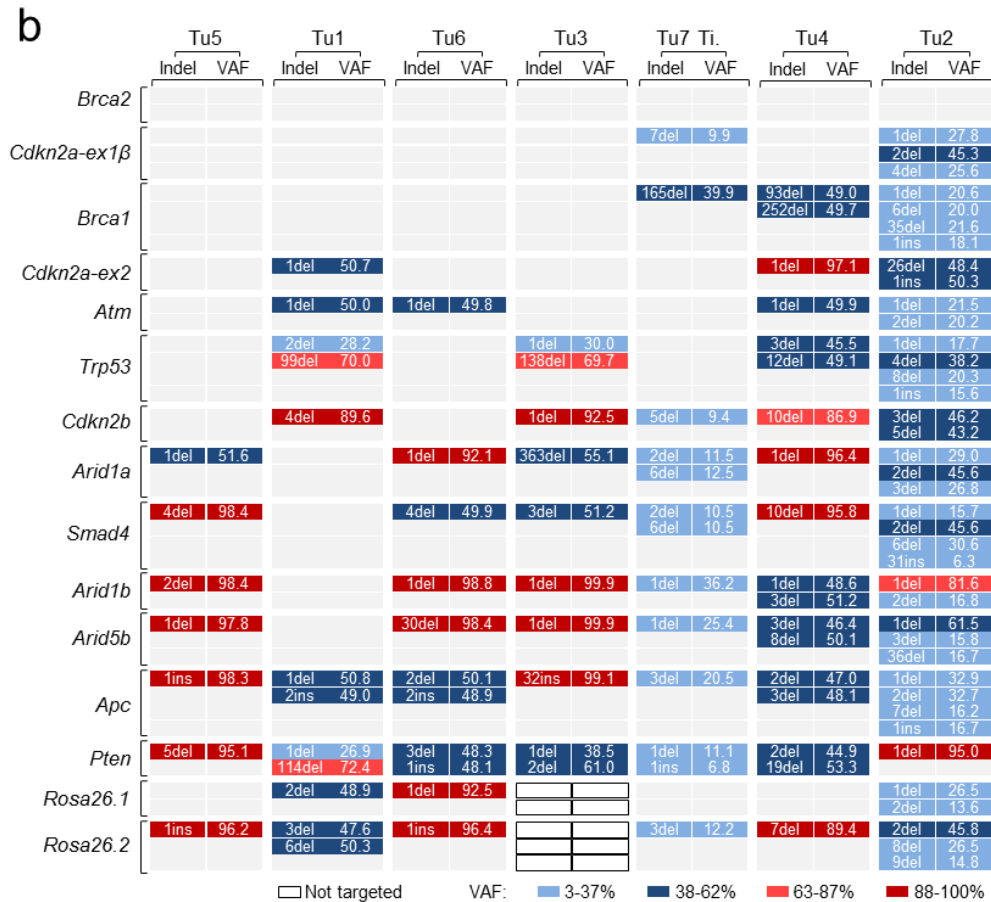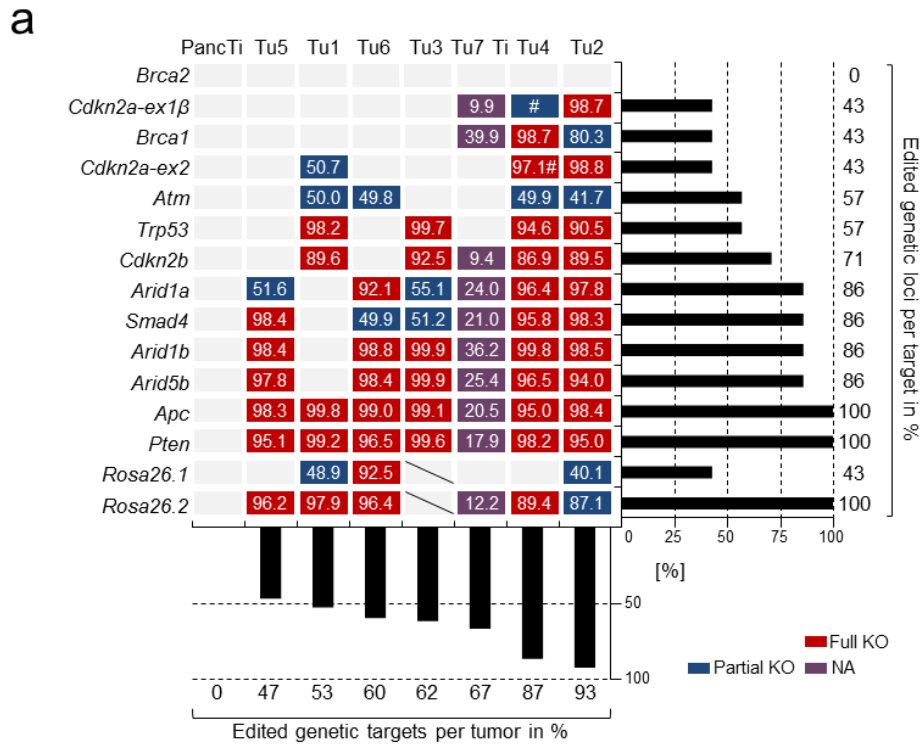
Figure 7 | Electroporation-based multiplexed CRISPR/Cas9-directed genome editing at sgRNA target sites in pancreatic cancer relevant genes. a, Combined variant allele frequencies (VAFs) in all gMix cohort cancers originating from primary cultures (Tu1-6) and cancer tissue (Tu7 Ti) and an exemplary reference "normal" pancreatic tissue are given. Individual cancers are sorted by increasing number of sgRNA target site mutations. Single boxes indicate cumulative VAFs of all different indel

63

mutations sequenced at sgRNA target sites. In case no wild-type reads were present, complete target gene inactivation (=homozygous) was assessed (red boxes). Partial gene knock-out (=heterozygous) was determined if wild-type reads of one chromosome was retained (blue boxes). As judged by indel mutations, Tu7 was only present in pancreatic cancer tissue and thus, no allelic status could be calculated (purple boxes). Healthy pancreatic tissue of all gMix-electroporated cancers showed absence of target gene mutations. *Cdkn2a* locus underwent intra-chromosomal fusion between both *Cdkn2a* target sites as indicated by # in Tu4. White boxes of Tu3 indicate that *Rosa26* locus was not targeted by respective sgRNAs. Bars on right site show the percentage of individual genes edited across all gMix cancers. The bars below present the percentage of genes targeted per individual tumour sample. Note the lack of *Brca2* inactivation. **b**, Detailed extension to Figure 8a. Sequenced type of indel and respective VAF of the same mutation are given per genetic target in a single cancer sample. Note that due to pre-existing aneuploidy to CRISPR/Cas9 electroporation more than two individual mutations can be found. **a-b**, adapted from (Maresch *et al.*, 2016).

When analysing targeted loci in detail, most diploid tumours comprised read frequencies of ~50% or ~100% mutated or wild-type reads (Figure 7b). This result suggested a clonal origin after CRISPR/Cas9-editing in these electroporated cancers, as there were no additional mutant reads from other targeted clones present. Targeted neutral *Rosa26* locus was also either hetero- or homozygously inactivated, which had been so far not assigned to possess tumour suppressive functions (Figure 7b) (Soriano, 1999). While *Apc* and *Pten* were completely deleted in all cancers, *Cdkn2a* and *Trp53* were mutated in 43% and 57% of electroporated tumours, respectively (Figure 7a).

To show the specificity of transient CRISPR/Cas9 activity after *in vivo* electroporation of the mouse pancreas, amplicon-based deep-sequencing was performed for each sgRNA's top-five off-target sites (Table 13). At least three exonic regions per sgRNA were also included into the analysis. In total, 648 genomic off-target sites (108 individual genomic positions from six primary cultures) were sequenced for detectable off-target mutations. The NGS-based analysis yielded no evidence for any CRISPR/Cas9-induced off-target mutations (Data not shown). Although we cannot completely exclude the possibility of unspecific sgRNA binding to other genomic sites, we concluded that transient electroporation-based *in vivo* delivery of CRISPR/Cas9 was highly specific, and undesired off-target effects were negligible.

9.8. High-level multiplexing allows for direct *in vivo* negative selection screening

In our gMix experimental cohort, *Brca2* was the only TSG, which was never target of somatic CRISPR/Cas9-based gene editing (Figure 7). Because *in vitro* SURVEYOR™ assay confirmed similar gene editing efficiencies of the *Brca2* sgRNA to all other used sgRNAs, this finding suggested negative selection for *Brca2* inactivation during pancreatic cancer formation. Skoulidis et al. had shown, that germline *Brca2* heterozygosity drives pancreatic tumour growth in patients (Skoulidis *et al.*, 2010). Likewise, germline *Brca2* heterozygosity in combination with the expression of oncogenic *Kras*^{G12D} accelerated pancreatic cancer formation in a mouse

model of familial pancreatic cancer (Skoulidis *et al.*, 2010). In contrast, in the presence of active oncogenic *Kras*^{G12D} signalling, concomitant complete/homozygous *Brca2* inactivation substantially blocked cancer induction in genetically engineered mouse pancreata (Skoulidis *et al.*, 2010; Rowley *et al.*, 2011). Mutations in *BRCA2* correlated with genomic instability and a mutational signature for DNA repair deficiency (Waddell *et al.*, 2015). The blockage of cancer progression was reversed and tumour development accelerated, if simultaneously *Trp53* was inactivated (Rowley *et al.*, 2011) or *TP53* loss-of-function variant was expressed (Skoulidis *et al.*, 2010). In both cases, the cancer escaped TP53-mediated growth arrest or cell death caused by massive chromosomal aberrations accumulating due to the loss of *Brca2* (Skoulidis *et al.*, 2010; Rowley *et al.*, 2011). In pancreatic cancer patients, *BRCA2* inactivation was consequentially associated with mutations in the *TP53* DNA damage repair gene (Waddell *et al.*, 2015).

In this study, CRISPR/Cas9 nuclease edited ~3/4 of all genetic targets homozygously (Figure 8c). Hence, it was conceivable, that inactivation of *Brca2* in the *Kras*^{G12D} background can lead to the growth arrest of the targeted cell. Despite of possible synchronous *Trp53* inactivation, the acute loss of the *Brca2* DNA maintenance gene might not overcome the DNA damage-mediated cell cycle arrest. These data could show that multiplexed CRISPR/Cas9-based mutagenesis by electroporation allowed for *in vivo* synthetic lethality screening of cancer essential genes in adult mice, a key feature to interrogate the cancer genome for new therapeutic drug vulnerabilities.

9.9. Characteristics of multiplexed CRISPR/Cas9-based gene editing

Most genetic mutations were found near the CRISPR/Cas9-induced double strand breakage sites (Cas9 introduces the DSB between the 3rd and 4th nucleotide 5' of the PAM; Figure 8a). Insertion sizes ranged from 1 to 32bp and deletions from 1 to 362bp (Figure 8a). Large indels >100bp caused by Cas9 enzyme were comparatively rare events. Notably, indels spanning further than ~300bp up- and downstream from the PAM could not be studied due to the primer binding limitations in our amplicon-based sequencing protocol.

In accordance with other reports, non-homologous end joining repair caused a strong tendency towards deletion-type mutations (~90% of all detected indels, Figure 8a). Furthermore, small indel mutations (≤10bp) comprised ~80% of all detected mutations (Figure 8a). In general, frequency and size of the indels were correlating inversely. In Figure 8b, three examples of CRISPR/Cas9-edited loci are shown aligned to the mouse reference gene sequence. In case large indels occurred in one allele, the affected truncated allele of the gene could be size separated by agarose gel electrophoresis (Figure 8b).

Of all detected CRISPR/Cas9 mutations, 76% of the respective genes were inactivated completely/homozygously, while only 24% of targeted loci retained at least one wild-type allele (Figure 8c). In one example, Tu3 contained a rare homozygous 32ins mutation in *Apc* (Figure 7b). Because it was very unlikely that Cas9 enzyme would edit both genetic copies with 32ins, complete *Apc* mutation must have occurred either by a pre-existing hemizygous allelic status of *Apc* before the electroporation procedure, or by selection for the heterozygous Cas9-edited 32ins variant during tumorigenesis of Tu3. This analysis showed the high gene editing efficiency (even only expressed transiently) of CRISPR/Cas9 coupled with the electroporation-based delivery in pancreatic cells of adult mice.
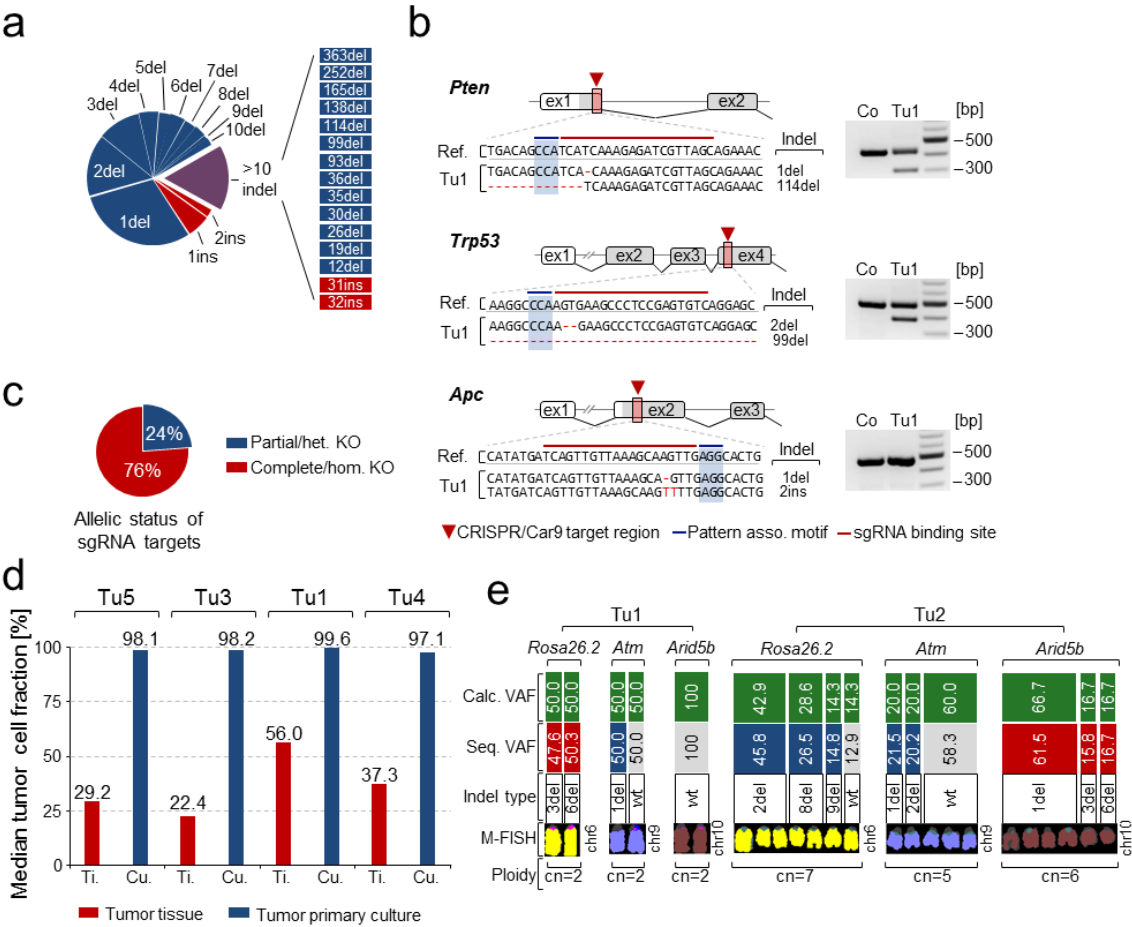
Figure 8 | Genetic analysis of multi-allelic CRISPR/Cas9-induced mutagenesis in mice. a, Pie chart shows distribution of different types of indel mutations detected in all gMix cancers. del, deletion; ins, insertion. **b**, Exemplary target loci of *Pten*, *Trp53* and *Apc* in Tu1 displayed aligned to the mouse reference sequence. Exon map, sgRNA target region (red arrow head) and mouse reference sequence with PAM (blue overlay) are shown. Indel mutations were usually found in close vicinity to the PAM. Indel mutations of mutant reads found in Tu1 are highlighted in red. Large deletion products (as well as theoretical large insertions) caused a shift in PCR product size (left). bp, base pair; co, control; ex, exon and Ref, reference. **c**, Allelic status of genomic targets in gMix cancer cohort. Data are derived from primary culture samples because of reduced stromal contamination. Complete/homozygous somatic inactivation was determined if no wild-type reads were detected. **d**, Comparison of tissue and primary culture samples of the same pancreatic tumour allowed determination of the median tumour cell fraction (and estimate level of "wild-type" stroma contamination). Only homozygously inactivated sgRNA

target sites were used for the equation. The median tumour cell fraction ranged from 22-56% in tumour tissues. Primary culture samples contained nearly pure cancer cells allowing the discrimination between homo- and heterozygously targeted samples. **e**, Comparison of chromosomal copies from M-FISH data to VAFs of CRISPR/Cas9 allowed assignment of wild-type and edited copies. A strictly diploid (Tu1, left) and a poly-/aneuploidy cancer (Tu2, right) are shown. VAF and M-FISH data originated from gMix primary cultures. Chromosomal copy number, calculated VAF (calculated from number of existing copies), sequenced VAF and type of indel are shown. CN, copy number. **a-e**, adapted from (Maresch *et al.*, 2016).

Haploinsufficiency of TSGs in cancer describes a phenomenon that already the functional loss of a single allele of a gene could cause a malignant phenotype. The allelic status showed the number of functional versus inactivated copies of a gene. Using multiplexed CRISPR/Cas9-based genome editing, increased presence of a distinct allelic status of a targeted TSG (wild-type, partial or complete inactivation) could be informative for cancer signalling. Essential genes would be never, classic TSGs completely and haploinsufficient TSGs both partially and completely edited by Cas9 nuclease activity. Hence, the exact determination of the allelic status is important to understand the mode of action of CRISPR/Cas9-targeted genes in the electroporated pancreatic tumours.

The analysis of genetic mutations caused by CRISPR/Cas9 editing can be confounded by two main factors: First, the high and variable stromal content of pancreatic cancers massively hampered the assignment of wild-type and variant reads to stroma or cancer cells. To overcome this issue, primary cultures from six pancreatic tumours were isolated to reduce the stromal content to a minimum. Counting only homozygously mutated target sites in four primary cultures, the median tumour cell fraction was calculated in these tissue samples (Figure 8d). Using this method, we found that these tissue cancer samples contained only 22-56% variant reads originating from Cas9 editing. Because of the unknown total non-cancer read fraction, only pure primary cancer cultures enabled the unambiguous determination of the allelic status of a CRISPR/Cas9 target site in an electroporated cancer.

Second, frequent copy number alterations of whole chromosomes (known as an- or polyploidy) introduced another level of complexity for the analysis of the allelic status in CRISPR/Cas9-based gene editing. Variating chromosomal copy numbers also affected the determination of the VAF for an individual Cas9-induced indel. To overcome these problems, multispectral karyotyping was performed on all primary cultures from electroporated gMix cancers to assess total chromosomal copy numbers. The composite karyotype (overlay of ten individual karyotypes) was used for the analysis. Next, the resulting chromosomal copy number was compared to individual variant reads from CRISPR/Cas9-induced mutagenesis of target sites (Figure 8e). This approach allowed the exact genetic classification of the allelic status of a CRISPR/Cas9 target site.

For example, M-FISH analysis revealed that Tu1 had a strictly diploid (2n) and stable composite karyotype. Consequentially, CRISPR/Cas9-based gene editing could only affect two possible copies in the genome of the targeted pancreatic cell. This was shown as both allelic copies of *Rosa26* on chromosome 6 (=homozygous/complete), one copy of *Atm* on chromosome 9 (=heterozygous/partial) and no allele of *Arid5b* on chromosome 10 (=wild-type) were edited (Figure 8e). Conversely, Tu2 featured an aneuploid karyotype and in total, more than two variant reads per target site. This heterogeneity originated not from a polyclonal primary culture because single cell clones from the primary culture were used for the analysis (Figure 8e and Figure 9). M-FISH revealed seven copies of chromosome 6, five copies of chromosome 9 and six for chromosome 10. The determination of the total chromosomal copy number allowed for the calculation of the theoretical variant read fraction originating from a single chromosomal copy (Figure 8e). Amplicon-based deep sequencing revealed multiple indel mutations and different VAFs for each genetic Cas9 target in Tu2 (Figure 7b). By assigning the theoretical VAF of one chromosomal copy to the sequenced VAF of one indel, the copy number of each indel variant could be determined for exemplary *Rosa26.2*, *Atm* and *Arid5b* target sites (Figure 8e). *Rosa26.2* and *Atm* were only partially inactivated because one out of seven, and three out of five copies of chromosome 9 remained wild-type, respectively. All six chromosomal copies of *Arid5b* were edited by Cas9 activity, yet affecting different copy numbers of the gene.

Interestingly, observed indel patterns in Tu2 could only be explained, if partial aneuploidy was already present before or during transient CRISPR/Cas9 gene targeting of the mouse pancreas. In summary, the characterisation of pure primary cancer cultures with tools determining the genetic sequence and variant read proportions (i.e. targeted amplicon-based sequencing or exome sequencing) as well as the chromosomal copy number (i.e. M-FISH or aCGH) provide useful information for the allelic status of CRISPR/Cas9-targeted genes in electroporated cancers.

9.10. Indel signatures for phylogenetic tracking of metastases

Metastasis formation in pancreatic cancer was often studied in PK mouse models predisposed to acquire a metastatic phenotype (Bardeesy *et al.*, 2006). A limitation to these models was that primary tumours have been arising multifocally from independent cancer clones (McGranahan *et al.*, 2017). This phenomenon confounded evolutionary studies or phylogenetic tracking of metastatic spread in mice. One option to deconvolute the complexity of metastatic dissemination could be the usage of unique DNA barcodes for individual cancer clones. Here, we anticipated that multiplexed *in vivo* CRISPR/Cas9-induced gene editing could allow the

establishment of unique mutational signatures in each targeted cellular clone. The edited pancreatic cells would carry different combinations of indels in known positions of the genome - similar to genetic barcodes.
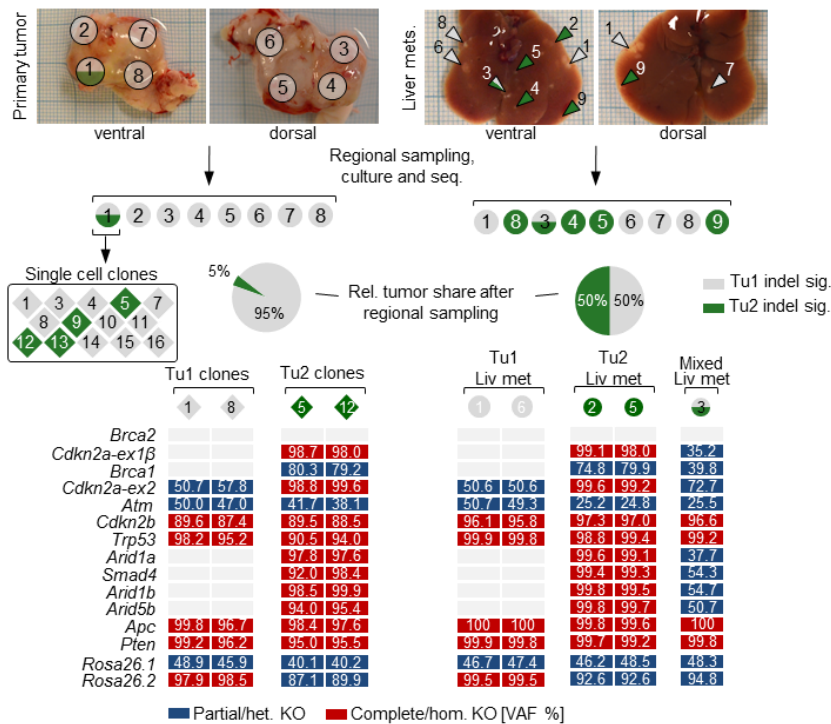
Figure 9 | Multiplexed CRISPR/Cas9 somatic genome-engineering for phylogenetic tracking of metastatic outgrowth in mouse PDAC. Electroporation of multiple sgRNA vectors into the pancreas of an adult PK mouse resulted in the development of metastatic pancreatic cancer. Eight regions from the primary mass (circles) and 9 liver metastases (arrow heads) were separately cultured and sequenced. Primary tumour region 1 contained indel signatures from an independent dominant (Tu1) and minor cancer clone (Tu2; diamonds). Individual liver metastases were phylogenetically tracked back to one of the clones based on the unique CRISPR/Cas9-based mutational signature. Adapted from (Maresch *et al.*, 2016).

To this end, regional sampling on the primary pancreatic cancer and extraction of >24 macroscopic metastatic colonies in the liver of one electroporated PK mouse was performed (Figure 9, upper panel). In total, nine liver metastases and eight regions from the primary tumour mass were cultured three passages to reduce stroma contamination. Subsequent amplicon-based deep sequencing of target sites revealed two genetically distinguishable cancer clones (Tu1 and Tu2) based on the CRISPR/Cas9-induced mutational signatures (Figure 9). In seven out of eight primary cancer regions, only the indel signature of Tu1 (dominant clone) was detected. Because region 1 contained additional variant reads in gMix target sites, 14 single cell clones were established by serial dilution cloning of the region 1 culture (Figure 9, central left panel). Thereby, Tu2 (minor clone) was clearly identified as independent cancer clone in region 1 of the pancreatic cancer (Figure 9, lower left panel). While the minor clone was only present in region 1, the dominant clone manifested in estimated ~95% of the total pancreatic cancer.

CRISPR/Cas9-induced indel signatures in the liver metastases were identical to either the dominant or minor primary cancer clone, except liver metastatic colony 3 containing variant reads from both clones (Figure 9, lower right panel). Of note, although the minor clone was only present in 5% of the total pancreatic cancer mass, this clone was able to establish 50% of disseminated liver colonies. Summarizing, multiplexed delivery of CRISPR/Cas9 vectors enabled unique barcoding of pancreatic cells by sequencing CRISPR/Cas9-edited target sites. The limited number of targeted pancreatic cells by electroporation guaranteed satisfactory unique indel combinations, thereby supporting phylogenetic tracking of metastatic disease.

9.11. *In vivo* electroporation for CRISPR/Cas9-induced chromosomal rearrangements

Two-thirds of human pancreatic cancers have been reported to harbour chromosomal rearrangements (Notta *et al.*, 2016). Furthermore, chromosomal rearrangements were associated with accelerated pancreatic tumour evolution in patients (Jones *et al.*, 2008; Griffin *et al.*, 2007; Karhu *et al.*, 2006; Waddell *et al.*, 2015; Notta *et al.*, 2016). We also found in PK mice that complex genetic changes involved clustered chromosomal rearrangements, aneuploidy and inter-chromosomal translocation, affecting known cancer genes such as *Cdkn2a* and *Myc* (Mueller *et al.*, 2018). PK mice losing *Cdkn2a* by complex rearrangements of the chromosome showed a shortened tumour-free survival compared to mice with a non-rearranged chromosome 4 (Mueller *et al.*, 2018). Using high-density array comparative genomic hybridisation (aCGH) and M-FISH data from 23 human PDAC cell lines, a median of 139 intra-chromosomal deletions/amplification and 8 inter-chromosomal translocations per tumour were detected (Data not shown). Frequently, chromosomes harbouring key pancreatic TSGs *CDKN2A* and *TP53* were affected by translocations in the PDAC cell lines. Other studies supported the notion that inter-chromosomal translocations were non-random in pancreatic cancers, because they affected key TSGs *CDKN2A*, *TP53* and *SMAD4* and, because they were predominantly unbalanced leading to the disruption of the genetic locus (Karhu *et al.*, 2006; Griffin *et al.*, 2007; Norris *et al.*, 2015; Notta *et al.*, 2016).

Our group and others had demonstrated that *in vivo* activity of CRISPR/Cas9 can cause large intra-chromosomal deletions between two sgRNA target sites (Weber *et al.*, 2015; Blasco *et al.*, 2014; Maddalo *et al.*, 2014). Hence, we examined whether transient electroporation of multiplexed CRISPR/Cas9 into the mouse pancreas was able to induce large intra-chromosomal rearrangements in the genome. To this end, all primary cancer cultures were screened by PCR for intra-chromosomal deletion events, if at least two sgRNAs binding sites existed on individual chromosomes (Figure 10a).
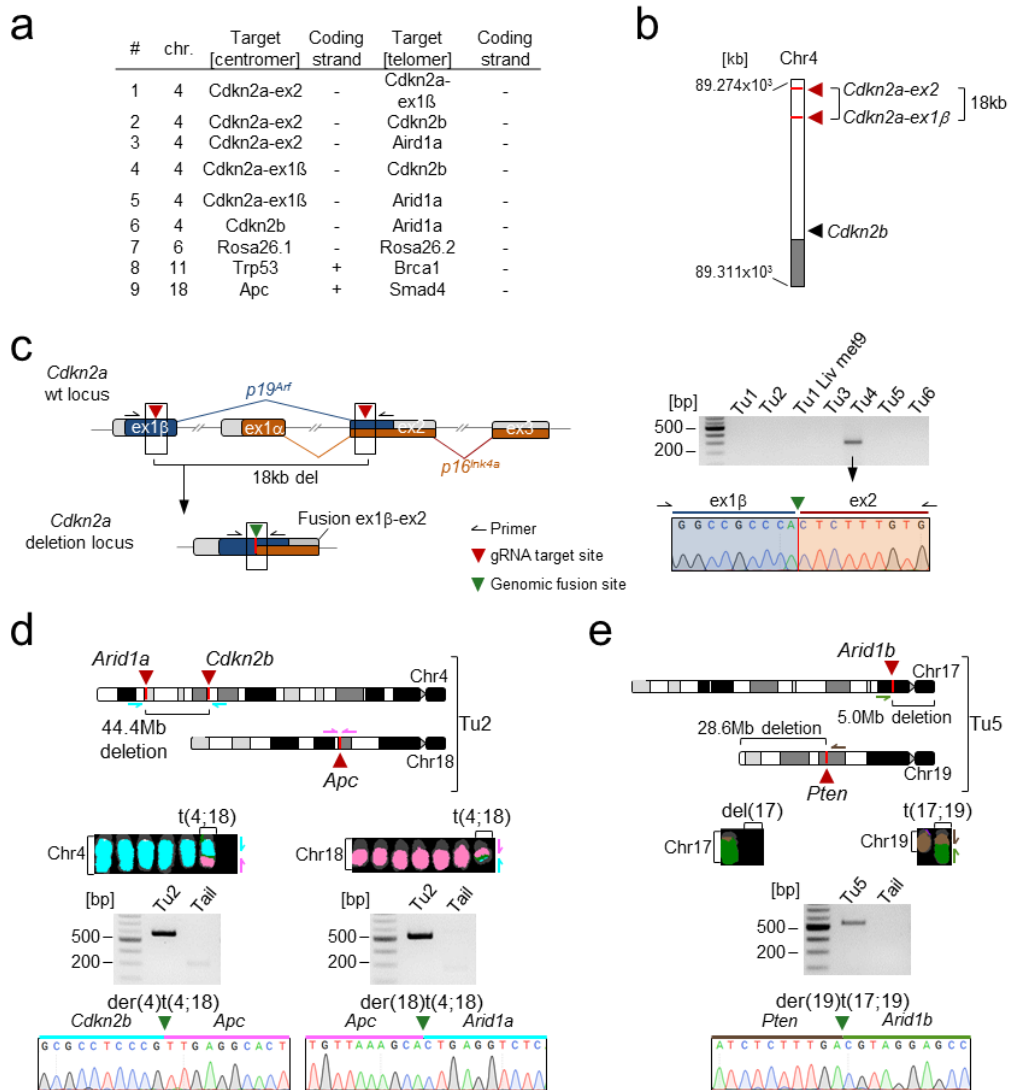
Figure 10 | Electroporation of multiple CRISPR/Cas9 vectors allowed for *in vivo* chromosomal engineering of the mouse pancreas. a, Overview of all nine possible intra-chromosomal rearrangements as indicated by sgRNA target sites. PCR-based screening for rearrangements between target sites was only positive in one cancer for combination 1 on chromosome 4. **b**, Outline of sgRNA binding sites (red arrow heads for exon1ß and common exon2) at *Cdkn2a* locus and associated 18kb intra-chromosomal deletion. kb, kilo bases. **c**, While exon1ß is distinct for *p19^Arf*, exon2-binding sgRNA targeted also alternative gene product *p16^Ink4a*. Fusion locus is shown below. Screening with respective primer pairs showed genomic fusion product and 18kb deletion in Tu4, which was further verified by Sanger sequencing. **d-e**, In two out of six cancers, M-FISH analysis and PCR-based screening revealed inter-chromosomal rearrangements between sgRNA target sites in primary cultures. In both cases, affected genes were inactivated by CRISPR/Cas9-induced loss of genetic information. t, translocation and der, derivative. **d**, Tu2 featured an unbalanced inter-chromosomal rearrangement between chromosome 4 (*Cdkn2b*) and chromosome 18 (*Apc*) and an associated 44.4Mb deletion between *Cdkn2b* and *Arid1a* on chromosome 4. M-FISH of affected chromosome pairs, agarose gel electrophoresis and Sanger sequencing at fusion sites (Green arrow) are shown. Mb, mega base. **e**, In Tu5, an unbalanced inter-chromosomal rearrangement between chromosome 17 (*Arid1b*) and chromosome 19 (*Pten*) leading to the loss of one copy of chromosome 17 and 28.6Mb on chromosome 19 was detected. del, deletion. **b-e**, adapted from (Maresch *et al.*, 2016).

Out of nine possible combinations in six primary cancer cultures, PCR using combination 1 primer pairs confirmed a deletion affecting 18kb of the *Cdkn2a* locus on chromosome 4 of Tu4 (Figure 10a and b). The *Cdkn2a* locus is harbouring two independent gene products that arise through alternative spicing of exon1ß (*p19^{Arf}*) or exon1α (*p16^{Ink4a}*, Figure 10c). Sanger sequencing of the rearranged *Cdkn2a* locus confirmed the genetic fusion of exon1ß to adjacent exon2 in close distance to the PAM of each sgRNA. Thereby, large parts of exon1ß and exon2 as well as complete exon1α were genetically lost to the cancer (Figure 10c). Preliminary aCGH analyses on Tu4 also discovered a large deletion involving *Cdkn2a* and highlighted a similar event on chromosome 4 in Tu2 (Data not shown). However, both chromosomal deletions were probably missed by our PCR screening because primer binding sites could be also lost during CRISPR/Cas9 genome editing. Additionally, we found a CRISPR/Cas9-associated 44.4Mb deletion on chromosome 4 in Tu2 and a 5Mb deletion resulting in a copy number loss of chromosome 17 in Tu5 (Figure 10d and e, upper panel). In summary, three out of six electroporated pancreatic cancers showed substantial evidence for intra-chromosomal deletions caused by transient *in vivo* activity of multiplexed CRISPR/Cas9 between two sgRNA targets sites and subsequent NHEJ.

M-FISH was conducted on the six electroporated primary cancer cultures to find evidence for complex rearrangements such as translocations. In two out of six cancers, we could identify striking patterns of translocated chromosomal arms fitting roughly to projected sgRNA target sites on the chromosomes (Figure 10d and e). Indeed, Tu2 featured an unbalanced reciprocal translocation affecting chromosomes 4 and 18 and an associated 44Mb loss between *Arid1a* and *Cdkn2b*. This event was presumably negatively selected for during tumorigenesis as indicated by the copy number gain of the non-translocated chromosome (Figure 10d). Sanger sequencing of respective Tu2 PCR products revealed the fusion of *Cdkn2b* and *Apc* (der(4)t(4;18)) as well as the fusion of *Apc* and *Arid1a* (der(18)t(4;18)) close to the PAM of each sgRNA target site (Figure 10d).

Evidence for a second unbalanced non-reciprocal inter-chromosomal translocation was found between chromosome 17 and 19 in Tu5 (Figure 10e). M-FISH revealed a loss of translocation-affected chromosome 17 (del(17)), presumably because of the short distance of the sgRNA target site to the centromere (5Mb). This proximity could have led to a destabilization and degradation of the chromosome (Figure 10e). Telomere-sided part of chromosome 17 translocated to chromosome 19 (der(19)t(17;19)). This caused the fusion of sgRNA targets *Pten* and *Arid1b* as shown by Sanger sequencing (Figure 10e). Presumably because telomere-sided part of chromosome 19 (downstream of *Pten* affecting 28.6Mb) missed a reciprocal

translocation partner on chromosome 17, it was also genetically lost to the cancer. In all electroporated cancers, the intra- as well as inter-chromosomal rearrangements were clonal and very close to the PAM of respective sgRNA binding sites. These data showed that multiplexed CRISPR/Cas9 electroporation could theoretically allow the study of locus-specific structural rearrangements during tumour development directly in the mouse pancreas.

9.12. CRISPR/Cas9-based mutational signatures for tracing of cancer cell phenotypes

Tu4 primary culture presented striking morphologic differences in 2D standard growth conditions. In general, mesenchymal "spindle-shaped" cells tend to grow individually but can migrate over each other in multiple layers. In contrast, epithelial cells strictly stay in dense mono-layered clusters and feature a rather cubic shape (Figure 11a,b).
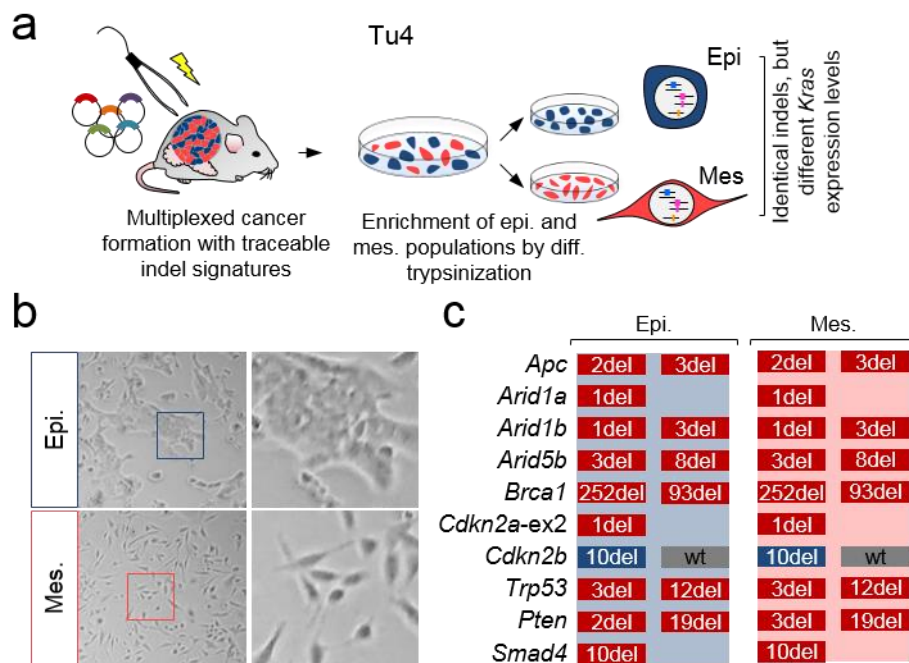

Figure 11 | Multiplexed *in vivo* CRISPR/Cas9-induced mutational signatures for clonal tracing in primary cultures. a, Scheme illustrating the workflow for separating epithelial and mesenchymal cell populations. **b**, Differential trypsinization of mixed Tu4 primary culture was performed to enrich epithelial and mesenchymal populations. Brightfield images; left 100x magnification and right zoom-in. **c**, Tu4-derived epithelial and mesenchymal cancer cell populations shared identical indel signatures pointing towards morphologic bifurcation after CRISPR/Cas9-induced mutagenesis. Red and blue boxes indicate complete/homozygous and partial/heterozygous target gene inactivation, respectively. wt, wild-type. **a-c**, adapted from (Mueller *et al.*, 2018).

Differential trypsinization of Tu4 was performed to separate cells with epithelial and mesenchymal phenotypes (Description of procedure in Method sections, Figure 11a,b). Both populations were analysed by amplicon-based deep sequencing to identify CRISPR/Cas9 target site mutations. Indel signatures would provide information on the origin of the mixed pancreatic cancer, suggesting three scenarios: (i) Different indels in both populations, which had originated

from different cells of origin, (ii) partial identical indels that were caused by asymmetric CRISPR/Cas9 gene editing during cell division or, (iii) identical indel signatures in both Tu4 cancer populations. The latter two scenarios would indicate a shared cell of origin in Tu4. Sequencing revealed complete concordance of indel signatures between epithelial and mesenchymal cell populations (Figure 11c). This result showed that morphologic and phenotypic diversification of Tu4 occurred after multiplexed CRISPR/Cas9gene editing. It also indicated that phenotypic bifurcation of Tu4 was not caused by differential Cas9-induced gene editing, but likely resulted from other genetic or epigenetic alterations during tumour evolution. Our group found evidence that the *Kras* gene dosage affected the histologic differentiation as well as the cellular morphology of pancreatic cancers from PK mice (Mueller *et al.*, 2018). Thus, the allelic status of the engineered *Kras* gene harbouring the oncogenic G12D mutation in exon 2 in both Tu4 cell populations was analysed by amplicon-based deep sequencing. While the epithelial population remained at ~50% *Kras*^{G12D} VAF, mesenchymal cells showed an increase of the *Kras*^{G12D} gene dosage (Figure 12a, upper panel). M-FISH indicated that epithelial Tu4 cells retained four copies of chromosome 6 after whole genome duplication. In contrast, mesenchymal cells featured a selective gain of the *Kras*^{G12D} copy number, likely through mitotic missegregation of chromosome 6 (Figure 12a, upper panel). qRT-PCR confirmed elevated *Kras* expression in mesenchymal compared to epithelial cell population on the mRNA level (Figure 12b). To substantiate this finding, 3'RNASeq (SCRBseq) was performed on both Tu4 populations. Gene set enrichment analysis of mesenchymal Tu4 population revealed significant upregulation of genes involved in *Kras* downstream signalling ("MAPK signalling pathway") and de-differentiation ("Epithelial to mesenchymal transdifferentiation"; Figure 12c).

For functional characterisation of the *Kras*^{G12D} dosage gain, MTT viability assay was performed on both Tu4 populations over the time course of 14 days. We had speculated whether selective *Kras*^{G12D} dosage gain would facilitate a tolerance of mesenchymal Tu4 to FCS depletion compared to the epithelial population. Secreted growth factors or cytokines from the cancer cultures were also removed by daily change of the medium. In 10% FCS conditions, no growth difference between epithelial and mesenchymal populations was observed (Figure 12d). Depletion of FCS and growth factors caused a dramatic drop of the viability in epithelial Tu4 cells already after 24h suggesting growth dependence on extrinsic or autocrine growth factors (Figure 12d). In contrast, mesenchymal Tu4 cells showed a resistance to serum deprivation by maintaining stable MTT viability levels from the first day. However, compared to 10% FCS conditions, mesenchymal Tu4 showed a relative growth deficiency (Figure 12d). Hence,

Kras^{G12D} gene dosage gain increased the tolerance of mesenchymal Tu4 primary cancer culture to continuous growth factor depletion.
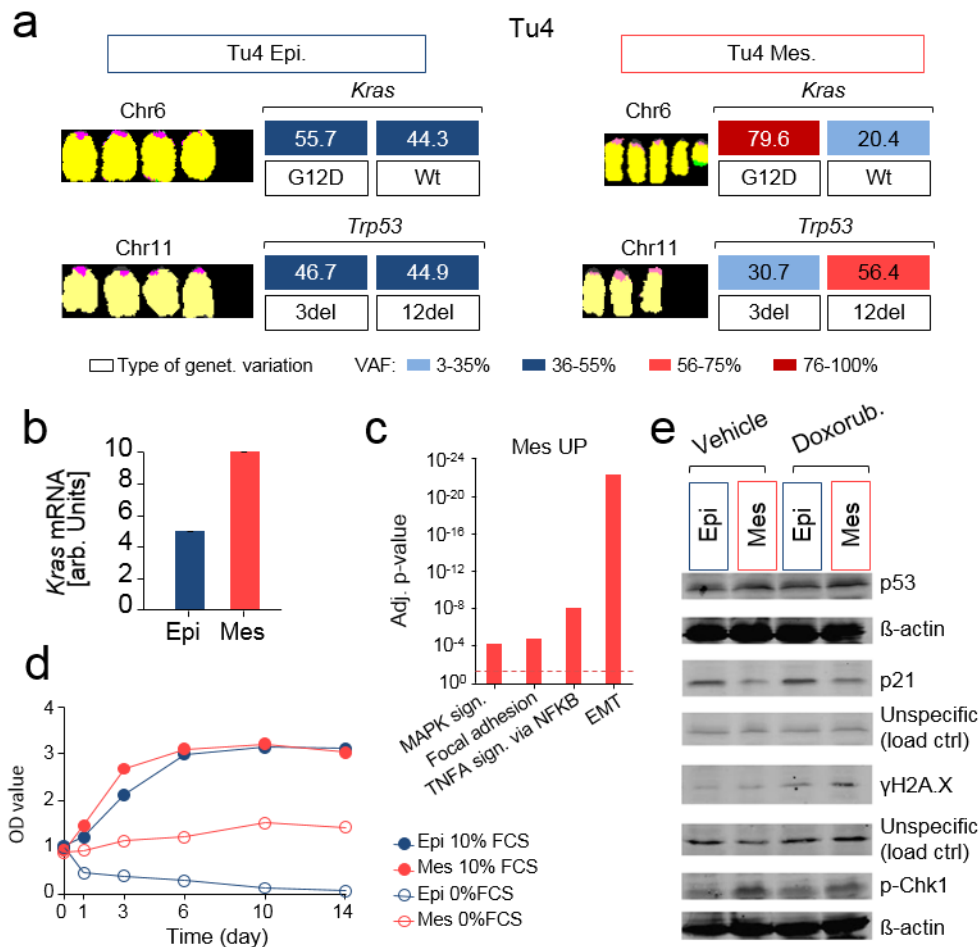
Figure 12 | Characterisation of epithelial and mesenchymal Tu4 cancer cell populations from the identical cell of origin. a, Identical indel signatures between epithelial and mesenchymal Tu4 cells indicated a shared cell of origin. M-FISH analysis and VAFs of the endogenous *Trp53* and *Kras* locus are shown. Note increasing *Kras^{G12D}* allelic ratios, loss of a g.175_177del (3del) *Trp53* and concomitant gain of g.168_179del (12del) copies in the mesenchymal clone. **b**, Total *Kras* transcript expression levels in both clonal pairs were determined using qRT-PCR and normalized to *Gapdh* housekeeping gene. n=2 technical replicates. Bars, mean; error bars, s.e.m. **c**, Transcriptomic characterization of selected gene sets enriched in mesenchymal Tu4 cells using MSigDB revealed an upregulation of genes involved in "MAPK signalling pathway" and "EMT" in comparison to the epithelial population. False discovery rate-adjusted *P* value is presented at the y-axis. Red dashed line indicates $P \leq 0.01$. Data originated from one experiment. **d**, MTT assay demonstrated increased serum-independence of mesenchymal Tu4 cells in contrast to the epithelial. Mean OD value of each condition at indicated time points are shown in technical duplicates. Experiment was repeated once with similar results. Points, mean; error bars, s.e.m.. **e**, Immunoblot analysis of differentially expressed proteins involved in major DNA response pathways are presented. Epithelial and mesenchymal cancer clones were treated with topoisomerase II inhibitor doxorubicin to induce DNA damage. ß-actin was used as loading control. **b,c**, adapted from (Mueller *et al.*, 2018).

M-FISH analysis of ten individual karyotypes in both Tu4 populations revealed a tetraploidization of the genome (Data not shown). The exclusive presence of maximally two different wild-type or CRISPR/Cas9-edited variant alleles also showed that the genome

duplication very likely occurred after the CRISPR/Cas9 gene editing in the pancreas (Figure 7b). Mesenchymal Tu4 population showed a relative gain of the CRISPR/Cas9-edited g.168_179del (12del) of *Trp53* on chromosome 11 by losing one of the other g.175_177del (3del) mutated chromosomal copies (Figure 12a). Consequentially, sequencing revealed an epithelial Tu4 VAF of 44.9% for the 12del mutation, whereas mesenchymal population increased the 12del VAF to 56.4% (Figure 12a). The sgRNA targeted *Trp53* protein outside of a functional domain. Hence, the 12del mutation affected the protein function more likely, compared to the in-frame deletion of the 3del removing only a single codon for glutamic acid. Because *Trp53* is a tetrameric TSG (Cho *et al.*, 1994), the chromosomal imbalance for the 12del loss-of-function mutation might have abrogated the function of *Trp53* as tumour-suppressor in the mesenchymal Tu4 population.

To gain further inside into the *Trp53* functional status, Western blot analysis of important DNA damage regulators was performed on both Tu4 populations. Similar expression levels of p53 protein in both Tu4 populations were observed (Figure 12e). The epithelial Tu4 population showed upregulation of the p53 main effector protein p21 (*Cdkn1a*) compared to the mesenchymal (Figure 12e, left panel). This result hinted towards an increased functional inactivation of p53 in the mesenchymal population compared to the epithelial Tu4 population. In contrast, phosphorylation of checkpoint kinase 1 (CHK1), a mediator of checkpoint-induced cell cycle arrest in response to DNA damage, was increased in the mesenchymal Tu4 population compared to the epithelial (Figure 12e, left panel). To investigate, if the DNA damage response could be further elevated, primary cultures were treated for 24h with 1μM doxorubicin. The drug can stall DNA replication in cells and thereby, γH2A.X recruitment would lead to a *Trp53*-dependent apoptotic response. Notably *Atm*, a critical factor for γH2A.X activation, was only mutated heterozygously by CRISPR/Cas9 in both Tu4 populations. As expected, treatment with doxorubicin caused the activation of a γH2A.X response compared to the vehicle treated cells (Figure 12e). However, doxorubicin failed to further increase p21 protein levels in both populations, suggesting a high *basal* p21 DNA damage response in the epithelial and no p53-mediated activation of p21 in the mesenchymal population (Figure 12e). γH2A.X activation can also lead to the inhibition of cell cycle progression through phosphorylation of CHK1 (Dietlein *et al.*, 2015). Again, phospho-CHK1 was not further increased in both populations due to doxorubicin treatment, however, it also suggested increased *basal* DNA damage response activity in the mesenchymal Tu4 population.

This result indicated that epithelial Tu4 population might regulate cell cycle progression mainly through p21 activation, while the mesenchymal switched to phospho-CHK1 signalling,

possibly because of the inactivation of *Trp53* by chromosomal imbalance of chromosome 11. However, this finding needs further in-depth validation. Further investigation is also required to elucidate the relationship of the oncogenic *Kras*^{G12D} dosage gain and the potential functional loss of *Trp53*-signalling in the mesenchymal Tu4 population, both occurring during tumour evolution after multiplexed CRISPR/Cas9 gene editing. It would also be interesting, whether mesenchymal Tu4 cells, in the absence of p53-mediated cell cycle regulation, have developed a checkpoint kinase dependence through synergistical inhibition of CHK1/MAPK Activated Protein Kinase 2 (MK2) (Dietlein *et al.*, 2015).

10. Discussion

10.1. Electroporation-based *in vivo* CRISPR/Cas9 genome editing

In this study we could demonstrate that the electroporation-based transfection of CRISPR/Cas9 plasmids allowed for the multiplexed gene editing in the adult mouse pancreas and subsequent cancer formation. We present several key applications for multiplexed *in vivo* CRISPR/Cas9 genome engineering, including (i) high-throughput studies of multiplexed gene interactions/functions in individual cancer clones, (ii) evolutionary tracking of cancer clones (e.g. in metastatic disease or by phenotypic differences) based on the unique indel signatures, (iii) *in vivo* negative selection screening and (iv) targeted *in vivo* chromosome engineering in pancreatic cells.

For the establishment of the multiplexed gene delivery protocol, optimized parameters for the efficient *in vivo* electroporation of the mouse pancreas were used. The in-depth analysis of different reporter constructs revealed the targeting performance of pancreatic cells by electroporation. The CRISPR/Cas9-induced inactivation of multiple relevant TSGs accelerated development of pancreatic cancer in PK mice compared to an equivalent control cohort (median tumour incidence of 54% in gMix compared to none in gControl cohort in the observation time of 24 weeks PE). Amplicon-based deep sequencing revealed indel mutations in at least ~50% out of 15 target regions showing the high level of multiplexing. The genomic characterization of primary cancer cultures determined the exact allelic status of genetic targets and allowed the phylogenetic association of indel signatures to individual cancer clones and other downstream applications including negative selection screening and chromosome engineering. In the following chapters, I will discuss the framework of multiplexed *in vivo* CRISPR/Cas9 electroporation for genome editing in the mouse.

For decades, scientists had to rely on patient-derived tumour cell lines or sophisticated GEMMs to study candidate cancer genes for their roles in tumour development. For the in-depth study of individual cancer genes in cell lines, researchers were restricted to study effects resulting from the downregulation of transcripts using RNA interference (RNAi), forced expression of cDNA or cross-correlation of several cancer cell lines genetically identical to the GOI. Furthermore, ZNFs, TALENs and meganucleases could never be effectively applied *in vivo* due to limitations in their applicability and efficiency.

The adoption of the prokaryotic CRISPR/Cas9 system to cut gDNA in eukaryotes was the basis of many further biotechnological developments and utilizations to study gene function *in vitro* and *in vivo*. The high efficiency and simplicity to introduce mutations in virtually all genes through the Cas9 endonuclease allowed the development of various techniques and models to investigate cancer genomics. For example, CRISPR/Cas9-based *ex vivo* genome editing was shown in haematopoietic stem cells, organoid systems or in 2D-cultured epithelial cells (Heckl *et al.*, 2014; Chen *et al.*, 2015; Matano *et al.*, 2015; Drost *et al.*, 2015; O'Rourke *et al.*, 2017). Additionally, several research groups have developed technologies to deliver CRISPR/Cas9 directly into specific organs of adult mice such as the liver (Xue *et al.*, 2014; Weber *et al.*, 2015; Yin *et al.*, 2014), brain (Zuckermann *et al.*, 2015; Cook *et al.*, 2017), lungs (Sanchez-Rivera *et al.*, 2014), pancreas (Chiou *et al.*, 2015) and colon (Roper *et al.*, 2017).

In this study, we aimed to combine electroporation, a somatic gene targeting approach, with the CRISPR/Cas9 gene editing tool to target multiple TSGs in the pancreata of PK mice. Electroporation is a transfection-based procedure, whereby local electric voltage can generate transient pores in the plasma membrane for the introduction of exogenous DNA into the cell. The delivery of the CRISPR/Cas9 vectors into the tail of the pancreas was performed by injection using a syringe and attached cannula. Now, the pancreatic parenchyma cells could potentially incorporate the pDNA. The forceps-type electrodes of the Nepa21 electroporator system allowed the application of an electric pulse of a defined amplitude and duration. Eventually, the electroporated pancreas was placed back into the abdomen and the wound closed. Mice were scored for clinical symptoms during the observation period; however, they never developed unusual symptoms after surgery.

A set of experiments was conducted to characterize the effects of electroporation to address potential tissue damage and to validate the range and types of transfected cells. Shortly after electroporation, electric pulses in mock electroporated pancreata of wild-type mice caused a localized acute pancreatitis with invading immune cells including macrophages and neutrophils. Lymphocytes could be detected at later time points in the area of electroporation. At day seven, the number of apoptotic cells regressed after an initial increase two days PE. Twenty-one days PE, pancreatic architecture was completely recovered (Figure 3). However, this inflammation caused by electroporation could still contribute unspecifically to the CRISPR/Cas9-induced pancreatic cancer formation. Especially, as it was shown that any type of inflammation in PK mice could boost ADM, electroporation itself could possibly increase PanIN and eventually cancer formation (Hausmann *et al.*, 2014). The findings that within the observation period of six months the electroporated gControl cohort showed no signs of cancer

formation and, that all isolated gMix cancers featured target site mutations, strongly argue for CRISPR/Cas9-mediated TSG inactivation as main driver of tumorigenesis. Yet, the electroporation-induced stimulation could still create a pro-tumorigenic environment. Further analysis would be required to study the effects of the acute inflammation on the long-term development of targeted "pre-neoplastic" pancreatic cells.

For the analysis of targeted cell types in the pancreas, a traceable GFP reporter gene was electroporated into wild-type mice. Unfortunately, the establishment of an amylase co-staining for acinar cells failed due to the high intrinsic proteinaceous background of acinar cells covering the comparatively weak positive GFP signal (Data not shown). Because acinar cells represent the overwhelming majority in the mouse pancreas and because cellular morphology of GFP-positive and haematoxylin-counterstained cells appeared rather acinar- than duct-like, the acinar cell compartment was very likely the most frequently targeted cell type. Quantification of targeted cells was performed by counting short-term (transient GFP expression) and long-term (genetically recombined permanent GFP expression) GFP-positive pancreatic cells. The number of electroporated cells ranged from only few hundreds to a few thousand cells (Figure 2). Thus, compared to other somatic gene delivery systems such as AAV (Rad Lab, unpublished data), the number of targeted cells was vanishingly low.

Pancreatic cancer has one of the most dismal prognoses of all cancer entities. Despite huge sequencing efforts of human patient samples and transposon-based genetic screens in mice, we are still far from understanding the complex natures of the underlying molecular processes. Because oncogenic *Kras* is the main driver of tumourigenesis in pancreatic cancer, it is of utmost interest to identify cancer gene networks that collaborate with the *Kras* driver gene. Multiplexed CRISPR/Cas9 gene editing in adult PK mice would allow a higher throughput and acceleration for the study of putative cancer genes during tumour development, progression and metastatic spread.

To achieve this, we had first started to flank sgRNA as well as the Cas9 nuclease with *SleepingBeauty* ITRs. The co-delivery of a *SleepingBeauty* transposase would stably integrate the complete construct into the genome, thus facilitating successful genome editing. Although this feature is still present in the modified CRISPR-SB vector, the CRISPR/Cas9 system has proved efficient enough to inactivate its genetic target also in a transient manner, without stable transposon mobilization. Advantages of this transient approach were the absence of confounding insertional mutagenesis of the transposon constructs and the gradual disappearance of potentially immunogenic Cas9 protein. In principal, *SleepingBeauty* ITRs could also allow the study of oncogenes. For example, another group could show that stable

electroporation of ITR-flanked *Kras* oncogene and *Trp53* inactivation elevated the tumour incidence dramatically, whereby 14/14 electroporated mice succumbed to pancreatic cancer development (Gurlevik *et al.*, 2016). However, also flanking of the CRISPRa system with *SleepingBeauty* ITRs would enable the stable overexpression and investigation of targeted oncogenes contributing to pancreatic cancer.

Human pancreatic cancer genome sequencing has created immense catalogues of potential cancer-relevant genetic alterations. However, these studies have also revealed that, besides an increased mutational heterogeneity, only a few highly recurrent altered genes such as *KRAS*, *TP53*, *CDKN2A* or *SMAD4* can be found in human PDAC. We have therefore selected a subset of 13 recurrent TSGs in the human pancreatic cancer context. Two sgRNAs against the neutral *Rosa26* locus were also included in the gMix experimental cohort and served as reference sgRNAs for the control cohort of electroporated PK mice. The disruption of the *Rosa26* locus causes no phenotype in mice (Soriano, 1999). At first, individual sgRNAs were tested for similar gene editing efficiencies. The SURVEYOR® nuclease assay showed homogenous indel frequencies between all used sgRNAs (Figure 4b). This validation was important because each sgRNA, when transfected simultaneously with multiple others into one cell, must have an equal cleavage efficiency. If this had not been the case, target inactivation would have been skewed by the sgRNA editing efficiency and no valid conclusion of the relevance of targeted genes during tumour formation would have been possible.

We hypothesized that collaborative mutations of the CRISPR/Cas9 targets would be positively selected during cancer development. Among targeted genes were negative regulators of frequently dysregulated oncogenic signalling pathways in pancreatic cancer such as PI3K/AKT (*Pten*) and Wnt signalling (*Apc*). The importance for the dysregulation of the involved pathways for pancreatic cancer development could be inferred from the complete inactivation in all electroporated gMix cancers (Figure 7). Interestingly, *Atm* was the only sgRNA target which was inactivated heterozygously in four out of seven cancers, even though CRISPR/Cas9 preferentially mutated all existing copies of a target gene (76% of all mutations in our model are homozygous/complete). In response to double strand breaks of the DNA, *Atm* functions as an induced cell cycle arresting factor. During pancreatic cancer development, it was reported that *Atm* could act in a haploinsufficient manner and PK mice heterozygous for *Atm* succumbed to pancreatic cancer significantly earlier than PK only mice (Tao *et al.*, 1999; Russell *et al.*, 2015). These results could partially explain, why *Atm* was only edited heterozygously in our gMix cohort. However, biologic proof, verifying *Atm* haploinsufficiency, must be shown in the

future to exclude a random observation. Hence, the exact determination of the allelic status of a targeted gene is important to understand the role of the gene in cancer development.

In summary, our electroporation protocol shows specific characteristics as compared to other methods that would allow gene transfer to the mouse pancreas: (i) Electroporation enabled the simultaneous delivery of multiple sgRNA vectors to a few individual cells. Hence, complex cancer genotypes could be generated showing up to 14 indels per cancer clone. This high level of sgRNA vector multiplexing is difficult to obtain in viral approaches such as AAV supporting 1-2 sgRNAs. (ii) Electroporation only targeted a few hundred to thousand pancreatic cells per electroporation. This low-frequency genetic mosaicism of differentially edited and non-transfected pancreatic cells reflected sporadic cancer formation of single transformed cells in human tumours. This finding was further substantiated by the observation of the mono- to oligo-clonal pancreatic cancer outgrowth in the gMix cohort. (iii) Multiplexed CRISPR/Cas9 gene editing created enough traceable genetic heterogeneity (= indels) enabling the barcoding of the "cancer-founding cell". The unique indel signatures allowed clonal tracing of cancer clones in the primary tumour and metastatic colonies. In stable viral approaches, one could integrate a unique barcode to the CRISPR/Cas9 vector(s); however multiplexed TSG inactivation would be again difficult to achieve. (iv) The insertional mutagenesis of viruses or transposons could disrupt molecular networks independently from CRISPR/Cas9 editing, thereby confounding downstream genetic analysis. (v) Because CRISPR/Cas9 plasmids can be directly electroporated, it is a fast protocol and would support high-throughput studies of putative cancer genes. (vi) *In vivo* gene transfer using viral vectors could induce an adaptive immune response of the host, which could severely affect the readouts in the somatic mouse cancer model. Transient plasmid DNA expression is reducing the risk of stimulating the immune system. (vii) In contrast to most viral approaches, S2 bio safety level is not required, which could be an issue in mouse research facilities.

10.2. CRISPR/Cas9 off-target effects

Multiplexed CRISPR/Cas9 delivery to individual cells of the mouse pancreas could cause unintentional editing of off-target loci, as a result of unspecific sgRNA binding in the genome. To address the off-target issue, amplicon-based deep sequencing of the top-ranked off-target regions of all sgRNAs was performed. This approach yielded a total of 648 off-target positions across all primary culture samples (108 predicted regions per tumour). Exclusively wild-type DNA sequences at sgRNA off-target binding sites were detected by NGS. Hence, we summarize that off-target mutation in our transient CRISPR/Cas9 gene editing approach could be neglected and was a very rare event.

10.3. Multiplexed in vivo gene editing for negative selection screening

Brca2 was the only genetic target that was never inactivated by multiplexed *in vivo* CRISPR/Cas9 editing in all pancreatic cancers. This was surprising because the efficiency of the sgRNA against *Brca2* to induce indels was comparable to the other used sgRNAs (Figure 4b) and, because of the high level of parallel vector delivery to individual cells during transfection-based delivery (Figure 7a). We reasoned that this selection against *Brca2* inactivation had a biological meaning to the cancer formation. Indeed, it was shown that the loss of *Brca2* without preceding *Trp53* signalling inactivation in the PK mouse model sensitized cancer cells towards genomic instability and eventually, growth arrest and apoptosis (Skoulidis *et al.*, 2010; Rowley *et al.*, 2011). In detail, in a *Trp53*-proficient background, *Brca2* inactivation in $Kras^{G12D}$ mice led to the abrogation of tumour formation, as cells would undergo lethal genomic instability. In contrast, defective *Trp53* signalling allowed *Brca2*-inactivated $Kras^{G12D}$ cells to evade the growth inhibition, or cell death caused by accumulation of chromosomal aberrations (Rowley *et al.*, 2011).

Electroporation for multiplexed delivery of CRISPR/Cas9 vectors to the mouse pancreas was the first experimental approach allowing direct *in vivo* negative-selection screening of genetic factors on a single cell level. Finding genetic vulnerabilities to *Kras*-driven cancers by performing systematic negative-selection screenings would open the possibility to determine essential cancer signalling components and translationally, to find novel treatment options for the patients. This approach would also make synthetic lethality screenings possible in the *in vivo* situation.

An important consideration for this application, however, is the fact that initially healthy un-transformed pancreatic cells would be edited by multiple CRISPR/Cas9 vectors, and not transformed neoplastic cells. Thus, resistance to synthetic lethality in normal un-transformed pancreatic cells or sensitivity in appropriate cancer models must be shown, as this would otherwise confound the interpretation negative selection process in the cancer. Yet, the *in vivo* implementation of such synthetic lethality screenings would integrate stroma-derived signalling factors, which could not be studied in conventional *in vitro* assays so far. Nevertheless, the consideration of extracellular signalling factors, originating from the pancreatic cancer stroma, has a high relevance for the understanding of the biology of pancreatic cancer.

10.4. Phylogenetic tracking using CRISPR/Cas9-induced mutational signatures

A consequence of delivering multiple sgRNAs to single cells through *in vivo* electroporation of the mouse pancreas was the generation of "mutational signatures", caused by CRISPR/Cas9 gene editing at numerous known positions in the genome. Different regional samples from

electroporated cancers were cultivated and amplicon-based deep sequencing performed. In case, the lengths and genomic positions of 15 different targeted indels overlapped perfectly from different regions of one cancer, it was very likely that all cancer cells were sharing the same founding clone. Obtained unique mutational signatures from different regional samples of a tumour can be used to study the evolution of the founding cancer clones. Hence, this method was applied to ascertain different founding cancer cell populations in each sample (e.g. specific primary tumour region or metastatic lesion). Because of the low-frequency mosaic targeting of pancreatic cells with sgRNA vector mix, CRISPR/Cas9-mutated cancers evolved from a very limited number of founding cells. Out of five regionally analysed cancers, we only found evidence for one sample comprising two different founder clones. In the remaining regional samples, no variant read support for other CRISPR/Cas9-edited cancer clones could be detected. To sum up, multiplexed CRISPR/Cas9-induced mutational signatures have sufficiently covered the number of *detectable* cancer clones in a targeted sample, especially if there were large (>10bp) marker indels present in the cancer clone.

Another application of multiplexed *in vivo* sgRNA electroporation of the mouse was the phylogenetic tracking of metastatic disease of a primary pancreatic cancer (Figure 9). We found one electroporated mouse that suffered from massive metastatic spreading to the liver. This mouse featured a mixed primary pancreatic tumour, where unique mutational signatures clearly discriminated two distinct cancer clones (Figure 9). These mutational patterns were used to assign individual metastatic colonies to either of the founding cancer clones.

In vivo electroporation of CRISPR/Cas9 would offer two critical advantages over other conventionally used metastasis mouse models. First, genetic barcodes, such as CRISPR/Cas9-induced mutational signatures, are very difficult to establish in traditional GEMM models. Second, orthotopically transplanted pancreatic cancer cells could comprise a genetic barcode, however, leakage at the site of transplantation could confound the metastatic phenotype. Hence, multiplexed electroporation of CRISPR/Cas9 is a very useful tool to study the biology of metastatic disease in pancreatic cancer.

In patients, early metastatic dissemination from the primary pancreatic cancer is frequently present at the time of diagnosis and thus, limiting the treatment options (Ryan *et al.*, 2014). *In vivo* electroporation could be deployed to monitor the blood circulation for the presence of targeted cancer cells. Thus, it would be possible to study the exact timing of systemic dissemination and open the possibility to test early metastasis detection applications, including tools screening for circulating cell-free DNA.

Furthermore, the study of factors facilitating metastasis is highly relevant in the pancreatic cancer research field, because it will lead to development of *screenable* marker genes and clinical treatment options. A potential experimental setup could be the addition of sgRNAs targeting *bona fide* factors enhancing the metastatic capacity to a "basal" vector mix. The enrichment of inactivated target gene(s) in the metastatic seeds could point towards the biologic relevance of the factor. Hence, there are many feasible applications to study not only the genetic basis of pancreatic cancer evolution, but also translational aspects of metastatic disease.

Recently, by the mouse-human species cross-comparison of PDAC exomes, we have found similar somatic mutational patterns in the tri-nucleotide context, however a significant reduction of somatic nucleotide variants (SNVs), indels, copy number alterations (CNAs) and translocations in the mouse situation (Mueller *et al.*, 2018). When analysing the allelic status of PDAC primary cultures derived from $Kras^{LSL-G12D/+}$ mouse model, we observed a correlation between a complete loss of *Cdkn2a* and concomitant amplification of the engineered mutant *Kras* allele. The consequential increased gene dosage of mutant *Kras* likely underlies the aggressive undifferentiated phenotype observed in this molecular cancer entity. In contrast, if a single functional copy of the *Cdkn2a* tumour suppressor is retained, an increased mutant *Kras* gene dosage was not tolerated and probably, would drive the cancer cell into oncogene-induced senescence. However, these cancers amplify alternative oncogenes including *Myc*, *Yap1* or *Nfkb2* collaborating with heterozygous mutant *Kras* signalling. This molecular PDAC sub-cluster was histologically well-differentiated and presented a rather epithelial morphology (Mueller *et al.*, 2018).

Interestingly, mixed cancer cell morphologies of epithelial and mesenchymal appearance were discovered in Tu4 primary culture. Differential trypsinization allowed separation of the morphologically distinct populations. Further, amplicon-based deep sequencing of sgRNA target sites revealed identical mutational signatures in both samples (Figure 11). This finding indicated, that both populations shared the same cancer cell clone of origin and, that the morphological difference could not be explained through differential CRISPR/Cas9 target gene editing. Notably, in both cases, *Cdkn2a* was completely inactivated by CRISPR/Cas9 editing. However, the mesenchymal population comprised a mutant *Kras* VAF of 80%, whereas the epithelial remained at 56%. This gain was explained by an additional chromosomal copy of the mutant *Kras* allele (Figure 12a). Consequentially, in the mesenchymal population, *Kras* mRNA levels were upregulated and transcriptomics revealed enriched gene sets for "EMT" and "MAPK signalling" (Figure 12b,d). Biologically, the mesenchymal cancer cell population became more serum-independent. Western blot analysis also showed dysregulation of the DDR,

as indicated by increased basal p-CHK1 levels and lack of a p21 response to doxorubicin, compared to the epithelial fraction (Figure 12e). We also found another example of increased mutant *Kras* dosage in the mesenchymal fraction of an otherwise mixed cancer culture (Data not shown). Again, the *Cdkn2a* tumour suppressor was completely inactivated by sgRNA editing. This case did not present $Kras^{LSL-G12D/+}$ amplification on the genomic, but elevated mutant *Kras* mRNA levels. Both examples point towards the conclusions that: (i) Already established cancer cells can undergo a morphological and likely a molecular evolution. (ii) The fate of the cancer phenotype is not necessarily pre-determined during the initial transformation process. (iii) Mutant *Kras* gene dosage variation is contributing to the histologic cancer phenotypes *in vivo* and the morphological appearance of PDAC-derived cultures *in vitro*. However, further examples must be studied to support the hypothesis, and whole exome or genome sequencing conducted to exclude the possibility of other unknown genomic factors explaining observed phenotypes.

In summary, electroporation-based CRISPR/Cas9 gene editing allowed not only the simultaneous delivery of multiple sgRNA to individual cells to induce complex (cancer) genotypes in the pancreas of adult mice, but also enabled the read-out of mutational sequences from targeted loci to phylogenetically trace back i.e. metastatic lesions or distinct cancer phenotypes.

10.5. *In vivo* CRISPR/Cas9-multiplexing for chromosome engineering

Structural rearrangements of chromosomes can occur in virtually all cancer entities. Thus, models to study the tremendous consequences of large structural aberrations in cancer biology are required to study this phenomenon (Ramirez-Solis *et al.*, 1995; Yu *et al.*, 2001). Furthermore, genomic instability is also a hallmark in human pancreatic cancer (Waddell *et al.*, 2015). By performing M-FISH analysis of CRISPR/Cas9 edited cancers, a subset of electroporated primary cancer cultures showed indications of chromosomal rearrangements, potentially involving sgRNA target sites. We speculated, whether the simultaneous cutting of multiple positions in the genome may lead to intra-chromosomal fusions (in case of targeting the same chromosome) or even to inter-chromosomal translocations (in case of different chromosomes). In both scenarios, this would cause inactivation of involved target genes and consequentially, the structural rearrangement of involved chromosome(s).

In case of intra-chromosomal fusions, PCR-based screening for all possible fusion products between two sgRNA target sites on one chromosome was performed. One out of six primary cultures showed evidence for such an event (Figure 10). By integrating M-FISH data, two inter-chromosomal rearrangements and associated large deletions between sgRNA target sites were

detected by PCR. To our knowledge, this was the first example of a targeted *in vivo* chromosomal translocation modelled in a higher organism.

The impact of structural alterations on tumorigenesis arising from human sequencing studies could so far only be studied laboriously in GEMMs. Manipulation of chromosomes in higher organisms is very challenging (Ramirez-Solis *et al.*, 1995). *Bona fide* oncogenic fusion proteins, arising from intra-chromosomal deletions, were mostly introduced to accessible loci in the germ line of mice (Maezawa *et al.*, 1985; Heisterkamp *et al.*, 1990). This approach carried the disadvantage of missing critical regulatory elements that would define the gene dosage of the oncogenic fusion protein. To account for this limitation, larger endogenous structural rearrangements could be modelled by using the *Cre-loxP* system (Review in (Yu *et al.*, 2001). Multiplexed sgRNA delivery to an autochthonous pancreatic cancer mouse model would allow the study of chromosome-level alterations comprising cancer-relevant coding as well as non-coding genetic regions. *In vivo* chromosome engineering would accelerate the potential to study structural alterations, frequently found in human pancreatic cancers (Childs *et al.*, 2015; Wolpin *et al.*, 2014). Targeting genomic breakpoints by multiple sgRNAs could increase the likelihood of the desired structural alteration. Subsequent genetic analysis of resulting malignant lesions would point towards most relevant chromosomal rearrangements and reveal essential genetic alterations for tumour development. Eventually, this finding also highlighted a conceptual limitation to *in vivo* electroporation in mice: Multiplexed CRISPR/Cas9 genome editing approaches require careful sgRNA design and testing, because already two concomitant double strand breaks in the genome could increase the likelihood of a chromosome-level alteration.

10.6. Conclusion

Human large-scale sequencing studies have established large catalogues of potential driver alterations, which need to be validated in suitable model systems. Traditional mouse models recapitulate human cancer biology and, thus have brought functional meaning to oncogenic mutations. However, the time required for generating these models and the cost- and labour-intensive nature have created the need for *in vivo* models suited for high-throughput functional genomics. Here, the newly developed method, electroporation-based multiplexed CRISPR/Cas9 genome editing in the adult mouse pancreas, will increase the speed and efficiency to model combinatorial candidate mutations in the organ. The mosaic pattern of CRISPR/Cas9-targeting in adult mice recapitulates sporadic tumorigenesis in humans. The genetic analyses of these "quantitative cancer genotypes" (Fraction of individual cancer clones among the total cancer population) within individual mice will accelerate the study of potential tumorigenic alterations. In summary, the development of scalable cancer models to accelerate

functional interrogation will open a comprehensive understanding of oncogenic networks driving respective tumours and eventually, a leverage for the translational aspects of cancer research.

11. Acknowledgements

12. References

Ryan, D.P., Hong, T.S., and Bardeesy, N. (2014). Pancreatic adenocarcinoma. N Engl J Med *371*, 1039-1049.

Rahib, L., Smith, B.D., Aizenberg, R., Rosenzweig, A.B., Fleshman, J.M., and Matrisian, L.M. (2014). Projecting cancer incidence and deaths to 2030: the unexpected burden of thyroid, liver, and pancreas cancers in the United States. Cancer Res *74*, 2913-2921.

Siegel, R.L., Miller, K.D., and Jemal, A. (2018). Cancer statistics, 2018. CA Cancer J Clin *68*, 7-30.

Rebours, V., Boutron-Ruault, M.C., Schnee, M., Ferec, C., Maire, F., Hammel, P., Ruszniewski, P., and Levy, P. (2008). Risk of pancreatic adenocarcinoma in patients with hereditary pancreatitis: a national exhaustive series. Am J Gastroenterol *103*, 111-119.

Giardiello, F.M., Brensinger, J.D., Tersmette, A.C., Goodman, S.N., Petersen, G.M., Booker, S.V., Cruz-Correa, M., and Offerhaus, J.A. (2000). Very high risk of cancer in familial Peutz-Jeghers syndrome. Gastroenterology *119*, 1447-1453.

Vasen, H.F., Gruis, N.A., Frants, R.R., van Der Velden, P.A., Hille, E.T., and Bergman, W. (2000). Risk of developing pancreatic cancer in families with familial atypical multiple mole melanoma associated with a specific 19 deletion of p16 (p16-Leiden). Int J Cancer *87*, 809-811.

Duell, E.J., Lucenteforte, E., Olson, S.H., Bracci, P.M., Li, D., Risch, H.A., Silverman, D.T., Ji, B.T., Gallinger, S., Holly, E.A., Fontham, E.H., Maisonneuve, P., Bueno-de-Mesquita, H.B., Ghadirian, P., Kurtz, R.C., Ludwig, E., Yu, H., Lowenfels, A.B., Seminara, D., Petersen, G.M., La Vecchia, C., and Boffetta, P. (2012). Pancreatitis and pancreatic cancer risk: a pooled analysis in the International Pancreatic Cancer Case-Control Consortium (PanC4). Ann Oncol *23*, 2964-2970.

Bosetti, C., Lucenteforte, E., Silverman, D.T., Petersen, G., Bracci, P.M., Ji, B.T., Negri, E., Li, D., Risch, H.A., Olson, S.H., Gallinger, S., Miller, A.B., Bueno-de-Mesquita, H.B., Talamini, R., Polesel, J., Ghadirian, P., Baghurst, P.A., Zatonski, W., Fontham, E., Bamlet, W.R., Holly, E.A., Bertuccio, P., Gao, Y.T., Hassan, M., Yu, H., Kurtz, R.C., Cotterchio, M., Su, J., Maisonneuve, P., Duell, E.J., Boffetta, P., and La Vecchia, C. (2012). Cigarette smoking and pancreatic cancer: an analysis from the International Pancreatic Cancer Case-Control Consortium (Panc4). Ann Oncol *23*, 1880-1888.

Ben, Q., Xu, M., Ning, X., Liu, J., Hong, S., Huang, W., Zhang, H., and Li, Z. (2011). Diabetes mellitus and risk of pancreatic cancer: A meta-analysis of cohort studies. Eur J Cancer *47*, 1928-1937.

Aune, D., Greenwood, D.C., Chan, D.S., Vieira, R., Vieira, A.R., Navarro Rosenblatt, D.A., Cade, J.E., Burley, V.J., and Norat, T. (2012). Body mass index, abdominal fatness and pancreatic cancer risk: a systematic review and non-linear dose-response meta-analysis of prospective studies. Ann Oncol *23*, 843-852.

Burris, H.A., 3rd, Moore, M.J., Andersen, J., Green, M.R., Rothenberg, M.L., Modiano, M.R., Cripps, M.C., Portenoy, R.K., Storniolo, A.M., Tarassoff, P., Nelson, R., Dorr, F.A., Stephens, C.D., and Von Hoff, D.D. (1997). Improvements in survival and clinical benefit with gemcitabine as first-line therapy for patients with advanced pancreas cancer: a randomized trial. J Clin Oncol *15*, 2403-2413.

Conroy, T., Desseigne, F., Ychou, M., Bouche, O., Guimbaud, R., Becouarn, Y., Adenis, A., Raoul, J.L., Gourgou-Bourgade, S., de la Fouchardiere, C., Bennouna, J., Bachet, J.B.,

Khemissa-Akouz, F., Pere-Verge, D., Delbaldo, C., Assenat, E., Chauffert, B., Michel, P., Montoto-Grillot, C., Ducreux, M., Groupe Tumeurs Digestives of, U., and Intergroup, P. (2011). FOLFIRINOX versus gemcitabine for metastatic pancreatic cancer. N Engl J Med *364*, 1817-1825.

Von Hoff, D.D., Ervin, T., Arena, F.P., Chiorean, E.G., Infante, J., Moore, M., Seay, T., Tjulandin, S.A., Ma, W.W., Saleh, M.N., Harris, M., Reni, M., Dowden, S., Laheru, D., Bahary, N., Ramanathan, R.K., Tabernero, J., Hidalgo, M., Goldstein, D., Van Cutsem, E., Wei, X., Iglesias, J., and Renschler, M.F. (2013). Increased survival in pancreatic cancer with nab-paclitaxel plus gemcitabine. N Engl J Med *369*, 1691-1703.

Hebrok, M., Kim, S.K., and Melton, D.A. (1998). Notochord repression of endodermal Sonic hedgehog permits pancreas development. Genes Dev *12*, 1705-1713.

Offield, M.F., Jetton, T.L., Labosky, P.A., Ray, M., Stein, R.W., Magnuson, M.A., Hogan, B.L., and Wright, C.V. (1996). PDX-1 is required for pancreatic outgrowth and differentiation of the rostral duodenum. Development *122*, 983-995.

Krapp, A., Knofler, M., Ledermann, B., Burki, K., Berney, C., Zoerkler, N., Hagenbuchle, O., and Wellauer, P.K. (1998). The bHLH protein PTF1-p48 is essential for the formation of the exocrine and the correct spatial organization of the endocrine pancreas. Genes Dev *12*, 3752-3763.

Kawaguchi, Y., Cooper, B., Gannon, M., Ray, M., MacDonald, R.J., and Wright, C.V. (2002). The role of the transcriptional regulator Ptf1a in converting intestinal to pancreatic progenitors. Nat Genet *32*, 128-134.

Kim, S.K., and MacDonald, R.J. (2002). Signaling and transcriptional control of pancreatic organogenesis. Curr Opin Genet Dev *12*, 540-547.

Horn, S., Kobberup, S., Jorgensen, M.C., Kalisz, M., Klein, T., Kageyama, R., Gegg, M., Lickert, H., Lindner, J., Magnuson, M.A., Kong, Y.Y., Serup, P., Ahnfelt-Ronne, J., and Jensen, J.N. (2012). Mind bomb 1 is required for pancreatic beta-cell formation. Proc Natl Acad Sci U S A *109*, 7356-7361.

Wells, J.M., Esni, F., Boivin, G.P., Aronow, B.J., Stuart, W., Combs, C., Sklenka, A., Leach, S.D., and Lowy, A.M. (2007). Wnt/beta-catenin signaling is required for development of the exocrine pancreas. BMC Dev Biol *7*, 4.

Pan, F.C., Bankaitis, E.D., Boyer, D., Xu, X., Van de Casteele, M., Magnuson, M.A., Heimberg, H., and Wright, C.V. (2013). Spatiotemporal patterns of multipotentiality in Ptf1a-expressing cells during pancreas organogenesis and injury-induced facultative restoration. Development *140*, 751-764.

Hruban, R.H., Goggins, M., Parsons, J., and Kern, S.E. (2000a). Progression model for pancreatic cancer. Clin Cancer Res *6*, 2969-2972.

Kanda, M., Matthaei, H., Wu, J., Hong, S.M., Yu, J., Borges, M., Hruban, R.H., Maitra, A., Kinzler, K., Vogelstein, B., and Goggins, M. (2012). Presence of somatic mutations in most early-stage pancreatic intraepithelial neoplasia. Gastroenterology *142*, 730-733 e739.

Mueller, S., Engleitner, T., Maresch, R., Zukowska, M., Lange, S., Kaltenbacher, T., Konukiewitz, B., Ollinger, R., Zwiebel, M., Strong, A., Yen, H.Y., Banerjee, R., Louzada, S., Fu, B., Seidler, B., Gotzfried, J., Schuck, K., Hassan, Z., Arbeiter, A., Schonhuber, N., Klein, S., Veltkamp, C., Friedrich, M., Rad, L., Barenboim, M., Ziegenhain, C., Hess, J., Dovey, O.M., Eser, S., Parekh, S., Constantino-Casas, F., de la Rosa, J., Sierra, M.I., Fraga, M., Mayerle, J., Kloppel, G., Cadinanos, J., Liu, P., Vassiliou, G., Weichert, W., Steiger, K., Enard, W., Schmid, R.M., Yang, F., Unger, K., Schneider, G., Varela, I., Bradley, A., Saur, D., and Rad, R. (2018).

Evolutionary routes and KRAS dosage define pancreatic cancer phenotypes. Nature *554*, 62-68.

Jones, S., Zhang, X., Parsons, D.W., Lin, J.C., Leary, R.J., Angenendt, P., Mankoo, P., Carter, H., Kamiyama, H., Jimeno, A., Hong, S.M., Fu, B., Lin, M.T., Calhoun, E.S., Kamiyama, M., Walter, K., Nikolskaya, T., Nikolsky, Y., Hartigan, J., Smith, D.R., Hidalgo, M., Leach, S.D., Klein, A.P., Jaffee, E.M., Goggins, M., Maitra, A., Iacobuzio-Donahue, C., Eshleman, J.R., Kern, S.E., Hruban, R.H., Karchin, R., Papadopoulos, N., Parmigiani, G., Vogelstein, B., Velculescu, V.E., and Kinzler, K.W. (2008). Core signaling pathways in human pancreatic cancers revealed by global genomic analyses. Science *321*, 1801-1806.

Biankin, A.V., Waddell, N., Kassahn, K.S., Gingras, M.C., Muthuswamy, L.B., Johns, A.L., Miller, D.K., Wilson, P.J., Patch, A.M., Wu, J., Chang, D.K., Cowley, M.J., Gardiner, B.B., Song, S., Harliwong, I., Idrisoglu, S., Nourse, C., Nourbakhsh, E., Manning, S., Wani, S., Gongora, M., Pajic, M., Scarlett, C.J., Gill, A.J., Pinho, A.V., Rooman, I., Anderson, M., Holmes, O., Leonard, C., Taylor, D., Wood, S., Xu, Q., Nones, K., Fink, J.L., Christ, A., Bruxner, T., Cloonan, N., Kolle, G., Newell, F., Pinese, M., Mead, R.S., Humphris, J.L., Kaplan, W., Jones, M.D., Colvin, E.K., Nagrial, A.M., Humphrey, E.S., Chou, A., Chin, V.T., Chantrill, L.A., Mawson, A., Samra, J.S., Kench, J.G., Lovell, J.A., Daly, R.J., Merrett, N.D., Toon, C., Epari, K., Nguyen, N.Q., Barbour, A., Zeps, N., Australian Pancreatic Cancer Genome, I., Kakkar, N., Zhao, F., Wu, Y.Q., Wang, M., Muzny, D.M., Fisher, W.E., Brunicardi, F.C., Hodges, S.E., Reid, J.G., Drummond, J., Chang, K., Han, Y., Lewis, L.R., Dinh, H., Buhay, C.J., Beck, T., Timms, L., Sam, M., Begley, K., Brown, A., Pai, D., Panchal, A., Buchner, N., De Borja, R., Denroche, R.E., Yung, C.K., Serra, S., Onetto, N., Mukhopadhyay, D., Tsao, M.S., Shaw, P.A., Petersen, G.M., Gallinger, S., Hruban, R.H., Maitra, A., Iacobuzio-Donahue, C.A., Schulick, R.D., Wolfgang, C.L., Morgan, R.A., Lawlor, R.T., Capelli, P., Corbo, V., Scardoni, M., Tortora, G., Tempero, M.A., Mann, K.M., Jenkins, N.A., Perez-Mancera, P.A., Adams, D.J., Largaespada, D.A., Wessels, L.F., Rust, A.G., Stein, L.D., Tuveson, D.A., Copeland, N.G., Musgrove, E.A., Scarpa, A., Eshleman, J.R., Hudson, T.J., Sutherland, R.L., Wheeler, D.A., Pearson, J.V., McPherson, J.D., Gibbs, R.A., and Grimmond, S.M. (2012). Pancreatic cancer genomes reveal aberrations in axon guidance pathway genes. Nature *491*, 399-405.

Waddell, N., Pajic, M., Patch, A.M., Chang, D.K., Kassahn, K.S., Bailey, P., Johns, A.L., Miller, D., Nones, K., Quek, K., Quinn, M.C., Robertson, A.J., Fadlullah, M.Z., Bruxner, T.J., Christ, A.N., Harliwong, I., Idrisoglu, S., Manning, S., Nourse, C., Nourbakhsh, E., Wani, S., Wilson, P.J., Markham, E., Cloonan, N., Anderson, M.J., Fink, J.L., Holmes, O., Kazakoff, S.H., Leonard, C., Newell, F., Poudel, B., Song, S., Taylor, D., Waddell, N., Wood, S., Xu, Q., Wu, J., Pinese, M., Cowley, M.J., Lee, H.C., Jones, M.D., Nagrial, A.M., Humphris, J., Chantrill, L.A., Chin, V., Steinmann, A.M., Mawson, A., Humphrey, E.S., Colvin, E.K., Chou, A., Scarlett, C.J., Pinho, A.V., Giry-Laterriere, M., Rooman, I., Samra, J.S., Kench, J.G., Pettitt, J.A., Merrett, N.D., Toon, C., Epari, K., Nguyen, N.Q., Barbour, A., Zeps, N., Jamieson, N.B., Graham, J.S., Niclou, S.P., Bjerkvig, R., Grutzmann, R., Aust, D., Hruban, R.H., Maitra, A., Iacobuzio-Donahue, C.A., Wolfgang, C.L., Morgan, R.A., Lawlor, R.T., Corbo, V., Bassi, C., Falconi, M., Zamboni, G., Tortora, G., Tempero, M.A., Australian Pancreatic Cancer Genome, I., Gill, A.J., Eshleman, J.R., Pilarsky, C., Scarpa, A., Musgrove, E.A., Pearson, J.V., Biankin, A.V., and Grimmond, S.M. (2015). Whole genomes redefine the mutational landscape of pancreatic cancer. Nature *518*, 495-501.

Bailey, P., Chang, D.K., Nones, K., Johns, A.L., Patch, A.M., Gingras, M.C., Miller, D.K., Christ, A.N., Bruxner, T.J., Quinn, M.C., Nourse, C., Murtaugh, L.C., Harliwong, I., Idrisoglu, S., Manning, S., Nourbakhsh, E., Wani, S., Fink, L., Holmes, O., Chin, V., Anderson, M.J., Kazakoff, S., Leonard, C., Newell, F., Waddell, N., Wood, S., Xu, Q., Wilson, P.J., Cloonan,

N., Kassahn, K.S., Taylor, D., Quek, K., Robertson, A., Pantano, L., Mincarelli, L., Sanchez, L.N., Evers, L., Wu, J., Pinese, M., Cowley, M.J., Jones, M.D., Colvin, E.K., Nagrial, A.M., Humphrey, E.S., Chantrill, L.A., Mawson, A., Humphris, J., Chou, A., Pajic, M., Scarlett, C.J., Pinho, A.V., Giry-Laterriere, M., Rooman, I., Samra, J.S., Kench, J.G., Lovell, J.A., Merrett, N.D., Toon, C.W., Epari, K., Nguyen, N.Q., Barbour, A., Zeps, N., Moran-Jones, K., Jamieson, N.B., Graham, J.S., Duthie, F., Oien, K., Hair, J., Grutzmann, R., Maitra, A., Iacobuzio-Donahue, C.A., Wolfgang, C.L., Morgan, R.A., Lawlor, R.T., Corbo, V., Bassi, C., Rusev, B., Capelli, P., Salvia, R., Tortora, G., Mukhopadhyay, D., Petersen, G.M., Australian Pancreatic Cancer Genome, I., Munzy, D.M., Fisher, W.E., Karim, S.A., Eshleman, J.R., Hruban, R.H., Pilarsky, C., Morton, J.P., Sansom, O.J., Scarpa, A., Musgrove, E.A., Bailey, U.M., Hofmann, O., Sutherland, R.L., Wheeler, D.A., Gill, A.J., Gibbs, R.A., Pearson, J.V., Waddell, N., Biankin, A.V., and Grimmond, S.M. (2016a). Genomic analyses identify molecular subtypes of pancreatic cancer. Nature *531*, 47-52.

Witkiewicz, A.K., McMillan, E.A., Balaji, U., Baek, G., Lin, W.C., Mansour, J., Mollaee, M., Wagner, K.U., Koduru, P., Yopp, A., Choti, M.A., Yeo, C.J., McCue, P., White, M.A., and Knudsen, E.S. (2015). Whole-exome sequencing of pancreatic cancer defines genetic diversity and therapeutic targets. Nat Commun *6*, 6744.

Cancer Genome Atlas Research Network. Electronic address, a.a.d.h.e., and Cancer Genome Atlas Research, N. (2017). Integrated Genomic Characterization of Pancreatic Ductal Adenocarcinoma. Cancer Cell *32*, 185-203 e113.

Griffin, C.A., Morsberger, L., Hawkins, A.L., Haddadin, M., Patel, A., Ried, T., Schrock, E., Perlman, E.J., and Jaffee, E. (2007). Molecular cytogenetic characterization of pancreas cancer cell lines reveals high complexity chromosomal alterations. Cytogenet Genome Res *118*, 148-156.

Notta, F., Chan-Seng-Yue, M., Lemire, M., Li, Y., Wilson, G.W., Connor, A.A., Denroche, R.E., Liang, S.B., Brown, A.M., Kim, J.C., Wang, T., Simpson, J.T., Beck, T., Borgida, A., Buchner, N., Chadwick, D., Hafezi-Bakhtiari, S., Dick, J.E., Heisler, L., Hollingsworth, M.A., Ibrahimov, E., Jang, G.H., Johns, J., Jorgensen, L.G., Law, C., Ludkovski, O., Lungu, I., Ng, K., Pasternack, D., Petersen, G.M., Shlush, L.I., Timms, L., Tsao, M.S., Wilson, J.M., Yung, C.K., Zogopoulos, G., Bartlett, J.M., Alexandrov, L.B., Real, F.X., Cleary, S.P., Roehrl, M.H., McPherson, J.D., Stein, L.D., Hudson, T.J., Campbell, P.J., and Gallinger, S. (2016). A renewed model of pancreatic cancer evolution based on genomic rearrangement patterns. Nature *538*, 378-382.

Kong, B., Michalski, C.W., Erkan, M., Friess, H., and Kleeff, J. (2011). From tissue turnover to the cell of origin for pancreatic cancer. Nat Rev Gastroenterol Hepatol *8*, 467-472.

Hruban, R.H., Wilentz, R.E., and Kern, S.E. (2000b). Genetic progression in the pancreatic ducts. Am J Pathol *156*, 1821-1825.

Kopp, J.L., von Figura, G., Mayes, E., Liu, F.F., Dubois, C.L., Morris, J.P.t., Pan, F.C., Akiyama, H., Wright, C.V., Jensen, K., Hebrok, M., and Sander, M. (2012). Identification of Sox9-dependent acinar-to-ductal reprogramming as the principal mechanism for initiation of pancreatic ductal adenocarcinoma. Cancer Cell *22*, 737-750.

Bailey, J.M., Hendley, A.M., Lafaro, K.J., Pruski, M.A., Jones, N.C., Alsina, J., Younes, M., Maitra, A., McAllister, F., Iacobuzio-Donahue, C.A., and Leach, S.D. (2016b). p53 mutations cooperate with oncogenic Kras to promote adenocarcinoma from pancreatic ductal cells. Oncogene *35*, 4282-4288.

Miyatsuka, T., Kaneto, H., Shiraiwa, T., Matsuoka, T.A., Yamamoto, K., Kato, K., Nakamura, Y., Akira, S., Takeda, K., Kajimoto, Y., Yamasaki, Y., Sandgren, E.P., Kawaguchi, Y., Wright,

C.V., and Fujitani, Y. (2006). Persistent expression of PDX-1 in the pancreas causes acinar-to-ductal metaplasia through Stat3 activation. Genes Dev *20*, 1435-1440.

Shi, C., Hong, S.M., Lim, P., Kamiyama, H., Khan, M., Anders, R.A., Goggins, M., Hruban, R.H., and Eshleman, J.R. (2009). KRAS2 mutations in human pancreatic acinar-ductal metaplastic lesions are limited to those with PanIN: implications for the human pancreatic cancer cell of origin. Mol Cancer Res *7*, 230-236.

Zhu, L., Shi, G., Schmidt, C.M., Hruban, R.H., and Konieczny, S.F. (2007). Acinar cells contribute to the molecular heterogeneity of pancreatic intraepithelial neoplasia. Am J Pathol *171*, 263-273.

Guerra, C., Schuhmacher, A.J., Canamero, M., Grippo, P.J., Verdaguer, L., Perez-Gallego, L., Dubus, P., Sandgren, E.P., and Barbacid, M. (2007). Chronic pancreatitis is essential for induction of pancreatic ductal adenocarcinoma by K-Ras oncogenes in adult mice. Cancer Cell *11*, 291-302.

Reichert, M., Blume, K., Kleger, A., Hartmann, D., and von Figura, G. (2016). Developmental Pathways Direct Pancreatic Cancer Initiation from Its Cellular Origin. Stem Cells Int *2016*, 9298535.

Murtaugh, L.C., and Keefe, M.D. (2015). Regeneration and repair of the exocrine pancreas. Annu Rev Physiol *77*, 229-249.

Morris, J.P.t., Cano, D.A., Sekine, S., Wang, S.C., and Hebrok, M. (2010). Beta-catenin blocks Kras-dependent reprogramming of acini into pancreatic cancer precursor lesions in mice. J Clin Invest *120*, 508-520.

Ferreira, R.M.M., Sancho, R., Messal, H.A., Nye, E., Spencer-Dene, B., Stone, R.K., Stamp, G., Rosewell, I., Quaglia, A., and Behrens, A. (2017). Duct- and Acinar-Derived Pancreatic Ductal Adenocarcinomas Show Distinct Tumor Progression and Marker Expression. Cell Rep *21*, 966-978.

Jakel, C., Bergmann, F., Toth, R., Assenov, Y., van der Duin, D., Strobel, O., Hank, T., Kloppel, G., Dorrell, C., Grompe, M., Moss, J., Dor, Y., Schirmacher, P., Plass, C., Popanda, O., and Schmezer, P. (2017). Genome-wide genetic and epigenetic analyses of pancreatic acinar cell carcinomas reveal aberrations in genome stability. Nat Commun *8*, 1323.

Capper, D., Jones, D.T.W., Sill, M., Hovestadt, V., Schrimpf, D., Sturm, D., Koelsche, C., Sahm, F., Chavez, L., Reuss, D.E., Kratz, A., Wefers, A.K., Huang, K., Pajtler, K.W., Schweizer, L., Stichel, D., Olar, A., Engel, N.W., Lindenberg, K., Harter, P.N., Braczynski, A.K., Plate, K.H., Dohmen, H., Garvalov, B.K., Coras, R., Holsken, A., Hewer, E., Bewerunge-Hudler, M., Schick, M., Fischer, R., Beschorner, R., Schittenhelm, J., Staszewski, O., Wani, K., Varlet, P., Pages, M., Temming, P., Lohmann, D., Selt, F., Witt, H., Milde, T., Witt, O., Aronica, E., Giangaspero, F., Rushing, E., Scheurlen, W., Geisenberger, C., Rodriguez, F.J., Becker, A., Preusser, M., Haberler, C., Bjerkvig, R., Cryan, J., Farrell, M., Deckert, M., Hench, J., Frank, S., Serrano, J., Kannan, K., Tsirigos, A., Bruck, W., Hofer, S., Brehmer, S., Seiz-Rosenhagen, M., Hanggi, D., Hans, V., Rozsnoki, S., Hansford, J.R., Kohlhof, P., Kristensen, B.W., Lechner, M., Lopes, B., Mawrin, C., Ketter, R., Kulozik, A., Khatib, Z., Heppner, F., Koch, A., Jouvet, A., Keohane, C., Muhleisen, H., Mueller, W., Pohl, U., Prinz, M., Benner, A., Zapatka, M., Gottardo, N.G., Driever, P.H., Kramm, C.M., Muller, H.L., Rutkowski, S., von Hoff, K., Fruhwald, M.C., Gnekow, A., Fleischhack, G., Tippelt, S., Calaminus, G., Monoranu, C.M., Perry, A., Jones, C., Jacques, T.S., Radlwimmer, B., Gessi, M., Pietsch, T., Schramm, J., Schackert, G., Westphal, M., Reifenberger, G., Wesseling, P., Weller, M., Collins, V.P., Blumcke, I., Bendszus, M., Debus, J., Huang, A., Jabado, N., Northcott, P.A., Paulus, W., Gajjar, A., Robinson, G.W., Taylor, M.D., Jaunmuktane, Z., Ryzhova, M., Platten, M.,

Unterberg, A., Wick, W., Karajannis, M.A., Mittelbronn, M., Acker, T., Hartmann, C., Aldape, K., Schuller, U., Buslei, R., Lichter, P., Kool, M., Herold-Mende, C., Ellison, D.W., Hasselblatt, M., Snuderl, M., Brandner, S., Korshunov, A., von Deimling, A., and Pfister, S.M. (2018). DNA methylation-based classification of central nervous system tumours. Nature *555*, 469-474.

Pylayeva-Gupta, Y., Grabocka, E., and Bar-Sagi, D. (2011). RAS oncogenes: weaving a tumorigenic web. Nat Rev Cancer *11*, 761-774.

Plowman, S.J., and Hancock, J.F. (2005). Ras signaling from plasma membrane and endomembrane microdomains. Biochim Biophys Acta *1746*, 274-283.

Bourne, H.R., Sanders, D.A., and McCormick, F. (1990). The GTPase superfamily: a conserved switch for diverse cell functions. Nature *348*, 125-132.

Field, J., Broek, D., Kataoka, T., and Wigler, M. (1987). Guanine nucleotide activation of, and competition between, RAS proteins from Saccharomyces cerevisiae. Mol Cell Biol *7*, 2128-2133.

Wittinghofer, A., and Pai, E.F. (1991). The structure of Ras protein: a model for a universal molecular switch. Trends Biochem Sci *16*, 382-387.

Hunter, J.C., Manandhar, A., Carrasco, M.A., Gurbani, D., Gondi, S., and Westover, K.D. (2015). Biochemical and Structural Analysis of Common Cancer-Associated KRAS Mutations. Mol Cancer Res *13*, 1325-1335.

Wolfman, A., and Macara, I.G. (1990). A cytosolic protein catalyzes the release of GDP from p21ras. Science *248*, 67-69.

Trahey, M., and McCormick, F. (1987). A cytoplasmic protein stimulates normal N-ras p21 GTPase, but does not affect oncogenic mutants. Science *238*, 542-545.

Scheidig, A.J., Burmester, C., and Goody, R.S. (1999). The pre-hydrolysis state of p21(ras) in complex with GTP: new insights into the role of water molecules in the GTP hydrolysis reaction of ras-like proteins. Structure *7*, 1311-1324.

Buhrman, G., Holzapfel, G., Fetics, S., and Mattos, C. (2010). Allosteric modulation of Ras positions Q61 for a direct role in catalysis. Proc Natl Acad Sci U S A *107*, 4931-4936.

Scheffzek, K., Ahmadian, M.R., Kabsch, W., Wiesmuller, L., Lautwein, A., Schmitz, F., and Wittinghofer, A. (1997). The Ras-RasGAP complex: structural basis for GTPase activation and its loss in oncogenic Ras mutants. Science *277*, 333-338.

Stacey, D.W., Watson, T., Kung, H.F., and Curran, T. (1987). Microinjection of transforming ras protein induces c-fos expression. Mol Cell Biol *7*, 523-527.

Gutman, A., Wasylyk, C., and Wasylyk, B. (1991). Cell-specific regulation of oncogene-responsive sequences of the c-fos promoter. Mol Cell Biol *11*, 5381-5387.

Urich, M., Senften, M., Shaw, P.E., and Ballmer-Hofer, K. (1997). A role for the small GTPase Rac in polyomavirus middle-T antigen-mediated activation of the serum response element and in cell transformation. Oncogene *14*, 1235-1241.

Westwick, J.K., Cox, A.D., Der, C.J., Cobb, M.H., Hibi, M., Karin, M., and Brenner, D.A. (1994). Oncogenic Ras activates c-Jun via a separate pathway from the activation of extracellular signal-regulated kinases. Proc Natl Acad Sci U S A *91*, 6030-6034.

Finco, T.S., Westwick, J.K., Norris, J.L., Beg, A.A., Der, C.J., and Baldwin, A.S., Jr. (1997). Oncogenic Ha-Ras-induced signaling activates NF-kappaB transcriptional activity, which is required for cellular transformation. J Biol Chem *272*, 24113-24116.

Filmus, J., Robles, A.I., Shi, W., Wong, M.J., Colombo, L.L., and Conti, C.J. (1994). Induction of cyclin D1 overexpression by activated ras. Oncogene *9*, 3627-3633.

Winston, J.T., Coats, S.R., Wang, Y.Z., and Pledger, W.J. (1996). Regulation of the cell cycle machinery by oncogenic ras. Oncogene *12*, 127-134.

Hanahan, D., and Weinberg, R.A. (2011). Hallmarks of cancer: the next generation. Cell *144*, 646-674.

Moodie, S.A., Willumsen, B.M., Weber, M.J., and Wolfman, A. (1993). Complexes of Ras.GTP with Raf-1 and mitogen-activated protein kinase kinase. Science *260*, 1658-1661.

Warne, P.H., Viciana, P.R., and Downward, J. (1993). Direct interaction of Ras and the amino-terminal region of Raf-1 in vitro. Nature *364*, 352-355.

Zhang, X.F., Settleman, J., Kyriakis, J.M., Takeuchi-Suzuki, E., Elledge, S.J., Marshall, M.S., Bruder, J.T., Rapp, U.R., and Avruch, J. (1993). Normal and oncogenic p21ras proteins bind to the amino-terminal regulatory domain of c-Raf-1. Nature *364*, 308-313.

Marais, R., Light, Y., Paterson, H.F., and Marshall, C.J. (1995). Ras recruits Raf-1 to the plasma membrane for activation by tyrosine phosphorylation. EMBO J *14*, 3136-3145.

Maurer, G., Tarkowski, B., and Baccarini, M. (2011). Raf kinases in cancer-roles and therapeutic opportunities. Oncogene *30*, 3477-3488.

Chambard, J.C., Lefloch, R., Pouyssegur, J., and Lenormand, P. (2007). ERK implication in cell cycle regulation. Biochim Biophys Acta *1773*, 1299-1310.

Dougherty, M.K., Muller, J., Ritt, D.A., Zhou, M., Zhou, X.Z., Copeland, T.D., Conrads, T.P., Veenstra, T.D., Lu, K.P., and Morrison, D.K. (2005). Regulation of Raf-1 by direct feedback phosphorylation. Mol Cell *17*, 215-224.

Navas, C., Hernandez-Porras, I., Schuhmacher, A.J., Sibilia, M., Guerra, C., and Barbacid, M. (2012). EGF receptor signaling is essential for k-ras oncogene-driven pancreatic ductal adenocarcinoma. Cancer Cell *22*, 318-330.

Ardito, C.M., Gruner, B.M., Takeuchi, K.K., Lubeseder-Martellato, C., Teichmann, N., Mazur, P.K., Delgiorno, K.E., Carpenter, E.S., Halbrook, C.J., Hall, J.C., Pal, D., Briel, T., Herner, A., Trajkovic-Arsic, M., Sipos, B., Liou, G.Y., Storz, P., Murray, N.R., Threadgill, D.W., Sibilia, M., Washington, M.K., Wilson, C.L., Schmid, R.M., Raines, E.W., Crawford, H.C., and Siveke, J.T. (2012). EGF receptor is required for KRAS-induced pancreatic tumorigenesis. Cancer Cell *22*, 304-317.

Eser, S., Reiff, N., Messer, M., Seidler, B., Gottschalk, K., Dobler, M., Hieber, M., Arbeiter, A., Klein, S., Kong, B., Michalski, C.W., Schlitter, A.M., Esposito, I., Kind, A.J., Rad, L., Schnieke, A.E., Baccarini, M., Alessi, D.R., Rad, R., Schmid, R.M., Schneider, G., and Saur, D. (2013). Selective requirement of PI3K/PDK1 signaling for Kras oncogene-driven pancreatic cell plasticity and cancer. Cancer Cell *23*, 406-420.

Blasco, R.B., Francoz, S., Santamaria, D., Canamero, M., Dubus, P., Charron, J., Baccarini, M., and Barbacid, M. (2011). c-Raf, but not B-Raf, is essential for development of K-Ras oncogene-driven non-small cell lung carcinoma. Cancer Cell *19*, 652-663.

Janku, F., Yap, T.A., and Meric-Bernstam, F. (2018). Targeting the PI3K pathway in cancer: are we making headway? Nat Rev Clin Oncol *15*, 273-291.

Engelman, J.A. (2009). Targeting PI3K signalling in cancer: opportunities, challenges and limitations. Nat Rev Cancer *9*, 550-562.

Baer, R., Cintas, C., Dufresne, M., Cassant-Sourdy, S., Schonhuber, N., Planque, L., Lulka, H., Couderc, B., Bousquet, C., Garmy-Susini, B., Vanhaesebroeck, B., Pyronnet, S., Saur, D., and Guillermet-Guibert, J. (2014). Pancreatic cell plasticity and cancer initiation induced by oncogenic Kras is completely dependent on wild-type PI 3-kinase p110alpha. Genes Dev *28*, 2621-2635.

Guillermet-Guibert, J., Bjorklof, K., Salpekar, A., Gonella, C., Ramadani, F., Bilancio, A., Meek, S., Smith, A.J., Okkenhaug, K., and Vanhaesebroeck, B. (2008). The p110beta isoform of phosphoinositide 3-kinase signals downstream of G protein-coupled receptors and is functionally redundant with p110gamma. Proc Natl Acad Sci U S A *105*, 8292-8297.

Cantley, L.C. (2002). The phosphoinositide 3-kinase pathway. Science *296*, 1655-1657.

Alessi, D.R., James, S.R., Downes, C.P., Holmes, A.B., Gaffney, P.R., Reese, C.B., and Cohen, P. (1997). Characterization of a 3-phosphoinositide-dependent protein kinase which phosphorylates and activates protein kinase Balpha. Curr Biol *7*, 261-269.

Samuels, Y., and Velculescu, V.E. (2004). Oncogenic mutations of PIK3CA in human cancers. Cell Cycle *3*, 1221-1224.

Cairns, P., Okami, K., Halachmi, S., Halachmi, N., Esteller, M., Herman, J.G., Jen, J., Isaacs, W.B., Bova, G.S., and Sidransky, D. (1997). Frequent inactivation of PTEN/MMAC1 in primary prostate cancer. Cancer Res *57*, 4997-5000.

Asano, T., Yao, Y., Zhu, J., Li, D., Abbruzzese, J.L., and Reddy, S.A. (2004). The PI 3-kinase/Akt signaling pathway is activated due to aberrant Pten expression and targets transcription factors NF-kappaB and c-Myc in pancreatic cancer cells. Oncogene *23*, 8571-8580.

Hill, R., Calvopina, J.H., Kim, C., Wang, Y., Dawson, D.W., Donahue, T.R., Dry, S., and Wu, H. (2010). PTEN loss accelerates KrasG12D-induced pancreatic cancer development. Cancer Res *70*, 7114-7124.

Ying, H., Elpek, K.G., Vinjamoori, A., Zimmerman, S.M., Chu, G.C., Yan, H., Fletcher-Sananikone, E., Zhang, H., Liu, Y., Wang, W., Ren, X., Zheng, H., Kimmelman, A.C., Paik, J.H., Lim, C., Perry, S.R., Jiang, S., Malinn, B., Protopopov, A., Colla, S., Xiao, Y., Hezel, A.F., Bardeesy, N., Turley, S.J., Wang, Y.A., Chin, L., Thayer, S.P., and DePinho, R.A. (2011). PTEN is a major tumor suppressor in pancreatic ductal adenocarcinoma and regulates an NF-kappaB-cytokine network. Cancer Discov *1*, 158-169.

Collisson, E.A., Trejo, C.L., Silva, J.M., Gu, S., Korkola, J.E., Heiser, L.M., Charles, R.P., Rabinovich, B.A., Hann, B., Dankort, D., Spellman, P.T., Phillips, W.A., Gray, J.W., and McMahon, M. (2012). A central role for RAF-->MEK-->ERK signaling in the genesis of pancreatic ductal adenocarcinoma. Cancer Discov *2*, 685-693.

Mendoza, M.C., Er, E.E., and Blenis, J. (2011). The Ras-ERK and PI3K-mTOR pathways: cross-talk and compensation. Trends Biochem Sci *36*, 320-328.

Zhang, Y., Morris, J.P.t., Yan, W., Schofield, H.K., Gurney, A., Simeone, D.M., Millar, S.E., Hoey, T., Hebrok, M., and Pasca di Magliano, M. (2013). Canonical wnt signaling is required for pancreatic carcinogenesis. Cancer Res *73*, 4909-4922.

David, C.J., Huang, Y.H., Chen, M., Su, J., Zou, Y., Bardeesy, N., Iacobuzio-Donahue, C.A., and Massague, J. (2016). TGF-beta Tumor Suppression through a Lethal EMT. Cell *164*, 1015-1030.

Blair, A.B., Groot, V.P., Gemenetzis, G., Wei, J., Cameron, J.L., Weiss, M.J., Goggins, M., Wolfgang, C.L., Yu, J., and He, J. (2018). BRCA1/BRCA2 Germline Mutation Carriers and Sporadic Pancreatic Ductal Adenocarcinoma. J Am Coll Surg *226*, 630-637 e631.

Tao, W., and Levine, A.J. (1999). P19(ARF) stabilizes p53 by blocking nucleo-cytoplasmic shuttling of Mdm2. Proc Natl Acad Sci U S A *96*, 6937-6941.

Russell, R., Perkhofer, L., Liebau, S., Lin, Q., Lechel, A., Feld, F.M., Hessmann, E., Gaedcke, J., Guthle, M., Zenke, M., Hartmann, D., von Figura, G., Weissinger, S.E., Rudolph, K.L., Moller, P., Lennerz, J.K., Seufferlein, T., Wagner, M., and Kleger, A. (2015). Loss of ATM accelerates pancreatic cancer formation and epithelial-mesenchymal transition. Nat Commun *6*, 7677.

Spring, K., Ahangari, F., Scott, S.P., Waring, P., Purdie, D.M., Chen, P.C., Hourigan, K., Ramsay, J., McKinnon, P.J., Swift, M., and Lavin, M.F. (2002). Mice heterozygous for mutation in Atm, the gene involved in ataxia-telangiectasia, have heightened susceptibility to cancer. Nat Genet *32*, 185-190.

Ueki, T., Toyota, M., Sohn, T., Yeo, C.J., Issa, J.P., Hruban, R.H., and Goggins, M. (2000). Hypermethylation of multiple genes in pancreatic adenocarcinoma. Cancer Res *60*, 1835-1839.

Campbell, P.J., Yachida, S., Mudie, L.J., Stephens, P.J., Pleasance, E.D., Stebbings, L.A., Morsberger, L.A., Latimer, C., McLaren, S., Lin, M.L., McBride, D.J., Varela, I., Nik-Zainal, S.A., Leroy, C., Jia, M., Menzies, A., Butler, A.P., Teague, J.W., Griffin, C.A., Burton, J., Swerdlow, H., Quail, M.A., Stratton, M.R., Iacobuzio-Donahue, C., and Futreal, P.A. (2010). The patterns and dynamics of genomic instability in metastatic pancreatic cancer. Nature *467*, 1109-1113.

Moffitt, R.A., Marayati, R., Flate, E.L., Volmar, K.E., Loeza, S.G., Hoadley, K.A., Rashid, N.U., Williams, L.A., Eaton, S.C., Chung, A.H., Smyla, J.K., Anderson, J.M., Kim, H.J., Bentrem, D.J., Talamonti, M.S., Iacobuzio-Donahue, C.A., Hollingsworth, M.A., and Yeh, J.J. (2015). Virtual microdissection identifies distinct tumor- and stroma-specific subtypes of pancreatic ductal adenocarcinoma. Nat Genet *47*, 1168-1178.

Wu, J., Matthaei, H., Maitra, A., Dal Molin, M., Wood, L.D., Eshleman, J.R., Goggins, M., Canto, M.I., Schulick, R.D., Edil, B.H., Wolfgang, C.L., Klein, A.P., Diaz, L.A., Jr., Allen, P.J., Schmidt, C.M., Kinzler, K.W., Papadopoulos, N., Hruban, R.H., and Vogelstein, B. (2011). Recurrent GNAS mutations define an unexpected pathway for pancreatic cyst development. Sci Transl Med *3*, 92ra66.

Patra, K.C., Kato, Y., Mizukami, Y., Widholz, S., Boukhali, M., Revenco, I., Grossman, E.A., Ji, F., Sadreyev, R.I., Liss, A.S., Screaton, R.A., Sakamoto, K., Ryan, D.P., Mino-Kenudson, M., Castillo, C.F., Nomura, D.K., Haas, W., and Bardeesy, N. (2018). Mutant GNAS drives pancreatic tumourigenesis by inducing PKA-mediated SIK suppression and reprogramming lipid metabolism. Nat Cell Biol *20*, 811-822.

Jackson, E.L., Willis, N., Mercer, K., Bronson, R.T., Crowley, D., Montoya, R., Jacks, T., and Tuveson, D.A. (2001). Analysis of lung tumor initiation and progression using conditional expression of oncogenic K-ras. Genes Dev *15*, 3243-3248.

Gannon, M., Herrera, P.L., and Wright, C.V. (2000). Mosaic Cre-mediated recombination in pancreas using the pdx-1 enhancer/promoter. Genesis *26*, 143-144.

Nakhai, H., Sel, S., Favor, J., Mendoza-Torres, L., Paulsen, F., Duncker, G.I., and Schmid, R.M. (2007). Ptf1a is essential for the differentiation of GABAergic and glycinergic amacrine cells and horizontal cells in the mouse retina. Development *134*, 1151-1160.

Hingorani, S.R., Petricoin, E.F., Maitra, A., Rajapakse, V., King, C., Jacobetz, M.A., Ross, S., Conrads, T.P., Veenstra, T.D., Hitt, B.A., Kawaguchi, Y., Johann, D., Liotta, L.A., Crawford, H.C., Putt, M.E., Jacks, T., Wright, C.V., Hruban, R.H., Lowy, A.M., and Tuveson, D.A. (2003). Preinvasive and invasive ductal pancreatic cancer and its early detection in the mouse. Cancer Cell *4*, 437-450.

Hingorani, S.R., Wang, L., Multani, A.S., Combs, C., Deramaudt, T.B., Hruban, R.H., Rustgi, A.K., Chang, S., and Tuveson, D.A. (2005). Trp53R172H and KrasG12D cooperate to promote chromosomal instability and widely metastatic pancreatic ductal adenocarcinoma in mice. Cancer Cell *7*, 469-483.

Aguirre, A.J., Bardeesy, N., Sinha, M., Lopez, L., Tuveson, D.A., Horner, J., Redston, M.S., and DePinho, R.A. (2003). Activated Kras and Ink4a/Arf deficiency cooperate to produce metastatic pancreatic ductal adenocarcinoma. Genes Dev *17*, 3112-3126.

Bardeesy, N., Aguirre, A.J., Chu, G.C., Cheng, K.H., Lopez, L.V., Hezel, A.F., Feng, B., Brennan, C., Weissleder, R., Mahmood, U., Hanahan, D., Redston, M.S., Chin, L., and Depinho, R.A. (2006). Both p16(Ink4a) and the p19(Arf)-p53 pathway constrain progression of pancreatic adenocarcinoma in the mouse. Proc Natl Acad Sci U S A *103*, 5947-5952.

Schonhuber, N., Seidler, B., Schuck, K., Veltkamp, C., Schachtler, C., Zukowska, M., Eser, S., Feyerabend, T.B., Paul, M.C., Eser, P., Klein, S., Lowy, A.M., Banerjee, R., Yang, F., Lee, C.L., Moding, E.J., Kirsch, D.G., Scheideler, A., Alessi, D.R., Varela, I., Bradley, A., Kind, A., Schnieke, A.E., Rodewald, H.R., Rad, R., Schmid, R.M., Schneider, G., and Saur, D. (2014). A next-generation dual-recombinase system for time- and host-specific targeting of pancreatic cancer. Nat Med *20*, 1340-1347.

Wiedenheft, B., Sternberg, S.H., and Doudna, J.A. (2012). RNA-guided genetic silencing systems in bacteria and archaea. Nature *482*, 331-338.

Fineran, P.C., and Charpentier, E. (2012). Memory of viral infections by CRISPR-Cas adaptive immune systems: acquisition of new information. Virology *434*, 202-209.

Horvath, P., and Barrangou, R. (2010). CRISPR/Cas, the immune system of bacteria and archaea. Science *327*, 167-170.

Barrangou, R., Fremaux, C., Deveau, H., Richards, M., Boyaval, P., Moineau, S., Romero, D.A., and Horvath, P. (2007). CRISPR provides acquired resistance against viruses in prokaryotes. Science *315*, 1709-1712.

Deltcheva, E., Chylinski, K., Sharma, C.M., Gonzales, K., Chao, Y., Pirzada, Z.A., Eckert, M.R., Vogel, J., and Charpentier, E. (2011). CRISPR RNA maturation by trans-encoded small RNA and host factor RNase III. Nature *471*, 602-607.

Jinek, M., Chylinski, K., Fonfara, I., Hauer, M., Doudna, J.A., and Charpentier, E. (2012). A programmable dual-RNA-guided DNA endonuclease in adaptive bacterial immunity. Science *337*, 816-821.

Cong, L., Ran, F.A., Cox, D., Lin, S., Barretto, R., Habib, N., Hsu, P.D., Wu, X., Jiang, W., Marraffini, L.A., and Zhang, F. (2013). Multiplex genome engineering using CRISPR/Cas systems. Science *339*, 819-823.

Wolfe, S.A., Nekludova, L., and Pabo, C.O. (2000). DNA recognition by Cys2His2 zinc finger proteins. Annu Rev Biophys Biomol Struct *29*, 183-212.

Urnov, F.D., Rebar, E.J., Holmes, M.C., Zhang, H.S., and Gregory, P.D. (2010). Genome editing with engineered zinc finger nucleases. Nat Rev Genet *11*, 636-646.

Joung, J.K., and Sander, J.D. (2013). TALENs: a widely applicable technology for targeted genome editing. Nat Rev Mol Cell Biol *14*, 49-55.

Mali, P., Yang, L., Esvelt, K.M., Aach, J., Guell, M., DiCarlo, J.E., Norville, J.E., and Church, G.M. (2013). RNA-guided human genome engineering via Cas9. Science *339*, 823-826.

Jinek, M., East, A., Cheng, A., Lin, S., Ma, E., and Doudna, J. (2013). RNA-programmed genome editing in human cells. Elife *2*, e00471.

Hwang, W.Y., Fu, Y., Reyon, D., Maeder, M.L., Tsai, S.Q., Sander, J.D., Peterson, R.T., Yeh, J.R., and Joung, J.K. (2013). Efficient genome editing in zebrafish using a CRISPR-Cas system. Nat Biotechnol *31*, 227-229.

Wang, H., Yang, H., Shivalila, C.S., Dawlaty, M.M., Cheng, A.W., Zhang, F., and Jaenisch, R. (2013). One-step generation of mice carrying mutations in multiple genes by CRISPR/Cas-mediated genome engineering. Cell *153*, 910-918.

Shen, B., Zhang, J., Wu, H., Wang, J., Ma, K., Li, Z., Zhang, X., Zhang, P., and Huang, X. (2013). Generation of gene-modified mice via Cas9/RNA-mediated gene targeting. Cell Res *23*, 720-723.

Li, D., Qiu, Z., Shao, Y., Chen, Y., Guan, Y., Liu, M., Li, Y., Gao, N., Wang, L., Lu, X., Zhao, Y., and Liu, M. (2013). Heritable gene targeting in the mouse and rat using a CRISPR-Cas system. Nat Biotechnol *31*, 681-683.

Yu, Z., Ren, M., Wang, Z., Zhang, B., Rong, Y.S., Jiao, R., and Gao, G. (2013). Highly efficient genome modifications mediated by CRISPR/Cas9 in Drosophila. Genetics *195*, 289-291.

Bassett, A.R., Tibbit, C., Ponting, C.P., and Liu, J.L. (2013). Highly efficient targeted mutagenesis of Drosophila with the CRISPR/Cas9 system. Cell Rep *4*, 220-228.

Wang, T., Wei, J.J., Sabatini, D.M., and Lander, E.S. (2014). Genetic screens in human cells using the CRISPR-Cas9 system. Science *343*, 80-84.

Gasiunas, G., Barrangou, R., Horvath, P., and Siksnys, V. (2012). Cas9-crRNA ribonucleoprotein complex mediates specific DNA cleavage for adaptive immunity in bacteria. Proc Natl Acad Sci U S A *109*, E2579-2586.

Qi, L.S., Larson, M.H., Gilbert, L.A., Doudna, J.A., Weissman, J.S., Arkin, A.P., and Lim, W.A. (2013). Repurposing CRISPR as an RNA-guided platform for sequence-specific control of gene expression. Cell *152*, 1173-1183.

Gilbert, L.A., Larson, M.H., Morsut, L., Liu, Z., Brar, G.A., Torres, S.E., Stern-Ginossar, N., Brandman, O., Whitehead, E.H., Doudna, J.A., Lim, W.A., Weissman, J.S., and Qi, L.S. (2013). CRISPR-mediated modular RNA-guided regulation of transcription in eukaryotes. Cell *154*, 442-451.

Kearns, N.A., Pham, H., Tabak, B., Genga, R.M., Silverstein, N.J., Garber, M., and Maehr, R. (2015). Functional annotation of native enhancers with a Cas9-histone demethylase fusion. Nat Methods *12*, 401-403.

Hilton, I.B., D'Ippolito, A.M., Vockley, C.M., Thakore, P.I., Crawford, G.E., Reddy, T.E., and Gersbach, C.A. (2015). Epigenome editing by a CRISPR-Cas9-based acetyltransferase activates genes from promoters and enhancers. Nat Biotechnol *33*, 510-517.

Kennedy, K.L., Steidle, C.P., and Letizia, T.M. (1995). Urinary incontinence: the basics. Ostomy Wound Manage *41*, 16-18, 20, 22 passim; quiz 33-14.

Sanchez-Rivera, F.J., Papagiannakopoulos, T., Romero, R., Tammela, T., Bauer, M.R., Bhutkar, A., Joshi, N.S., Subbaraj, L., Bronson, R.T., Xue, W., and Jacks, T. (2014). Rapid

modelling of cooperating genetic events in cancer through somatic genome editing. Nature *516*, 428-431.

Chiou, S.H., Winters, I.P., Wang, J., Naranjo, S., Dudgeon, C., Tamburini, F.B., Brady, J.J., Yang, D., Gruner, B.M., Chuang, C.H., Caswell, D.R., Zeng, H., Chu, P., Kim, G.E., Carpizo, D.R., Kim, S.K., and Winslow, M.M. (2015). Pancreatic cancer modeling using retrograde viral vector delivery and in vivo CRISPR/Cas9-mediated somatic genome editing. Genes Dev *29*, 1576-1585.

Senis, E., Fatouros, C., Grosse, S., Wiedtke, E., Niopek, D., Mueller, A.K., Borner, K., and Grimm, D. (2014). CRISPR/Cas9-mediated genome engineering: an adeno-associated viral (AAV) vector toolbox. Biotechnol J *9*, 1402-1412.

Chow, R.D., Guzman, C.D., Wang, G., Schmidt, F., Youngblood, M.W., Ye, L., Errami, Y., Dong, M.B., Martinez, M.A., Zhang, S., Renauer, P., Bilguvar, K., Gunel, M., Sharp, P.A., Zhang, F., Platt, R.J., and Chen, S. (2017). AAV-mediated direct in vivo CRISPR screen identifies functional suppressors in glioblastoma. Nat Neurosci *20*, 1329-1341.

Yang, Y., Wang, L., Bell, P., McMenamin, D., He, Z., White, J., Yu, H., Xu, C., Morizono, H., Musunuru, K., Batshaw, M.L., and Wilson, J.M. (2016). A dual AAV system enables the Cas9-mediated correction of a metabolic liver disease in newborn mice. Nat Biotechnol *34*, 334-338.

Chew, W.L., Tabebordbar, M., Cheng, J.K., Mali, P., Wu, E.Y., Ng, A.H., Zhu, K., Wagers, A.J., and Church, G.M. (2016). A multifunctional AAV-CRISPR-Cas9 and its host response. Nat Methods *13*, 868-874.

Kotterman, M.A., and Schaffer, D.V. (2014). Engineering adeno-associated viruses for clinical gene therapy. Nat Rev Genet *15*, 445-451.

Glass, Z., Lee, M., Li, Y., and Xu, Q. (2018). Engineering the Delivery System for CRISPR-Based Genome Editing. Trends Biotechnol *36*, 173-185.

Xue, W., Chen, S., Yin, H., Tammela, T., Papagiannakopoulos, T., Joshi, N.S., Cai, W., Yang, G., Bronson, R., Crowley, D.G., Zhang, F., Anderson, D.G., Sharp, P.A., and Jacks, T. (2014). CRISPR-mediated direct mutation of cancer genes in the mouse liver. Nature *514*, 380-384.

Weber, J., Ollinger, R., Friedrich, M., Ehmer, U., Barenboim, M., Steiger, K., Heid, I., Mueller, S., Maresch, R., Engleitner, T., Gross, N., Geumann, U., Fu, B., Segler, A., Yuan, D., Lange, S., Strong, A., de la Rosa, J., Esposito, I., Liu, P., Cadinanos, J., Vassiliou, G.S., Schmid, R.M., Schneider, G., Unger, K., Yang, F., Braren, R., Heikenwalder, M., Varela, I., Saur, D., Bradley, A., and Rad, R. (2015). CRISPR/Cas9 somatic multiplex-mutagenesis for high-throughput functional cancer genomics in mice. Proc Natl Acad Sci U S A *112*, 13982-13987.

Kobayashi, R., Endo, K., Ohmori, Y., and Hondo, E. (2017). A novel method of gene transduction to the murine endometrium using in vivo electroporation. J Vet Med Sci *79*, 1573-1577.

Renaud, J., Kerjan, G., Sumita, I., Zagar, Y., Georget, V., Kim, D., Fouquet, C., Suda, K., Sanbo, M., Suto, F., Ackerman, S.L., Mitchell, K.J., Fujisawa, H., and Chedotal, A. (2008). Plexin-A2 and its ligand, Sema6A, control nucleus-centrosome coupling in migrating granule cells. Nat Neurosci *11*, 440-449.

Barnabe-Heider, F., Meletis, K., Eriksson, M., Bergmann, O., Sabelstrom, H., Harvey, M.A., Mikkers, H., and Frisen, J. (2008). Genetic manipulation of adult mouse neurogenic niches by in vivo electroporation. Nat Methods *5*, 189-196.

Seehawer, M., Heinzmann, F., D'Artista, L., Harbig, J., Roux, P.F., Hoenicke, L., Dang, H., Klotz, S., Robinson, L., Dore, G., Rozenblum, N., Kang, T.W., Chawla, R., Buch, T., Vucur,

M., Roth, M., Zuber, J., Luedde, T., Sipos, B., Longerich, T., Heikenwalder, M., Wang, X.W., Bischof, O., and Zender, L. (2018). Necroptosis microenvironment directs lineage commitment in liver cancer. Nature *562*, 69-75.

Aihara, H., and Miyazaki, J. (1998). Gene transfer into muscle by electroporation in vivo. Nat Biotechnol *16*, 867-870.

Michaelis, M., Sobczak, A., and Weitzel, J.M. (2014). In vivo microinjection and electroporation of mouse testis. J Vis Exp.

Zuckermann, M., Hovestadt, V., Knobbe-Thomsen, C.B., Zapatka, M., Northcott, P.A., Schramm, K., Belic, J., Jones, D.T., Tschida, B., Moriarity, B., Largaespada, D., Roussel, M.F., Korshunov, A., Reifenberger, G., Pfister, S.M., Lichter, P., Kawauchi, D., and Gronych, J. (2015). Somatic CRISPR/Cas9-mediated tumour suppressor disruption enables versatile brain tumour modelling. Nat Commun *6*, 7391.

Guschin, D.Y., Waite, A.J., Katibah, G.E., Miller, J.C., Holmes, M.C., and Rebar, E.J. (2010). A rapid and general assay for monitoring endogenous gene modification. Methods Mol Biol *649*, 247-256.

Muzumdar, M.D., Tasic, B., Miyamichi, K., Li, L., and Luo, L. (2007). A global double-fluorescent Cre reporter mouse. Genesis *45*, 593-605.

Liu, F., and Huang, L. (2002). Electric gene transfer to the liver following systemic administration of plasmid DNA. Gene Ther *9*, 1116-1119.

Dean, D.A., Machado-Aranda, D., Blair-Parks, K., Yeldandi, A.V., and Young, J.L. (2003). Electroporation as a method for high-level nonviral gene transfer to the lung. Gene Ther *10*, 1608-1615.

Braren, R., Altomonte, J., Settles, M., Neff, F., Esposito, I., Ebert, O., Schwaiger, M., Rummeny, E., and Steingoetter, A. (2011). Validation of preclinical multiparametric imaging for prediction of necrosis in hepatocellular carcinoma after embolization. J Hepatol *55*, 1034-1040.

Hruban, R.H., Adsay, N.V., Albores-Saavedra, J., Anver, M.R., Biankin, A.V., Boivin, G.P., Furth, E.E., Furukawa, T., Klein, A., Klimstra, D.S., Kloppel, G., Lauwers, G.Y., Longnecker, D.S., Luttges, J., Maitra, A., Offerhaus, G.J., Perez-Gallego, L., Redston, M., and Tuveson, D.A. (2006). Pathology of genetically engineered mouse models of pancreatic exocrine cancer: consensus report and recommendations. Cancer Res *66*, 95-106.

Brinkman, E.K., Chen, T., Amendola, M., and van Steensel, B. (2014). Easy quantitative assessment of genome editing by sequence trace decomposition. Nucleic Acids Res *42*, e168.

Bronner, I.F., Quail, M.A., Turner, D.J., and Swerdlow, H. (2014). Improved Protocols for Illumina Sequencing. Curr Protoc Hum Genet *80*, 18 12 11-42.

Li, H., Handsaker, B., Wysoker, A., Fennell, T., Ruan, J., Homer, N., Marth, G., Abecasis, G., Durbin, R., and Genome Project Data Processing, S. (2009). The Sequence Alignment/Map format and SAMtools. Bioinformatics *25*, 2078-2079.

Koboldt, D.C., Chen, K., Wylie, T., Larson, D.E., McLellan, M.D., Mardis, E.R., Weinstock, G.M., Wilson, R.K., and Ding, L. (2009). VarScan: variant detection in massively parallel sequencing of individual and pooled samples. Bioinformatics *25*, 2283-2285.

Jentsch, I., Adler, I.D., Carter, N.P., and Speicher, M.R. (2001). Karyotyping mouse chromosomes by multiplex-FISH (M-FISH). Chromosome Res *9*, 211-214.

Parekh, S., Ziegenhain, C., Vieth, B., Enard, W., and Hellmann, I. (2016). The impact of amplification on differential expression analyses by RNA-seq. Sci Rep *6*, 25533.

Macosko, E.Z., Basu, A., Satija, R., Nemesh, J., Shekhar, K., Goldman, M., Tirosh, I., Bialas, A.R., Kamitaki, N., Martersteck, E.M., Trombetta, J.J., Weitz, D.A., Sanes, J.R., Shalek, A.K., Regev, A., and McCarroll, S.A. (2015). Highly Parallel Genome-wide Expression Profiling of Individual Cells Using Nanoliter Droplets. Cell *161*, 1202-1214.

Love, M.I., Huber, W., and Anders, S. (2014). Moderated estimation of fold change and dispersion for RNA-seq data with DESeq2. Genome Biol *15*, 550.

Laemmli, U.K. (1970). Cleavage of structural proteins during the assembly of the head of bacteriophage T4. Nature *227*, 680-685.

Towbin, H., Staehelin, T., and Gordon, J. (1979). Electrophoretic transfer of proteins from polyacrylamide gels to nitrocellulose sheets: procedure and some applications. Proc Natl Acad Sci U S A *76*, 4350-4354.

Somiari, S., Glasspool-Malone, J., Drabick, J.J., Gilbert, R.A., Heller, R., Jaroszeski, M.J., and Malone, R.W. (2000). Theory and in vivo application of electroporative gene delivery. Mol Ther *2*, 178-187.

Neumann, E., Schaefer-Ridder, M., Wang, Y., and Hofschneider, P.H. (1982). Gene transfer into mouse lyoma cells by electroporation in high electric fields. EMBO J *1*, 841-845.

Maresch, R., Mueller, S., Veltkamp, C., Ollinger, R., Friedrich, M., Heid, I., Steiger, K., Weber, J., Engleitner, T., Barenboim, M., Klein, S., Louzada, S., Banerjee, R., Strong, A., Stauber, T., Gross, N., Geumann, U., Lange, S., Ringelhan, M., Varela, I., Unger, K., Yang, F., Schmid, R.M., Vassiliou, G.S., Braren, R., Schneider, G., Heikenwalder, M., Bradley, A., Saur, D., and Rad, R. (2016). Multiplexed pancreatic genome engineering and cancer induction by transfection-based CRISPR/Cas9 delivery in mice. Nat Commun *7*, 10770.

Schmidt-Supprian, M., and Rajewsky, K. (2007). Vagaries of conditional gene targeting. Nat Immunol *8*, 665-668.

Jiao, Y., Yonescu, R., Offerhaus, G.J., Klimstra, D.S., Maitra, A., Eshleman, J.R., Herman, J.G., Poh, W., Pelosof, L., Wolfgang, C.L., Vogelstein, B., Kinzler, K.W., Hruban, R.H., Papadopoulos, N., and Wood, L.D. (2014). Whole-exome sequencing of pancreatic neoplasms with acinar differentiation. J Pathol *232*, 428-435.

Furlan, D., Sahnane, N., Bernasconi, B., Frattini, M., Tibiletti, M.G., Molinari, F., Marando, A., Zhang, L., Vanoli, A., Casnedi, S., Adsay, V., Notohara, K., Albarello, L., Asioli, S., Sessa, F., Capella, C., and La Rosa, S. (2014). APC alterations are frequently involved in the pathogenesis of acinar cell carcinoma of the pancreas, mainly through gene loss and promoter hypermethylation. Virchows Arch *464*, 553-564.

Shain, A.H., Giacomini, C.P., Matsukuma, K., Karikari, C.A., Bashyam, M.D., Hidalgo, M., Maitra, A., and Pollack, J.R. (2012). Convergent structural alterations define SWItch/Sucrose NonFermentable (SWI/SNF) chromatin remodeler as a central tumor suppressive complex in pancreatic cancer. Proc Natl Acad Sci U S A *109*, E252-259.

Lynch, H.T., Deters, C.A., Lynch, J.F., and Brand, R.E. (2004). Familial pancreatic carcinoma in Jews. Fam Cancer *3*, 233-240.

Goggins, M., Schutte, M., Lu, J., Moskaluk, C.A., Weinstein, C.L., Petersen, G.M., Yeo, C.J., Jackson, C.E., Lynch, H.T., Hruban, R.H., and Kern, S.E. (1996). Germline BRCA2 gene mutations in patients with apparently sporadic pancreatic carcinomas. Cancer Res *56*, 5360-5364.

Ozcelik, H., Schmocker, B., Di Nicola, N., Shi, X.H., Langer, B., Moore, M., Taylor, B.R., Narod, S.A., Darlington, G., Andrulis, I.L., Gallinger, S., and Redston, M. (1997). Germline BRCA2 6174delT mutations in Ashkenazi Jewish pancreatic cancer patients. Nat Genet *16*, 17-18.

Caldas, C., Hahn, S.A., da Costa, L.T., Redston, M.S., Schutte, M., Seymour, A.B., Weinstein, C.L., Hruban, R.H., Yeo, C.J., and Kern, S.E. (1994). Frequent somatic mutations and homozygous deletions of the p16 (MTS1) gene in pancreatic adenocarcinoma. Nat Genet *8*, 27-32.

Schutte, M., Hruban, R.H., Geradts, J., Maynard, R., Hilgers, W., Rabindran, S.K., Moskaluk, C.A., Hahn, S.A., Schwarte-Waldhoff, I., Schmiegel, W., Baylin, S.B., Kern, S.E., and Herman, J.G. (1997). Abrogation of the Rb/p16 tumor-suppressive pathway in virtually all pancreatic carcinomas. Cancer Res *57*, 3126-3130.

Redston, M.S., Caldas, C., Seymour, A.B., Hruban, R.H., da Costa, L., Yeo, C.J., and Kern, S.E. (1994). p53 mutations in pancreatic carcinoma and evidence of common involvement of homocopolymer tracts in DNA microdeletions. Cancer Res *54*, 3025-3033.

Hahn, S.A., Schutte, M., Hoque, A.T., Moskaluk, C.A., da Costa, L.T., Rozenblum, E., Weinstein, C.L., Fischer, A., Yeo, C.J., Hruban, R.H., and Kern, S.E. (1996). DPC4, a candidate tumor suppressor gene at human chromosome 18q21.1. Science *271*, 350-353.

Soriano, P. (1999). Generalized lacZ expression with the ROSA26 Cre reporter strain. Nat Genet *21*, 70-71.

Skoulidis, F., Cassidy, L.D., Pisupati, V., Jonasson, J.G., Bjarnason, H., Eyfjord, J.E., Karreth, F.A., Lim, M., Barber, L.M., Clatworthy, S.A., Davies, S.E., Olive, K.P., Tuveson, D.A., and Venkitaraman, A.R. (2010). Germline Brca2 heterozygosity promotes Kras(G12D) -driven carcinogenesis in a murine model of familial pancreatic cancer. Cancer Cell *18*, 499-509.

Rowley, M., Ohashi, A., Mondal, G., Mills, L., Yang, L., Zhang, L., Sundsbak, R., Shapiro, V., Muders, M.H., Smyrk, T., and Couch, F.J. (2011). Inactivation of Brca2 promotes Trp53-associated but inhibits KrasG12D-dependent pancreatic cancer development in mice. Gastroenterology *140*, 1303-1313 e1301-1303.

McGranahan, N., and Swanton, C. (2017). Clonal Heterogeneity and Tumor Evolution: Past, Present, and the Future. Cell *168*, 613-628.

Karhu, R., Mahlamaki, E., and Kallioniemi, A. (2006). Pancreatic adenocarcinoma -- genetic portrait from chromosomes to microarrays. Genes Chromosomes Cancer *45*, 721-730.

Norris, A.L., Kamiyama, H., Makohon-Moore, A., Pallavajjala, A., Morsberger, L.A., Lee, K., Batista, D., Iacobuzio-Donahue, C.A., Lin, M.T., Klein, A.P., Hruban, R.H., Wheelan, S.J., and Eshleman, J.R. (2015). Transflip mutations produce deletions in pancreatic cancer. Genes Chromosomes Cancer *54*, 472-481.

Blasco, R.B., Karaca, E., Ambrogio, C., Cheong, T.C., Karayol, E., Minero, V.G., Voena, C., and Chiarle, R. (2014). Simple and rapid in vivo generation of chromosomal rearrangements using CRISPR/Cas9 technology. Cell Rep *9*, 1219-1227.

Maddalo, D., Manchado, E., Concepcion, C.P., Bonetti, C., Vidigal, J.A., Han, Y.C., Ogrodowski, P., Crippa, A., Rekhtman, N., de Stanchina, E., Lowe, S.W., and Ventura, A. (2014). In vivo engineering of oncogenic chromosomal rearrangements with the CRISPR/Cas9 system. Nature *516*, 423-427.

Cho, Y., Gorina, S., Jeffrey, P.D., and Pavletich, N.P. (1994). Crystal structure of a p53 tumor suppressor-DNA complex: understanding tumorigenic mutations. Science *265*, 346-355.

Dietlein, F., Kalb, B., Jokic, M., Noll, E.M., Strong, A., Tharun, L., Ozretic, L., Kunstlinger, H., Kambartel, K., Randerath, W.J., Jungst, C., Schmitt, A., Torgovnick, A., Richters, A., Rauh, D., Siedek, F., Persigehl, T., Mauch, C., Bartkova, J., Bradley, A., Sprick, M.R., Trumpp, A., Rad, R., Saur, D., Bartek, J., Wolf, J., Buttner, R., Thomas, R.K., and Reinhardt, H.C. (2015). A Synergistic Interaction between Chk1- and MK2 Inhibitors in KRAS-Mutant Cancer. Cell *162*, 146-159.

Heckl, D., Kowalczyk, M.S., Yudovich, D., Belizaire, R., Puram, R.V., McConkey, M.E., Thielke, A., Aster, J.C., Regev, A., and Ebert, B.L. (2014). Generation of mouse models of myeloid malignancy with combinatorial genetic lesions using CRISPR-Cas9 genome editing. Nat Biotechnol *32*, 941-946.

Chen, S., Sanjana, N.E., Zheng, K., Shalem, O., Lee, K., Shi, X., Scott, D.A., Song, J., Pan, J.Q., Weissleder, R., Lee, H., Zhang, F., and Sharp, P.A. (2015). Genome-wide CRISPR screen in a mouse model of tumor growth and metastasis. Cell *160*, 1246-1260.

Matano, M., Date, S., Shimokawa, M., Takano, A., Fujii, M., Ohta, Y., Watanabe, T., Kanai, T., and Sato, T. (2015). Modeling colorectal cancer using CRISPR-Cas9-mediated engineering of human intestinal organoids. Nat Med *21*, 256-262.

Drost, J., van Jaarsveld, R.H., Ponsioen, B., Zimberlin, C., van Boxtel, R., Buijs, A., Sachs, N., Overmeer, R.M., Offerhaus, G.J., Begthel, H., Korving, J., van de Wetering, M., Schwank, G., Logtenberg, M., Cuppen, E., Snippert, H.J., Medema, J.P., Kops, G.J., and Clevers, H. (2015). Sequential cancer mutations in cultured human intestinal stem cells. Nature *521*, 43-47.

O'Rourke, K.P., Loizou, E., Livshits, G., Schatoff, E.M., Baslan, T., Manchado, E., Simon, J., Romesser, P.B., Leach, B., Han, T., Pauli, C., Beltran, H., Rubin, M.A., Dow, L.E., and Lowe, S.W. (2017). Transplantation of engineered organoids enables rapid generation of metastatic mouse models of colorectal cancer. Nat Biotechnol *35*, 577-582.

Yin, H., Xue, W., Chen, S., Bogorad, R.L., Benedetti, E., Grompe, M., Koteliansky, V., Sharp, P.A., Jacks, T., and Anderson, D.G. (2014). Genome editing with Cas9 in adult mice corrects a disease mutation and phenotype. Nat Biotechnol *32*, 551-553.

Cook, P.J., Thomas, R., Kannan, R., de Leon, E.S., Drilon, A., Rosenblum, M.K., Scaltriti, M., Benezra, R., and Ventura, A. (2017). Somatic chromosomal engineering identifies BCAN-NTRK1 as a potent glioma driver and therapeutic target. Nat Commun *8*, 15987.

Roper, J., Tammela, T., Cetinbas, N.M., Akkad, A., Roghanian, A., Rickelt, S., Almeqdadi, M., Wu, K., Oberli, M.A., Sanchez-Rivera, F.J., Park, Y.K., Liang, X., Eng, G., Taylor, M.S., Azimi, R., Kedrin, D., Neupane, R., Beyaz, S., Sicinska, E.T., Suarez, Y., Yoo, J., Chen, L., Zukerberg, L., Katajisto, P., Deshpande, V., Bass, A.J., Tsichlis, P.N., Lees, J., Langer, R., Hynes, R.O., Chen, J., Bhutkar, A., Jacks, T., and Yilmaz, O.H. (2017). In vivo genome editing and organoid transplantation models of colorectal cancer and metastasis. Nat Biotechnol *35*, 569-576.

Hausmann, S., Kong, B., Michalski, C., Erkan, M., and Friess, H. (2014). The role of inflammation in pancreatic cancer. Adv Exp Med Biol *816*, 129-151.

Gurlevik, E., Fleischmann-Mundt, B., Brooks, J., Demir, I.E., Steiger, K., Ribback, S., Yevsa, T., Woller, N., Kloos, A., Ostroumov, D., Armbrecht, N., Manns, M.P., Dombrowski, F., Saborowski, M., Kleine, M., Wirth, T.C., Oettle, H., Ceyhan, G.O., Esposito, I., Calvisi, D.F., Kubicka, S., and Kuhnel, F. (2016). Administration of Gemcitabine After Pancreatic Tumor Resection in Mice Induces an Antitumor Immune Response Mediated by Natural Killer Cells. Gastroenterology *151*, 338-350 e337.

Ramirez-Solis, R., Liu, P., and Bradley, A. (1995). Chromosome engineering in mice. Nature *378*, 720-724.

Yu, Y., and Bradley, A. (2001). Engineering chromosomal rearrangements in mice. Nat Rev Genet *2*, 780-790.

Maezawa, A., Ogiwara, T., Matsui, K., Suzuki, Y., Nakamura, T., Oite, T., and Shimizu, F. (1985). Long-term observation of passive Heymann nephritis. Nephron *41*, 348-353.

Heisterkamp, N., Jenster, G., ten Hoeve, J., Zovich, D., Pattengale, P.K., and Groffen, J. (1990). Acute leukaemia in bcr/abl transgenic mice. Nature *344*, 251-253.

Childs, E.J., Mocci, E., Campa, D., Bracci, P.M., Gallinger, S., Goggins, M., Li, D., Neale, R.E., Olson, S.H., Scelo, G., Amundadottir, L.T., Bamlet, W.R., Bijlsma, M.F., Blackford, A., Borges, M., Brennan, P., Brenner, H., Bueno-de-Mesquita, H.B., Canzian, F., Capurso, G., Cavestro, G.M., Chaffee, K.G., Chanock, S.J., Cleary, S.P., Cotterchio, M., Foretova, L., Fuchs, C., Funel, N., Gazouli, M., Hassan, M., Herman, J.M., Holcatova, I., Holly, E.A., Hoover, R.N., Hung, R.J., Janout, V., Key, T.J., Kupcinskas, J., Kurtz, R.C., Landi, S., Lu, L., Malecka-Panas, E., Mambrini, A., Mohelnikova-Duchonova, B., Neoptolemos, J.P., Oberg, A.L., Orlow, I., Pasquali, C., Pezzilli, R., Rizzato, C., Saldia, A., Scarpa, A., Stolzenberg-Solomon, R.Z., Strobel, O., Tavano, F., Vashist, Y.K., Vodicka, P., Wolpin, B.M., Yu, H., Petersen, G.M., Risch, H.A., and Klein, A.P. (2015). Common variation at 2p13.3, 3q29, 7p13 and 17q25.1 associated with susceptibility to pancreatic cancer. Nat Genet *47*, 911-916.

Wolpin, B.M., Rizzato, C., Kraft, P., Kooperberg, C., Petersen, G.M., Wang, Z., Arslan, A.A., Beane-Freeman, L., Bracci, P.M., Buring, J., Canzian, F., Duell, E.J., Gallinger, S., Giles, G.G., Goodman, G.E., Goodman, P.J., Jacobs, E.J., Kamineni, A., Klein, A.P., Kolonel, L.N., Kulke, M.H., Li, D., Malats, N., Olson, S.H., Risch, H.A., Sesso, H.D., Visvanathan, K., White, E., Zheng, W., Abnet, C.C., Albanes, D., Andreotti, G., Austin, M.A., Barfield, R., Basso, D., Berndt, S.I., Boutron-Ruault, M.C., Brotzman, M., Buchler, M.W., Bueno-de-Mesquita, H.B., Bugert, P., Burdette, L., Campa, D., Caporaso, N.E., Capurso, G., Chung, C., Cotterchio, M., Costello, E., Elena, J., Funel, N., Gaziano, J.M., Giese, N.A., Giovannucci, E.L., Goggins, M., Gorman, M.J., Gross, M., Haiman, C.A., Hassan, M., Helzlsouer, K.J., Henderson, B.E., Holly, E.A., Hu, N., Hunter, D.J., Innocenti, F., Jenab, M., Kaaks, R., Key, T.J., Khaw, K.T., Klein, E.A., Kogevinas, M., Krogh, V., Kupcinskas, J., Kurtz, R.C., LaCroix, A., Landi, M.T., Landi, S., Le Marchand, L., Mambrini, A., Mannisto, S., Milne, R.L., Nakamura, Y., Oberg, A.L., Owzar, K., Patel, A.V., Peeters, P.H., Peters, U., Pezzilli, R., Piepoli, A., Porta, M., Real, F.X., Riboli, E., Rothman, N., Scarpa, A., Shu, X.O., Silverman, D.T., Soucek, P., Sund, M., Talar-Wojnarowska, R., Taylor, P.R., Theodoropoulos, G.E., Thornquist, M., Tjonneland, A., Tobias, G.S., Trichopoulos, D., Vodicka, P., Wactawski-Wende, J., Wentzensen, N., Wu, C., Yu, H., Yu, K., Zeleniuch-Jacquotte, A., Hoover, R., Hartge, P., Fuchs, C., Chanock, S.J., Stolzenberg-Solomon, R.S., and Amundadottir, L.T. (2014). Genome-wide association study identifies multiple susceptibility loci for pancreatic cancer. Nat Genet *46*, 994-1000.

13. Publications resulting from my thesis

December 2014

A conditional piggyBac transposition system for genetic screening in mice identifies oncogenic networks in pancreatic cancer. Rad R*, Rad L, Wang W, Strong A, Ponstingl H, Bronner IF, Mayho M, Steiger K, Weber J, Hieber M, Veltkamp C, Eser S, Geumann U, Öllinger R, Zukowska M, Barenboim M, **Maresch R**, Cadiñanos J, Friedrich M, Varela I, Constantino-Casas F, Sarver A, Ten Hoeve J, Prosser H, Seidler B, Bauer J, Heikenwälder M, Metzakopian E, Krug A, Ehmer U, Schneider G, Knösel T, Rümmele P, Aust D, Grützmann R, Pilarsky C, Ning Z, Wessels L, Schmid RM, Quail MA, Vassiliou G, Esposito I, Liu P, Saur D, Bradley A.; Nat Genet. 2015 Jan;47(1):47-56.

October 2015

CRISPR/Cas9 somatic multiplex-mutagenesis for high-throughput functional cancer genomics in mice. Weber J*, Öllinger R*, Friedrich M, Ehmer U, Barenboim M, Steiger K, Heid I, Mueller S, **Maresch R**, Engleitner T, Gross N, Geumann U, Fu B, Segler A, Yuan D, Lange S, Strong A, de la Rosa J, Esposito I, Liu P, Cadiñanos J, Vassiliou GS, Schmid RM, Schneider G, Unger K, Yang F, Braren R, Heikenwälder M, Varela I, Saur D, Bradley A, Rad R.; Proc Natl Acad Sci U S A. 2015 Nov 10;112(45):13982-7.

February 2016

Multiplexed pancreatic genome engineering and cancer induction by transfection-based CRISPR/Cas9 delivery in mice. Maresch R*, Mueller S*, Veltkamp C, Öllinger R, Friedrich M, Heid I, Steiger K, Weber J, Engleitner T, Barenboim M, Klein S, Louzada S, Banerjee R, Strong A, Stauber T, Gross N, Geumann U, Lange S, Ringelhan M, Varela I, Unger K, Yang F, Schmid RM, Vassiliou GS, Braren R, Schneider G, Heikenwalder M, Bradley A, Saur D, Rad R.; Nat Commun. 2016 Feb 26;7:10770.

November 2017

PD-1 is a haploinsufficient suppressor of T cell lymphomagenesis. Wartewig T*, Kurgyis Z, Keppler S, Pechloff K, Hameister E, Öllinger R, **Maresch R**, Buch T, Steiger K, Winter C, Rad R, Ruland J. Nature. 2017 Dec 7;552(7683):121-125.

January 2018

Evolutionary routes and KRAS dosage define pancreatic cancer phenotypes. Mueller S*, Engleitner T*, **Maresch R***, Zukowska M, Lange S, Kaltenbacher T, Konukiewitz B, Öllinger

R, Zwiebel M, Strong A, Yen HY, Banerjee R, Louzada S, Fu B, Seidler B, Götzfried J, Schuck K, Hassan Z, Arbeiter A, Schönhuber N, Klein S, Veltkamp C, Friedrich M, Rad L, Barenboim M, Ziegenhain C, Hess J, Dovey OM, Eser S, Parekh S, Constantino-Casas F, de la Rosa J, Sierra MI, Fraga M, Mayerle J, Klöppel G, Cadiñanos J, Liu P, Vassiliou G, Weichert W, Steiger K, Enard W, Schmid RM, Yang F, Unger K, Schneider G, Varela I, Bradley A, Saur D, Rad R. Nature. 2018 Feb 1;554(7690):62-68.

February 2020

Computational pipelines for cancer genome sequencing in mice. Sebastian Lange*, Thomas Engleitner*, Sebastian Mueller*, **Roman Maresch***, Maximilian Zwiebel, Laura Gonzalez-Silva, Günter Schneider, George S. Vassiliou, Mathias J. Friedrich1, Dieter Saur, Ignacio Varela, Roland Rad. Nat Protoc. 2020 Feb;15(2):266-315.

*First author